Physics – Uspekhi **41** (10) 945 – 982 (1998)

REVIEWS OF TOPICAL PROBLEMS PACS numbers: **95.35.+d**, **98.35.–a**

Gravitational microlensing

A F Zakharov, M V Sazhin

Contents

Abstract. The foundations of standard microlensing theory are discussed as applied to stars in the Galactic bulge, Magellanic Clouds or other nearby galaxies and gravitational microlenses assumed to lie in-between these stars and the terrestrial observer. In contrast to the review article by Gurevich et al. [48], microlensing by compact objects is mainly considered. Criteria for the identification of microlensing events are discussed as also are microlensing events not satisfying these criteria, such as non-symmetrical light curves and chromatic and polarization effects. The Large Magellanic Cloud (LMC) and Galactic bulge microlensing data of the MACHO group are discussed in detail and also the LMC data of EROS and the Galactic bulge data of OGLE are presented. A detailed comparison of theoretical predictions and observations is given.

A F Zakharov Institute of Theoretical and Experimental Physics,
ul. B. Cheremushkinskaya 25, 117259 Moscow, Russia
Tel. (7-095) 125 91 22
E-mail: zakharov@vitep5.itep.ru
M V Sazhin Sternberg State Astronomical Institute,
Universitetskiĭ prosp., 119889 Moscow,
Tel. (7-095) 939 50 06
E-mail: sazhin@sai.msu.su

Received 29 December 1997, revised 22 April 1998
Uspekhi Fizicheskikh Nauk **168** (10) 1041 – 1082 (1998)
Translated by A F Zakharov; edited by S D Danilov

1. Standard model

1.1 Equation of motion of light rays

A standard microlens model is based on a simple approximation of a point mass for a gravitational microlens. Therefore, before discussing the microlensing effect we consider a simple gravitational lens model and the principles of image formation by a gravitational lens with a spherically symmetrical density distribution.

If we suppose that the gravitational field is weak then photons are emitted from infinity and are bent by a gravitational mass (a gravitational lens) and move away from the neighborhood of the gravitational mass to infinity. First we consider the photon motion in the framework of the Newtonian gravitational theory. We suppose that a photon is a particle with mass $m = h\nu/c^2$.

Let us consider photon motion near a star with a mass M_*. If a photon is emitted by a source S then we denote the impact distance of the photon motion by p. If we use the Cartesian coordinate frame Oxy then the equation of motion of a light ray has the following form:

$$m\,\frac{\mathrm{d}^2\mathbf{r}}{\mathrm{d}t^2} = -\frac{GmM_*}{|\mathbf{r}|^3}\,\mathbf{r}\,. \tag{1}$$

As follows from Eqn (1), the photon mass is shortened, so there is a light bending effect even in the framework of the Newtonian theory. This effect was noted by Newton, but the first derivation for the bending angle of a light ray by a gravitating body was published by J Soldner at the beginning of the nineteenth century [1].

It is well-known from the analysis of the Newtonian equations of motion that a test particle trajectory may be a hyperbola, a parabola or an ellipse. The quantitative criteria of different types of particle trajectory consist in the comparison of the potential energy of a particle in the gravitational field [$U = GM_*hv/(c^2p)$] and the kinetic energy ($E = hv$ for the case). Since the test particle is a photon in our case, the criterion is a ratio of the gravitational potential of the body and the square of the speed of light $GM_*/(c^2p)$. The ratio is much smaller than unity for the astronomical models considered, so the trajectory is a hyperbola and the kinetic energy of the photon is much greater than its potential energy.

Below we will analyse a light ray's displacement along the axis Oy, which is perpendicular to the original velocity of the photon. Since the light ray in effect moves along the axis Ox, in zeroth order in the parameter $GM_*/(c^2p)$ we have the following equation of motion $x = ct$. If we express t via x and substitute it into Eqn (1), then we obtain the equation in the parametric form $y(x)$

$$\frac{\mathrm{d}^2y}{\mathrm{d}x^2} = -\frac{GM_*y}{c^2(x^2+y^2)^{3/2}}\,. \tag{2}$$

We suppose that the displacement is very small, thus, we assume $y \approx p$ in the right hand side of Eqn (2). So, it is possible to calculate an integral of the right hand side of Eqn (2). Really, using the substitution $x = p\tan\phi$, we obtain

$$-p\int_{-\infty}^{x}\frac{\mathrm{d}x}{(x^2+p^2)^{3/2}} = -p^{-1}(\sin\phi+1)\,. \tag{3}$$

We note that $\mathrm{d}y/\mathrm{d}x$ is a tangent line for the photon trajectory, the difference of the values $\mathrm{d}y/\mathrm{d}x$ for $+\infty$ and $-\infty$ is equal to the bending angle of the photon in the gravitational field of the star M_*:

$$\begin{aligned}\Delta\varphi &= \left.\frac{\mathrm{d}y}{\mathrm{d}x}\right|_{x=-\infty} - \left.\frac{\mathrm{d}y}{\mathrm{d}x}\right|_{x=+\infty}\\ &= \left.\frac{\mathrm{d}y}{\mathrm{d}x}\right|_{\phi=-\pi/2} - \left.\frac{\mathrm{d}y}{\mathrm{d}x}\right|_{\phi=+\pi/2} = -\frac{2GM_*}{c^2p}\,.\end{aligned} \tag{4}$$

So, we have obtained a value for the bending angle which is a half of the correct value. The difference is connected with the usage of a non-relativistic approximation, but a photon is a relativistic particle moving with the limiting speed (the speed of light).

In the framework of general relativity using a weak gravitational field approximation the correct bending angle is described by an expression which differs from the right hand side of Eqn (4) by a factor of 2. Really the bending angle is defined by the following expression:

$$\delta\varphi = -\frac{4GM_*}{c^2p}\,. \tag{5}$$

The derivation of Einstein's famous formulae for the bending angle of light rays in gravitational field of a point mass M_* is in practically all monographs and textbooks on general relativity and gravity theory (see, for example books of Landau & Lifshitz [3], Möller [2]).

In the framework of general relativity the light ray bending effect was predicted by Einstein in 1915 and was first confirmed by Sir A Eddington for observations of light ray bending by the Solar gravitational field near its surface. The angle was equal to 1.75″, and Einstein's prediction was confirmed by observations.

The first researcher who used the term 'lens' for the gravitational deflection of light curves was O Lodge. In the short letter "Gravitation and Light" which was published in *Nature* in 1919 he wrote "that the solar gravitational field acts like a lens, for it has no focal length..."

In 1924 Russian physicist O Chwolson published a short paper in *Astronomische Nachrichten* where he considered the possibility of the appearance of a fictitious double star due to the deflection of light rays by a star lying between the background star and an observer. He noted that a reversed mirror image appeared but the separation angle between the two images is very small in this case. He closed his short paper with the cautious sentence "I cannot judge whether the case of a fictitious double star mentioned here really exists". Chwolson considered the case when the background and foreground stars were perfectly aligned and a ring-shape image of the background star would appear. So, as American astronomer J. Barnothy wrote in 1969, such rings should be called 'Chwolson rings' but they are usually called 'Einstein rings' and Schneider, Ehlers and Falco, who are the authors of the first remarkable monograph on gravitational lensing in English, wrote about this tradition that "the biggest cat gets all the milk". Thus, following the terminology of Schneider et al., we call such rings Einstein – Chwolson rings.

In 1936 A Einstein published a short letter in *Science* where he mentioned the appearance of 'a luminous circle' if the background and foreground stars are aligned, but Einstein noted that "of course, there is not much hope of observing this phenomenon directly". Moreover, he also mentioned the increase of the apparent brightness of the background due to the gravitational deflection of light rays. So, both Chwolson and Einstein thought that it impossible to detect the gravitational lens effect if the source and deflector (gravitational lens) are stars. Really, it is impossible to resolve two images of a background star, since the separation angle is too small in this case. But now there are technical possibilities for monitoring several million stars, in our Galaxy or in nearby galaxies, over several years and to select those few light curves with typical properties of gravitational lensing. So, now it is possible to detect typical light curves due the gravitational lens phenomenon. It is clear that it is necessary to use modern techniques for observation and powerful computers to collect, process and fit the observational data. Below we will discuss these problems in detail.

1.2 Point lens equation

Since a photon moves practically along straight lines far from a gravitating body, we approximate the photon trajectory by two straight lines which intersect near the body D (Fig. 1). The angle between the lines α demonstrates the photon bending in the gravitational field of the body D.

Two rays of light, which lie on opposite sides of the gravitating body, are deflected to the gravitating body. If a source S lies far away from the body D then the rays begin to converge and intersect at some distant point O (see Fig. 1). If we suppose that an observer is at the point O, he will see two images (I_1, I_2) of one source S. This is gravitational lens effect. In Figure 1 three physical bodies are shown, namely the source S, the gravitating body D and the observer O. The trajectories of light rays from S to O are shown by two bold solid lines. We use also the following notation: D_{ds} is the distance from the source S to the lens D; D_d is the distance

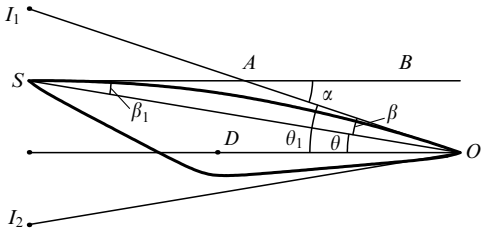

Figure 1. Formation of images and light rays bent by the gravitational field of a body.

from the lens D to the observer O; D_s is the distance from the source S to the observer O. We draw a plane via the point S and suppose that the plane is perpendicular to the light ray trajectory. The plane is called the source plane. Similarly, we draw a plane via the gravitational lens D. This plane is called lens source. We also use the following notation for the angles: θ is the angle between the direction to the gravitating body D and the direction to the source S, θ_1 is the angle between the direction to the gravitating body D and the apparent direction to the source S, I_1 and I_2 are images (mirages) of the source.

It can be seen from the figure that we have the following expressions for the angles:

$$\alpha = \beta_1 + \beta\,, \tag{6}$$

$$\theta_1 = \theta + \beta\,, \tag{7}$$

$$\beta_1 D_{ds} = \beta D_d\,, \tag{8}$$

where the angle β is expressed in radians. From Eqns (7), (8) we obtain a quadratic equation for the angle θ_1 which determines apparent positions of images relative to the direction toward the gravitational lens,

$$\theta_1^2 - \theta\theta_1 - \theta_0^2 = 0\,, \tag{9}$$

where θ_0 is the angular radius of the Einstein–Chwolson cone which is defined as

$$\theta_0^2 = \frac{4GM}{c^2}\,\frac{D_{ds}}{(D_{ds}+D_d)D_d}\,.$$

Equation (9) is called the gravitational lens (GL) equation for the case of a spherically symmetric point lens. The equation has two real roots, namely

$$\theta_1 = \frac{1}{2}\,\theta + \frac{1}{2}\sqrt{\theta^2 + 4\theta_0^2}\,,$$

$$\theta_2 = \frac{1}{2}\,\theta - \frac{1}{2}\sqrt{\theta^2 + 4\theta_0^2}\,,$$

corresponding to two images of the source S. The angular distance between the images is equal to $(\theta^2 + 4\theta_0^2)^{1/2}$.

According to previous arguments we have written about two images. However, these two images are not always formed. Really, we used the assumption that the size of the gravitating body D is infinitesimal and Eqn (5) is valid for any impact parameter p. Actually, if the impact parameter is smaller than the radius R_D of the gravitating body D or

$$R_D > D_d\,\theta_2\,,$$

then the image I_2 disappears for an observer O (the light ray moving along a trajectory with a small impact parameter is absorbed by the matter of the gravitational lens if it is non-transparent). Therefore, only one image of the source is formed for this case. That is the reason why an Earth observer does not see two images during a solar eclipse in spite of the existence of a set of stars which lie near the line drawn via the solar center and the observer [we recall that the angular solar size is about a half a degree, which is much greater than the Einstein–Chwolson cone size of the Sun since the distance between an Earth observer and the gravitational lens (the Sun) is equal to 1 astronomical unit].

For a spherically symmetric gravitational field of a body D an image of a circular star S is transformed by the gravitational lens into two crescents, which are reflected relative to each other (Fig. 2a) [4–9]. Their sizes and brightnesses are different, but the total luminosity is greater than the original luminosity of the (unlensed) source S. The discovery of microlensing effects is based on this effect.

It is necessary to note that according to the equivalence principle two bodies with different masses fall with the same acceleration in a gravitational field. Therefore, two photons having different frequencies (different energies and thus different masses) are accelerated identically in a gravitational field. In other words, photons lying in different bands are bent

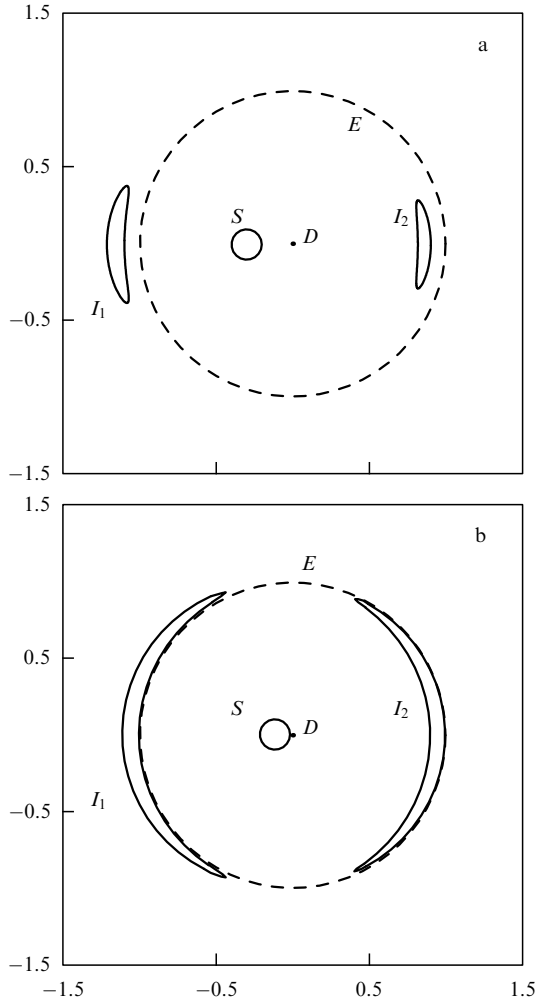

Figure 2. Two images of a circular source, which are formed by a point gravitational lens (for the case when the angular distance between the gravitational lens and the source center is (a) $d = 0.3$, (b) $d = 0.11$ in Einstein–Chwolson units). Sources and images are shown in Einstein–Chwolson units.

identically in the gravitational field of body D. This property is called the achromatism of the microlensing effect. Possible violations of this property may be connected with the complicated structure of the source S; the violations will be discussed below.

The gravitational lens effect is the formation of several images instead of one. We have two images for a point lens model (Schwarzschild lens model). The angular distance between the two images is about the angular size of the so-called Einstein – Chwolson cone. The angular size of the Einstein – Chwolson cone is proportional to the lens mass divided by the distance between the lens and observer. Therefore, if we consider a gravitational lens with typical galactic mass and a typical galactic distance between the gravitational lens and observer then the angular distance between images will be about a few angular seconds; if we suppose that the gravitational lens has a solar mass and a distance between the lens and observer is several kiloparsecs then the angular distance between the images will be about an angular millisecond.

If the separation angle is $\sim 1''$, then one may observe two images in the optical band although this problem is complex, but one cannot observe directly two images on Earth in the optical band if the separation angle is $\sim 0.001''$. Therefore, the effect is observed on changing of the luminosity of the source S.

Let us consider a change of a luminosity of images during microlensing. First, we determine the luminosity of either of the two images. It is possible to evade formal and cumbersome calculations if we use the following assumption for the simplification of our analysis. We suppose that the shape of any image is an ellipse (Fig. 2a) [really the shapes of the images are more complex figures, for example, for great amplifications the shapes are like crescents (Fig. 2b), although behind a gravitational lens the source image is a circle]. Both I_1 and I_2 are slightly squeezed along a line which connects $I_1 D I_2$ and the images are extended in the perpendicular direction. The ellipse area is determined by the following expression $\Omega = \pi ab$, where a and b are the major and minor semiaxes respectively. Using proportionality relations we find the semiaxes a and b through the parameters of the lens and source (Fig. 2a). So, the area of the first image is determined (in steradians) by the following expression

$$\Omega_1 = \pi\varphi_s^2\left(\frac{1}{2}+\frac{u}{4}+\frac{1}{4u}\right),$$

and the area of the second image by the expression

$$\Omega_2 = \pi\varphi_s^2\left(-\frac{1}{2}+\frac{u}{4}+\frac{1}{4u}\right),$$

where $u = (1+4\theta_0^2\theta^{-2})^{1/2}$ is an auxiliary variable. The sizes and luminosities of the images are different, but their total luminosity is greater than the luminosity of an unlensed source S, actually

$$\Omega_1 + \Omega_2 = \frac{1}{2}\,\pi\varphi_s^2\left(u+\frac{1}{u}\right) > \pi\varphi_s^2\,. \tag{10}$$

Really, the discovery of microlensing effects is based on the usage of this property. Since photons belonging to different spectral bands are deflected identically in the gravitational field of a body D, the amplification is the same for different spectral bands.

The sum of the luminosity of two images divided by the undistorted luminosity is called the amplification factor and is usually denoted as A, so

$$A = \frac{\Omega_1 + \Omega_2}{\pi\varphi_s^2}\,.$$

If the impact parameter for a source S is small, that is defined formally as $\theta \ll \theta_0$, then the parameter u is great and the amplification factor $A = \theta_0/\theta$ is much greater than unity.

If $\theta \to 0$ or the source center S, an observer O and a gravitational lens D lie on a straight line, the total luminosity will be defined by Eqn (10) and formally tend to infinity as $\Omega_1 + \Omega_2 \to \infty$. We obtain this incorrect conclusion since we made an incorrect assumption about the shapes of the images for small impact parameters and carried out approximate calculations of the semiaxes a and b.

If the source center S, an observer O and a gravitational lens D lie on a straight line, the gravitational lens will form an image like a luminous ring or the Einstein–Chwolson ring. It has a radius θ_0, a circumference $2\pi\theta_0$ and a width:

$$2\phi_s\left.\frac{\mathrm{d}\theta_1}{\mathrm{d}\theta}\right|_{\theta_0} = \phi_s\,,$$

which is equal to the source radius. In other words, the solid angle Ω corresponding to the ring on the celestial sphere is equal to $2\pi\theta_0\phi_s$. The amplification factor is equal to $2\pi\theta_0/\phi_s$ for this case.

Let us return to Fig. 1. A light source S, a dark body D and an observer O have a peculiar motion. It is possible to decompose the motion of each of these three bodies into two vectors, one of which is perpendicular to the straight line OD and the second is parallel to the line. The parallel component of the velocity changes the basic astrophysical parameters of the model, for example the size of the Einstein – Chwolson cone. However, the change is very small and we will neglect its influence. Perpendicular components of the velocity are added together and there is motion of the source S in the gravitational lens plane relatively to the dark body D.

Let us consider the source motion across the Einstein – Chwolson cone. (Fig. 3a). The real motion of a light source S is shown by a solid straight line, but the motions of images are drawn by two dashed lines I_1 and I_2. The Einstein – Chwolson circle is also shown by the dashed line. It is possible to find θ which is the angular distance between the light source S and the gravitational lens D from the following expression

$$\theta^2(t) = \Omega^2 t^2 + \theta_p^2\,.$$

We choose the time $t = 0$ according to the following rule: the time $t = 0$ corresponds to the minimal angular distance (θ_p) between S and D. If we assume that the observer and lens are fixed then Ω is the angular velocity of the source on the celestial sphere. Thus, the distances between the dark body and the first and the second images are equal to

$$\theta_1(t) = \frac{1}{2}\sqrt{\Omega^2 t^2 + \theta_p^2} + \frac{1}{2}\sqrt{\Omega^2 t^2 + \theta_p^2 + 4\theta_0^2}$$

and

$$\theta_2(t) = \frac{1}{2}\sqrt{\Omega^2 t^2 + \theta_p^2} - \frac{1}{2}\sqrt{\Omega^2 t^2 + \theta_p^2 + 4\theta_0^2}$$

respectively.

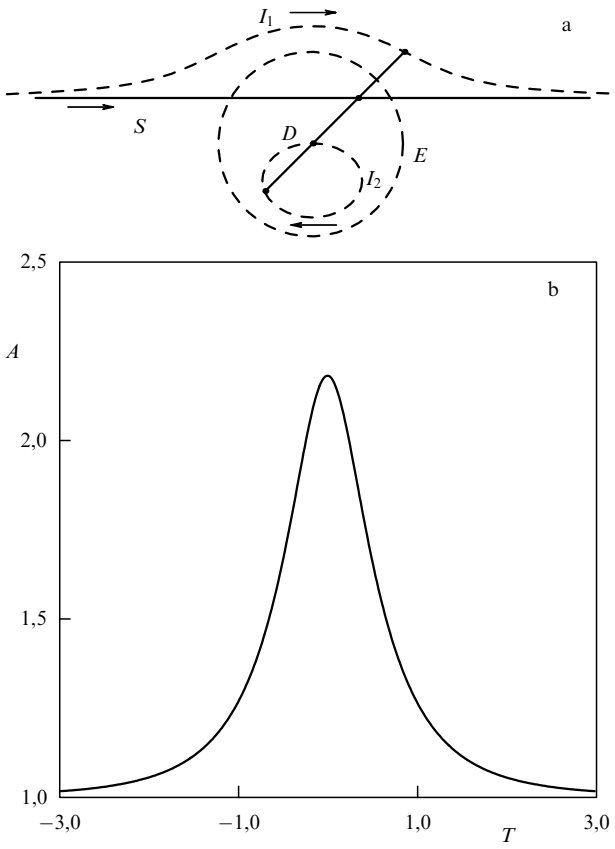

Figure 3. (a) Motion of a source and its images which are formed by a point gravitational lens. The straight line motion of a source is considered. The directions of motions of the source and images are shown by arrows. (b) Typical dependence of the amplification factor on time (in units $T_0/2$).

According to these expressions, we draw the trajectories of the visible motions of these two images [$I_1(t)$ and $I_2(t)$] on the celestial sphere. The trajectories are shown by dashed lines in Fig. 3a. The direction of motion of the source S is shown by the arrow. The direction of motion of the image I_1 coincides with that of the source, but the motion of image I_2 is opposite relative to the motion of the source.

The auxiliary variable $u(t)$ introduced above is determined by the expression

$$u(t) = \sqrt{1 + \frac{4\theta_0^2}{\Omega^2 t^2 + \theta_p^2}},$$

therefore the total luminosity of the two images

$$I(t) = \frac{I_0\big(u(t) + u^{-1}(t)\big)}{2}$$

is a symmetrical function of time with respect to $t = 0$ (Fig. 3b).

If the source S lies on the boundary of the Einstein–Chwolson cone [$\theta(t) = \theta_0$], then we have $A = 1.34$. Note, that the total time of crossing the Einstein–Chwolson cone T_0 is

$$T_0 = 2\,\frac{\sqrt{\theta_0^2 - \theta_p^2}}{\Omega}\,.$$

Sometimes the microlensing time is defined as a half of T_0. If we suppose that $D_d < D_{ds}$, then

$$T_0 = 3.5 \text{ months} \sqrt{\frac{M}{M_\odot}\,\frac{D_d}{10 \text{ kpc}}}\,\frac{300 \text{ km s}^{-1}}{v}\,,$$

where v is the perpendicular component of the velocity of a dark body.

We will give numerical estimations for parameters of the microlensing effect. If the distance between a dark body and the Sun is ~ 10 kpc, then the angular size of the Einstein–Chwolson cone of the dark body with a solar mass is equal to $\sim 0.001''$ or the linear size of the Einstein–Chwolson cone is equal to about 10 astronomical units. If we suppose that the perpendicular component of the velocity of a dark body is equal to ~ 300 km s^{-1} (that is a typical stellar velocity in the Galaxy), then a typical time of crossing the Einstein–Chwolson cone is about 3.5 months. The luminosity of the source S changes with time.

For observations of an extragalactic gravitational lens a typical time for changes of the light curve is very long ($\sim 10^5$ years) for direct observations. Therefore, extragalactic gravitational lenses are discovered and observed by resolving different optical components (images) since typical angular distances between images are several angular seconds because of the great mass of the gravitational lens. If the gravitational lens is a galaxy cluster then the angular distances between images may be several minutes. For the identification of gravitational lenses, observers compare typical features and spectra of different images. It is clear that one cannot resolve different components during microlensing but it is possible to obtain and analyse a light curve in different spectral bands.

2. Gravitational lens equation

Let us consider gravitational lenses with arbitrary density distributions, i.e. the gravitational lens equation in the general form.

For the case of a spherically symmetric distribution, the light motion is on the plane that is determined by three points: the observer, the source and the gravitational lens. Both light rays emitted by a point source and coming to the observer form images lying in the plane. For the case of an arbitrary mass distribution the trajectories may be non-planar. For the explanation of the formation of images we again consider the figure of the light motion in the field of a gravitational lens and introduce two auxiliary planes: the source plane, drawn via the source and perpendicular to the straight line connecting the observer and the barycenter (the center of mass) of the gravitational lens, and the lens plane, drawn via the gravitational lens and perpendicular to the same line (Fig. 4). These two planes coincide with the celestial plane for an Earth observer. The line connecting the observer and the barycenter of the gravitational lens is projected as a point on the celestial sphere. We suppose that this point is the origin of the coordinates on the plane.

We approximate the trajectory of a light ray by a broken straight line (the approximation is correct for weak gravitational fields) and the break is the gravitational lens plane. For this case the photon trajectory is determined by the sum of two vectors, one of which connects the light source with the break point, the second vector connects the break point with

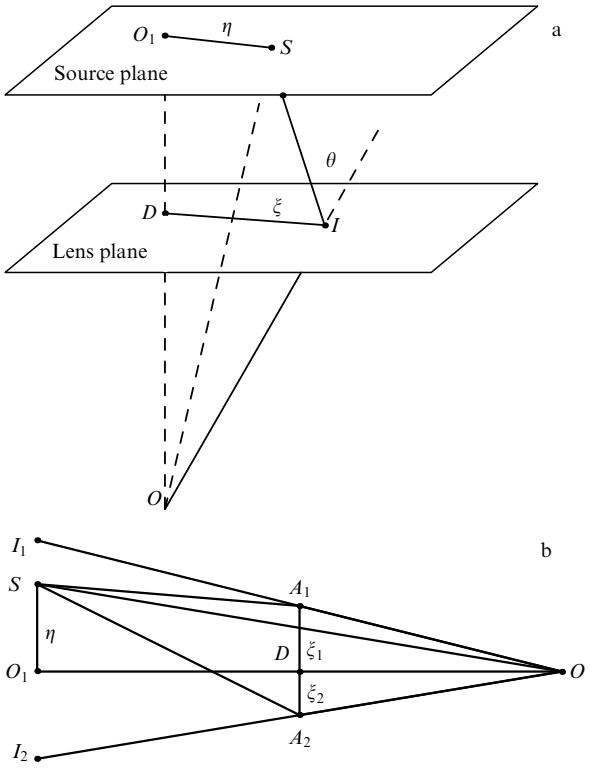

Figure 4. (a) Geometry of a gravitational lens. (b) Light rays illustrating the geometry of the gravitational lens equation.

the observer. So, the sum of the vectors is the vector drawn from the light source to the observer, the difference of the vectors determines the deflection angle in the gravitational field of the lens. Therefore, the absolute value of the sum is the distance between the light source and the observer, but the vector sum of the transverse components determines the gravitational lens equation.

We introduce a 2-dimensional vector $\boldsymbol{\eta}$, lying in the source plane. This vector shows the source position on the celestial sphere. We introduce a 2-dimensional vector $\boldsymbol{\xi}$, lying in the lens plane. This vector shows the positions of the images on the celestial sphere with respect to the barycenter. The enlargement of the light ray trajectory in 3-dimensional space is characterized by the tangent vector $\mathbf{u}$. For a derivation of the gravitational lens equation, it is necessary to find a simple geometrical relation between two straight lines, one of which starts from the source, and another one hits the observer. Both lines are an approximation of the light trajectory. The lines intersect at the lens plane. The unit tangent vector for the lines is the tangent vector for the photon trajectory. Under the approximation chosen the vector is constant and has a break at the point of intersection of the lines. The difference of the vectors belongs to the lens plane, so the difference is isomorphic to the 2-dimensional vector which is denoted as $\boldsymbol{\Theta}$. The projection of the light ray trajectories is determined by the vector sum of the vector projections reduced onto one plane (for example, the source plane). The reducing factor connecting the 2-dimensional vectors on the lens plane and the 2-dimensional vectors on the source plane is the ratio of the distance between the observer and the lens and the distance between the observer and the light source.

If we consider a non-planar light ray trajectory, then we obtain the gravitational lens equation in the general form:

$$\boldsymbol{\eta} = \frac{D_s}{D_d}\,\boldsymbol{\xi} - D_{ds}\boldsymbol{\Theta}(\boldsymbol{\xi})\,, \tag{11}$$

where $\boldsymbol{\Theta}(\boldsymbol{\xi})$ is the function describing the deflection of the light ray in the gravitational field of an auxiliary planar density distribution, and $\boldsymbol{\xi}$ is the 2-dimensional impact parameter. This function is expressed through the gravitational potential of the gravitational lens as

$$\boldsymbol{\Theta} = \frac{2}{c^2}\int_{-\infty}^{\infty} \boldsymbol{\nabla}\varphi\,\mathrm{d}l\,,$$

where ∇ is the 2-dimensional gradient operator in the celestial plane, but l is the affine parameter along the light ray trajectory.

We rewrite the equation using a 2-dimensional density distribution $[\Sigma(\boldsymbol{\xi})]$,

$$\boldsymbol{\Theta} = \frac{4G}{c^2}\int \mathrm{d}^2\xi'\,\Sigma(\boldsymbol{\xi}')\frac{\boldsymbol{\xi}'-\boldsymbol{\xi}}{|\boldsymbol{\xi}'-\boldsymbol{\xi}|^2}\,.$$

We write the gravitational lens equation using the normalization of angle variables on the Einstein – Chwolson angle [12], namely using the following variables $\mathbf{x} = \boldsymbol{\xi}/\xi_0$, $\mathbf{y} = D_s\boldsymbol{\eta}/(\xi_0 D_d)$, $\boldsymbol{\alpha} = \boldsymbol{\Theta}D/\xi_0$, where

$$\xi_0 = \sqrt{\frac{4GM}{c^2}\,\frac{(D_s - D_d)D_d}{D_s}}$$

is the Einstein – Chwolson radius with length dimensionality.

Therefore, the gravitational lens equation has the following form

$$\mathbf{y} = \mathbf{x} - \boldsymbol{\alpha}(\mathbf{x})\,. \tag{12}$$

The change of the solid angle during the transformation from the source to the image characterizes the magnification factor of the gravitational lens [10]. So, if the solid angle $\Delta\Omega_0$ corresponds to the source and the solid angle $\Delta\Omega$ corresponds to the images then the magnification factor will be

$$A = \frac{\Delta\Omega}{\Delta\Omega_0} = \left|\det\frac{\mathrm{d}\mathbf{y}}{\mathrm{d}\mathbf{x}}\right|^{-1}, \tag{13}$$

where $\mathbf{y}$ are the normalized coordinates of the source, and $\mathbf{x}$ are the normalized coordinates of the images.

The vectors $\boldsymbol{\alpha}$ and $\mathbf{x}$ are collinear for a spherically symmetric mass density distribution of a gravitational lens. The vectors may be non-collinear for an arbitrary mass density distribution, therefore, the number of images may change. There are an odd number of different images for the general case (for a smooth gravitational potential), but there are an even number of different images in a special degenerate case (as in a spherically symmetric Schwarzschild lens or a lens having a non-smooth gravitational potential) [11, 12, 9].

There is a single point in the source plane for a spherically symmetric lens formed by a point mass, for which the amplification factor is infinite. Let us consider the inverse mapping with respect to the gravitational lens mapping. The inverse mapping of the single point on the source plane determines the circumference and the circumference dia-

meter is equal to the Einstein – Chwolson cone diameter. The inverse mapping is not single-valued because the unique point is mapped onto the circumference. The gravitational lens mapping transforms the circumference into a point and is single-valued. The single-valuedness of the gravitational lens mapping and the absence of the single-valuedness of the inverse mapping are the general properties of the gravitational lens equation for the general case. Let us consider a set of points on the lens plane: the set is defined by vanishing the Jacobian for the gravitational lens mapping and forms a curve which is called a critical curve. The transform of the critical curve onto the source plane is called a caustic curve. The Jacobian (13) of the reverse mapping is infinite on the caustic curve, therefore the amplification factor is also infinite on the caustic curve.

Let us consider the following elementary case of the general situation. Namely we add together the monopole field of a point mass and the gravitational field of another point mass located at a distance $\mathbf{r}_2$ from the primary point mass. So, the gravitational lens potential has the following form

$$\varphi(\mathbf{r}) = \frac{GM}{r} + \frac{Gm}{|\mathbf{r}-\mathbf{r}_2|}\,.$$

Therefore, in the gravitational field of the system of fixed gravity points the deflection angle of a light ray is approximately equal to

$$\boldsymbol{\Theta}(\xi) = \frac{4GM}{c^2}\,\frac{\xi}{\xi^2} + \frac{4Gm}{c^2}\,\frac{\xi-\xi_2}{|\xi-\xi_2|^2}\,,$$

where ξ and ξ_2 are variables of length dimensionality, ξ is the light ray impact parameter with respect to the primary point mass, and ξ_2 is the lens plane projection of the distance between the points. One can choose the coordinates in the following way: the position of the second point mass is defined by the expression $\xi_2 = (a, 0)$.

Light motion in the gravitational field of two fixed gravity points and the respective gravitational lens equation are very complicated [13]. We simplify the expression for the deflection angle $\boldsymbol{\Theta}(\xi)$ as far as possible for the analysis of major optical effects of the formation of images, their intensities etc. For this simplification we decompose $\boldsymbol{\Theta}(\xi)$ into a Taylor series with respect to ξ, leaving terms up to the first order in ξ inclusively:

$$\boldsymbol{\Theta}(\xi) = \frac{2r_g\xi}{\xi^2} - \mu\,\frac{2r_g\xi_2}{\xi_2^2} + \mu\,\frac{2r_g\xi}{\xi_2^2} - \mu\,\frac{4r_g\xi_2(\xi_2\xi)}{\xi_2^4}\,,$$

where μ is the mass ratio. We write the gravitational lens equation for the case

$$\boldsymbol{\eta} = \frac{D_s}{D_d}\,\xi - 2r_g D_{ds}\,\frac{\xi}{\xi^2} + \mu D_{ds}\,\frac{2r_g\xi_2}{\xi_2^2} + \mu D_{ds}\,\frac{2r_g\xi}{\xi_2^2} - \mu D_{ds}\,\frac{4r_g\xi_2(\xi_2\xi)}{\xi_2^4}\,.$$

We have added a second fixed point mass. In spite of its apparent simplicity, the gravitational lens equation became more complicated. First, the constant shift $\mu D_{ds} 2r_g\xi_2/\xi_2^2$ appeared. Second, the vector ξ_2 appeared, and if the real position of the light source is characterized by the vector $\boldsymbol{\eta}$, then the visible image position characterized by the vector ξ is shifted and does not lie on the line connecting the gravitational lens center and the light source as in the case of a spherically symmetric gravitational field.

We also introduce the following variables

$$\mathbf{y} = \frac{\boldsymbol{\eta}}{R_\mathrm{E}}\,\frac{D_d}{D_s} + \mu\,\frac{D_{ds}D_d}{R_\mathrm{E}D_s}\,\frac{2r_g\xi_2}{\xi_2^2} \quad\text{and}\quad \mathbf{x} = \frac{\xi}{R_\mathrm{E}}\,,$$

which are normalized on the Einstein – Chwolson radius $R_\mathrm{E}^2 = 4GMD_{ds}D_d/(c^2D_s)$ and respective distances. Thus, the gravitational lens equation (the relation between $\mathbf{y}$ and $\mathbf{x}$) has the following form:

$$\mathbf{y} = \mathbf{x} - \frac{\mathbf{x}}{|x|^2} + \gamma\begin{pmatrix}1 & 0\\ 0 & -1\end{pmatrix}\mathbf{x}\,,$$

where $\gamma = \mu(R_\mathrm{E}/a)^2$ is a parameter characterizing the action of the second mass on the light ray. To obtain a simpler form of the gravitational lens equation we change variables again

$$\mathbf{X} = \mathbf{x}\sqrt{1+\gamma}\,, \qquad \mathbf{Y} = \frac{\mathbf{y}}{\sqrt{1+\gamma}}\,. \tag{14}$$

We rewrite the gravitational lens equation using these variables. The equation looks more compact and clear now, and has the following form:

$$\mathbf{Y} = \begin{pmatrix}1 & 0\\ 0 & \Lambda\end{pmatrix}\mathbf{X} - \frac{\mathbf{X}}{|\mathbf{X}|^2}\,, \tag{15}$$

where

$$\Lambda = \frac{1-\gamma}{1+\gamma}\,.$$

The amplification factor A is equal to the inverse of the determinant (the inverse of the Jacobian of the gravitational lens mapping):

$$A = \left|\frac{\partial\mathbf{y}}{\partial\mathbf{x}}\right|^{-1}\,,$$

but the critical curves for the gravitational lens (the geometric locus on the lens plane, where the amplification factor is equal to infinity) and caustic curves (the geometric locus on the source plane, where the amplification factor is equal to infinity) are determined from the condition of vanishing determinant, namely

$$\det A = \det\frac{\partial\mathbf{Y}}{\partial\mathbf{X}} = 0\,.$$

We rewrite the condition for the components $\mathbf{X}$ in the explicit form:

$$\Lambda(X_1^2 + X_2^2)^2 + (\Lambda - 1)(X_1^2 - X_2^2) - 1 = 0\,. \tag{16}$$

These curves are called Cassini ovals [14]. This condition looks clearer in polar coordinates on the lens plane. We introduce the following notation for polar coordinates:

$$X_1 = \rho\cos\phi\,, \qquad X_2 = \rho\sin\phi\,.$$

Using the coordinates ρ, ϕ we rewrite the equation for Cassini ovals:

$$\Lambda\rho^4 + (\Lambda - 1)\rho^2\cos 2\phi - 1 = 0\,.$$

We have the following solution

$$\rho^2 = 1 + \lambda \sin^2 \phi \,, \tag{17}$$

for small $\lambda = 1 - \Lambda$. We see from this solution that the curve is an oval extended slightly along the axis OX_2. More exactly, the oval size along the axis OX_1 is equal to 1, the oval size along the axis OX_2 is equal to $1 + \lambda$.

If we use the gravitational lens mapping then the map of the oval onto the source plane will form a caustic curve. To obtain the mapping equation we substitute the equation of the Cassini oval into the gravitational lens equation and obtain

$$Y_1 = \lambda \cos^3 \phi \,, \qquad Y_2 = -\lambda \sin^3 \phi \,. \tag{18}$$

So, the critical curve (Cassini oval) is close to a unit circle, but the caustic curve is an astroid in the approximation used.

If we suppose that one point mass is much greater than the other ($m_2 \ll m_1$), and the major semiaxis is equal to the Einstein – Chwolson radius $a = R_E$, we will have $\lambda = 2m_2/m_1$. The caustic curve (the astroid) for such a case is shown in Fig. 5. If we use the normalized variables **X** the Einstein – Chwolson radius will be equal to unity, but the transverse caustic size will be m_2/m_1 times smaller.

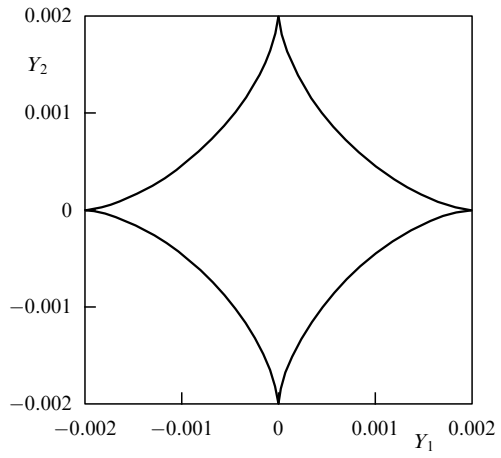

Figure 5. Caustic curve for the case of two point masses when one of the masses is much greater than the other ($\mu = 0.001$, $a = R_E$).

3. Dark matter problem

Searches for gravitational microlenses are connected closely with the cosmological dark matter problem which is one of the most important in modern physics and astrophysics. In consequence of the doubtless importance of the problem we briefly set forth its main points.

3.1 Basic points

Let us discuss the basic points of the dark matter problem (one can find a brief discussion of the problem in the article by Doroshkevich [15] or in the book by Dolgov et al. [16]). The modern discussion of the problem is in the reviews by Carr [17], Turner [18] and in the fundamental monograph of Peebles [19], where there is a detailed analysis of the problem and a very interesting historical introduction. The connection of the dark matter problem with microlensing is discussed in the review by Ferlet [20].

We recall that the parameter Ω is very often used in cosmology for the density [16]. We shall use this parameter too. We recall its definition

$$\Omega = \frac{\rho}{\rho_c} \,, \qquad \rho_c = \frac{3H_0^2}{8\pi G} = 2 \times 10^{-29} h^{-2} \text{ g cm}^{-3} \,, \tag{19}$$

where G is the gravity constant, H_0 is the Hubble constant, ρ_c is the critical constant,

$$h = \frac{H_0}{100 \text{ km s}^{-1} \text{ Mpc}} \,.$$

Comparison of the density parameter Ω and unity yields a very important criterion because in the framework of the Friedmann models the Universe has different topologies depending on the parameter Ω. If $\Omega > 1$ ($\rho > \rho_c$), the Universe is closed in 3-dimensional space and after the observable present expansion it will collapse. If $\Omega \leqslant 1$, the Universe is open and the expansion will be eternal. The case $\rho = \rho_c$ corresponds to a spatially flat Universe with normal Euclidean geometry. With the consideration of more non-trivial topologies of the Universe, cosmologists have concluded that the connection between Ω and the Universe topology may be more complicated than the connection for Friedmann models. However, the comparison of Ω and unity yields important information showing how much greater (or smaller respectively) is the kinetic energy of our Universe than its potential energy.

Visible matter is distributed hierarchically. It is possible to distinguish several scales which characterize the visible matter distribution. We disregard small scales and consider only galaxies and galactic clusters. The hierarchy of the dark matter distribution is characterized similarly to the usual astronomical hierarchy of scales. Below we will be interested only in distributions of dark matter on typical galactic scales.

Before a discussion of the dark matter in our Galaxy we will briefly recall the structure and distribution of the visible matter in the Galaxy.

Our Solar System, nearby stars and the background of faint unresolvable stars, the so-called Milky Way, belong to the great star system which is called our Galaxy. About 150 billions stars, interstellar gas and dust belong to the Galaxy. The stars form a flat subsystem of the Galaxy or the so-called disk component. It is like a giant discus. Its diameter is ~ 30 kpc, and its depth is ~ 5 kpc. The Sun is located at ~ 10 kpc from the Galactic center.

Astronomers determined the shape of the Galaxy having found the distribution of stars in space, or the visible matter in the Galaxy. The determination of the star distribution represents the most interesting subject of investigations but the discussion leads far away from the subject under consideration. It is natural to suppose that the gravitational field distribution corresponds to the distribution of visible stars. But observations do not confirm this assumption. Most researchers have no doubts of the basic physical laws, therefore it is necessary to introduce the concept of dark (or invisible) matter. Oort first pointed out the dark matter problem using observations of star velocities and the density distribution in the direction perpendicular to the Galactic disk [21]. He found that the disk density is about $0.1 M_\odot \text{ pc}^{-3}$, which is much greater than the density estimated of observable visible stars. Let us introduce the following (formal) definition. Dark matter does not radiate photons

(in any spectral band) or radiates so few that the photons are not detectable by direct observations. The Galactic component consisting of the dark matter is called the halo of our Galaxy. Soon after Oort's discovery Zwicky found the presence of dark matter in galactic clusters [36] and after that it became obvious that the dark matter problem is universal and peculiar not only to our Galaxy, but to the Universe on the whole. The nature of dark matter has remained a subject of discussions for a long time.

Stars of most galaxies are involved in rotational motion around their centers. One can consider stars as test particles moving around the mean center of the galaxy. Since stars move in the gravitational field of the galaxy, for a system of particles moving in the gravitational potential $1/r$ the virial theorem for a star moving on a circular orbit is valid:

$$\frac{GM(r)m}{r^2} = \frac{v^2(r)m}{r} ,$$

where $v(r)$ is the star velocity, that is a measurable variable, r is the distance from the Galactic center, and m is the star mass (our test particle). So, using the virial equation, one can calculate the density distribution $M(r)$ for the galaxy. Star velocities (or velocities of gas clouds) are measured using observations of Doppler shift of spectral lines. The rotation curve of a typical spiral galaxy is shown in Fig. 6. The solid line corresponds to the observable velocity distribution on the galactic radius, the dashed line corresponds to the velocity distribution calculated on the visible mass of the galaxy. It can be seen from Fig. 6 that an invisible mass must exist to satisfy the observable distribution of velocities. The invisible mass must be distributed much more uniformly in the galaxy in contrast to the visible matter which is concentrated usually to the galactic center.

A deviation of the observable rotation curve from the rotation curve corresponding to the visible matter is also observed in our Galaxy. So, our Sun rotates around the Galactic center with a speed of 220 km s^{-1} at a distance of about 10 kpc from the center. In other words, it takes our Sun 225 millions years to revolve around the Galactic center. The parameters are typical for galaxies of *Sc* type. The Sun is at the distance which approximately coincides with the distance corresponding to the maximal value of the rotation curve. For large scales, for example, 20 kpc $< r <$ 100 kpc the rotation curve is flat (confirmed by observations in the optical and radio bands [22–24]). The rotation curve is determined for scales of about 100 kpc using observations of dynamics of globular clusters and dwarf clusters, which are satellites of our Galaxy [25, 26].

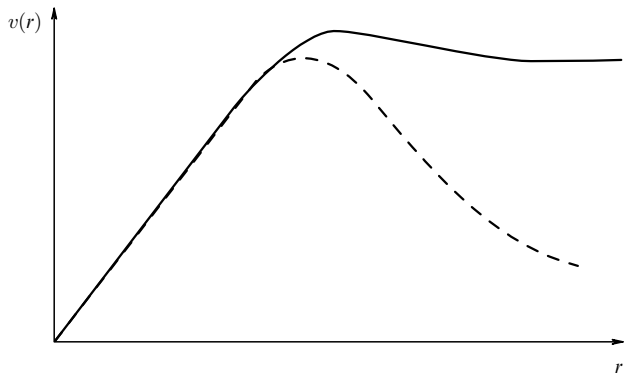

Figure 6. Typical example of a galactic rotation curve.

Now the hypothesis of the existence of dark matter in our Galaxy is not disputed usually but the amount of dark matter and its distribution over Galactic components is still an open problem. So, using observations of F dwarf stars and K-giants, Bahcall et al. [27] concluded that the hypothesis of the absence of dark matter can be accepted at a confidence level of 14%, and the most probable density of dark matter is about $0.15 M_\odot$ pc^{-3}, so the corresponding dark matter density is 53% greater than the visible matter density.

The best evidence for the existence of dark matter in spiral galaxies are the rotation curves of spirals, or the rotation velocity dependence on the galactocentric coordinate R. So, one can measure the density profile $\rho(R)$ [17]. In the opinion of Rubin et al. [22], an important feature of the existence of dark matter is the observational fact that the rotation curve shows a linear growth for small R and is approximately constant for great R. Therefore, we conclude that the mass inside a ball with radius R increases approximately as R, or much faster than the mass of visible stars. One can suppose that spiral galaxies have much dust, which influences the opacity, therefore a much smaller number of stars could be observed, but apparently the probability of this effect is negligibly small [28, 29].

The existence of a Galactic halo whose radius is greater than 30 kpc follows from investigations of the dynamics of globular clusters, but using investigations of the dynamics of the Local Group of galaxies it is possible to conclude that the halo radius is about 70 kpc [30]. However, one can conclude using observations of satellite galaxies that spiral galaxies have halos whose radii are about 200 kpc [31]. So, coming from an analysis of flat rotation curves [33] and the dynamics of satellite galaxies [32] it is possible to assume the existence of dark matter in galaxies.

Dark matter detection attempts in elliptic and dwarf galaxies are discussed in the review by Carr [17]. In particular, there are reports about the existence of a dark matter halo in dwarf spheroidal galaxies [34, 35].

The measurement of velocity dispersion demonstrates the existence of dark matter in small groups of galaxies and in rich clusters of galaxies, and the dark matter density may be at least in 10 times greater than the density of visible matter formed by stars and gas in rich clusters of galaxies [36, 37]. A similar estimate was also obtained using X-ray observations in clusters [37] and investigations of weak gravitational lensing [38].

Coming from observational data, one can assume that the dark matter density is characterized by the parameter $\Omega_d \sim 0.001$ in the disks of galaxies, $\Omega_d \sim 0.01-0.1$ in halo, $\Omega_d \sim 0.1-0.2$ in clusters of galaxies, while in the most popular inflationary cosmological theories the density must be critical ($\Omega = 1$), or more exactly as Linde noted [39], the density must be equal to the critical value to within a small correction $\delta\rho/\rho \sim 10^{-3}-10^{-4}$.

3.2 Baryonic or non-baryonic dark matter?

The problem of the origin of the dark matter is one of the most important in modern physics. One of the possibilities considered is the baryonic dark matter model, in other words, one can assume that the dark matter is formed from ordinary baryonic matter (protons and neutrons).

There is an important restriction on the total number of baryons in the Universe, obtained from the observational

data on the abundances of light elements (D, ^{3}He, ^{4}He, ^{7}Li) and predictions based on the theory of primordial nucleosynthesis. If we introduce the following dimensionless variable $\Omega_b = \rho_b/\rho_c$, characterizing the average density of baryons ρ_b, then it is possible to write the restriction in the following form: $0.009 < \Omega_b < 0.14$ [40]. Since there are following restrictions on the density of visible matter $0.003 < \Omega_{lum} \lesssim 0.007$ [41], we therefore obtain from the inequalities that even if Ω_b is minimal it would be necessary to recognize the existence of the baryonic dark matter.

One can remark that the upper limit of the parameter Ω_b is consistent with the dark matter density on galactic scales $\Omega \gtrsim 0.1$ [42]. However, the dark matter density is characterized by the parameter $\Omega_{tot} > 0.2-0.3$ for scales greater than typical galactic cluster radii [44], but as we mentioned above the dark matter density must be $\Omega_{tot} \simeq 1$ in inflationary cosmological models, therefore the necessity of the existence of non-baryonic dark matter follows from the limit on the baryonic dark matter density $\Omega_b < 0.14$.

The discussion of different candidates (objects) which may form baryonic dark matter is presented in the reviews [45, 17]. The possibilities of laboratory detection of elementary particles forming non-baryonic dark matter such as axions, light neutrinos (having non-vanishing mass), weakly interacting massive particles (WIMP's), for example, neutralinos (we shall discuss below the possibility of detection of neutralino stars during microlensing) are considered in the review [46].

The attractive peculiarity of non-baryonic dark matter is that this matter is very important in the models where density perturbations originally arise in non-baryonic dark matter and after that baryons fall into the potential hole [47, 48, 42]. If we use these scenarios then the non-baryonic dark matter will be kept somewhere in the galaxies and apparently the halo is a 'natural' enough place where the non-baryonic dark matter can be kept.

As mentioned neutrinos with non-vanishing masses and neutralinos may be considered as candidates for elementary particles forming the non-baryonic dark matter [45–48].

Baryonic dark matter can be made up of brown dwarfs, because fragmentation can lead to the formation of objects formed of H and He, but the object mass is too low to provide thermonuclear fusion, or $m < m_{HB} \simeq 0{,}08\ M_\odot$, where m_{HB} is the minimum star mass for H burning to take place. The Jeans mass (or minimum mass) for which the gravitational forces of an isolated gas cloud fragment can be greater than the pressure forces and lead to star formation, is estimated as $4-7 \times 10^{-3}\ M_\odot$ [49, 50]. Objects having a mass of about $10^{-3} M_\odot$ are usually called Jupiters. Brown dwarfs could be observed in the infrared band. Their mass is estimated using observations of quasar microlensing. The possibility of determining the mass distribution of brown dwarfs is considered in paper [51].

A component of the baryonic dark matter may be formed by faint red stars (M-dwarfs). To define limits on the concentration of such stars Bahcall et al. found several stars using the Hubble Space Telescope (HST) and the deep Wide Field Camera (WFC2) [52]. The astronomers got images of the celestial sphere element with galactic coordinates $l = 241$, $b = -51$. The images cover 4.4 square arcmins and the exposure was 2.00 h in V' and 2.83 in I'. The field contains 5 stars (four from which are in the disk or the thick disk) with $2.0 < V - I < 3.0$ and no stars with $V - I > 3.0$ down to the magnitude limit $I < 25.3$. If the dark matter of our Galaxy was formed by main-sequence stars $M_I = 14$, they would be visible in the HST field to a distance of $d = 1.8$ kpc. Before the observations of Bahcall et al. [52] about $N = 65$ such stars were expected in the field (assuming a local halo density). Using the observations Bahcall et al. conclude that the faint red stars contribute $< 6\%$ of unseen matter of our Galaxy but M-dwarfs contribute at most 15% to the mass of the disk [52]. However, one can remark that 5 M-dwarfs form too small a sample to obtain a strong statistical estimate of the mass density distribution of faint stars. The results of Mao and Paczynski [53], which will be discussed below, may be an illustration of this statement.

Clouds of molecular hydrogen are also considered as an essential component of the baryonic dark matter in the Galactic halo [54, 55]. One can conclude that cold dense clouds of gas could provide an essential contribution to the baryonic dark matter [56]. Neutron stars may contribute to the baryonic dark matter, but probably the contribution is at most 1% of the dark matter in the halo [17].

The most widespread hypothesis concerning the character of gravitational microlenses assumes that they are compact faint stars such as brown or red dwarfs [57, 58]. However, it is possible to consider a dark matter model of our Galaxy where dark matter is formed from a mixture of baryonic and non-baryonic dark matter and the parameters of the model are to be made consistent with microlensing data [59].

3.3 Dark matter in halos

The assumption about the existence of dark matter is 'natural' enough since more than 90%, and probably even 99% of the matter in the Universe is invisible or emits too little electromagnetic radiation to be observable in the electromagnetic band [42].

The existence of dark matter halos surrounding visible galaxies could be one of the possible solutions (probably not a unique solution) of the dark matter problem [60]. In this case halo densities fall as r^{-2} with the galactocentric coordinate r, as long as the rotation curves stay flat. Usually it is assumed that a spherically symmetric halo density is modeled by the following expression [42]:

$$\rho^H(r) = \rho_0^H \frac{R_0^2 + a^2}{r^2 + a^2}\,, \tag{20}$$

where a is the halo core radius, which is typically a few kpc. For our Galaxy, taking R_0 as the solar galactocentric distance, ρ_0^H is the local halo density in Eqn (20). The estimate for the solar galactocentric distance is $R_0 = 8.5$ kpc, but the local halo density is estimated as $\rho_0^H \simeq 10^{-2} M_\odot/\mathrm{pc}^3$ [61, 62, 59].

If we assume that the Milky Way circular speed $v_c \simeq 220$ km s^{-1} stays constant up to a galactocentric distance r_{max}, the total mass of the Galaxy within that radius results

$$M_{tot} \simeq \frac{v_c^2 r_{max}}{G} \simeq 5.6 \times 10^{11} \left(\frac{v_c}{220\ \mathrm{km\ s^{-1}}}\right)^2 \frac{r_{max}}{50\ \mathrm{kpc}}\, M_\odot\,, \tag{21}$$

which is an order larger than the disk mass if $r_{max} > 50$ kpc, and hence should mainly be due to the halo.

However, the profile and extent of the Galactic halo and other components of our Galaxy are not well known, which is partly due to the poor knowledge of rotation curves. The

rotation curve has been measured only up ~ 20 kpc for our Galaxy and the curve is determined with essential uncertainties [30]. There is also an uncertainty in the halo density in the inner region of the Galaxy which is related to the imprecise knowledge of the contribution to the rotation curve coming from the Galactic disk. For example, there are maximum disk models which lead to small halo mass inside the solar galactocentric radius [63].

It is necessary to remark that ellipticity is also a poorly known parameter, for instance our Galaxy may not be axisymmetric and may be tilted with respect to the disk plane [42]. Associated with the density uncertainties, there is also an uncertainty in the motion of the halo constituents. The simplest assumption that is usually adopted is that the halo objects move with isotropic velocities having a Maxwellian distribution with a constant (space independent) one-dimensional velocity dispersion σ^2, which is related to the circular speed $\sigma = v_c/\sqrt{2} \simeq 155$ km s^{-1} [42]. The halo model (isothermal sphere model) is known to lead to a density profile falling as r^{-2} at large radii. There are more complicated models of the halo. For example, Evans proposed a self-consistent halo density distribution in an elliptical halo for either a rising or declining rotation curve [43].

4. Components of our Galaxy

Since gravitational lensing is a very useful instrument for investigating the density distribution of our Galaxy, one may wish to recall the basic information about its structure and main components. A detailed and compact presentation of the information is in the article by Suchkov [64]. Some parameters of the subsystems of our Galaxy given in that article were offered by Einasto's group. They slightly differ from those which we will use below. There is much more detailed information about our Galaxy in the monograph by Marochnik and Suchkov [65].

Most of the visible stars in our Galaxy lie in the disk, generally assumed to be double exponential in galactocentric cylindrical coordinates (R, z)

$$\rho^D(R,z) = \rho_0^D \exp\left(-\frac{R-R_0}{h_R} - \frac{|z|}{h_z}\right), \tag{22}$$

where ρ_0^D is the local disk density, $h_R \simeq 3.5$ kpc is the disk scale length [62] (estimates of h_R vary over a wide range from 1.8 to 6 kpc [66]), h_z is the scale height which is $\sim$100 pc for very young stars and gas, and $\sim$325 pc for the older disk stars [62]. Paczynski et al. noted that there are some indications that at distances larger than ~ 3 kpc towards the Galactic center the disk star density falls below what would follow from Eqn (22) [67], suggesting that the scale decreases with decreasing R [66], or that the disk is actually 'hollow' ($\rho^D \simeq 0$ for $R < 2-4$ kpc) [42]. It is clear that Eqn (22) does not describe the existence of a spiral structure which is probably responsible for an excess in the star counts at distances ~ 2 kpc from the Sun (Sagitarius arm) in the direction of the Galactic center [42].

The disk is formed by the rotation of its stars $v_{\rm rot}^D \simeq 220$ km s^{-1}. The velocity dispersion $(\sigma^D)^2$ is small: $\sigma^D \simeq 20$ km s^{-1} locally [42], at smaller R [68].

The disk column density could be estimated in several ways, for example, $\Sigma_0^D(|z| < 1.1 \text{ kpc}) = (48 \pm 9) M_\odot/\text{pc}^2$ [71] or $\Sigma_0^D(|z| < 1.1 \text{ kpc}) = (54 \pm 8) M_\odot/\text{pc}^2$ [72, 27], thus the estimates are very close. Therefore, one can conclude that the disk does not contain an essential mass of dark matter. The statement is consistent with the observable local distribution of main sequence stars [73, 70]; these stars have been observed almost down to the hydrogen burning limit. The distribution is approximately flat below $m \simeq 0.4 M_\odot$, so that the extrapolation of the curve below $m_{\rm HB}$ does not hint at a significant contribution to the disk mass coming from brown dwarfs.

If we consider the upper limit for the disk column density within ± 1.1 kpc of the value $70 M_\odot/\text{pc}^2$ and subtract from it the disk column density of known matter this will allow a maximum dark contribution to the thin disk density of $\Sigma_0^D \simeq 30\ M_\odot/\text{pc}^2$.

Note, that the total mass associated with the disk, in terms of the local column density Σ_0, and if the scale length is assumed to be 3.5 kpc, is (upon integration of Eqn (22) [42])

$$M^{\rm D} = 4.4 \times 10^{10} M_\odot \left(\frac{\Sigma_0}{50 M_\odot \text{pc}^{-2}}\right). \tag{23}$$

The galactic halo (spheroid) is a galactic component formed by stars which are observed both looking at high latitudes far above the disk and locally by studying high velocity stars which cannot be bound to the disk [42]. The halo is formed of old metal poor stars, probably of protogalactic origin with a little rotation, supported by a large velocity dispersion $\sigma^{\rm S} \simeq 120$ km s^{-1} km s^{-1} and a density falling as $r^{-3.5}$. This is consistent with the expectation $\sigma = v_c/\sqrt{n}$ for an isotropic component with density falling as r^{-n} in a potential leading to a constant rotation velocity [74]. Probably there are some deviations from sphericity in the spheroid density and from isotropy in the velocity distribution [75–77].

The local density in luminous spheroid stars, i.e. those more massive than $m_{\rm HB} \simeq 0.08 M_\odot$ was estimated by Bahcall et al. to be $\rho_0^{\rm S}(m > m_{\rm HB}) \simeq 10^{-4} M_\odot/\text{pc}^3$ [78]. Therefore, the distribution of luminous spheroid stars weakly influences the dynamics of our Galaxy. However, dynamical models of our Galaxy in which the same spheroid population accounts for the dynamic and photometric observations in the inner Galaxy suggested that the spheroid mass should be much larger with $\rho_0^{\rm S} \simeq 10^{-3} M_\odot/\text{pc}^3$ [61, 79]. The difference between the density of luminous stars and the dynamical estimate of the density may be due to the presence of large numbers of stars with masses below $m_{\rm HB}$, as seems to be suggested by the measured mass function of spheroid field stars, which rises as $(\text{d}n/\text{d}m \propto m^{-4.5\pm1.2})$ below $0.5 M_\odot$ and down to the lowest measured value of $0.14 M_\odot$ [80]. However, low mass stars may be observed (in principle) during microlensing [81].

The inner component 1–2 kpc of our Galaxy is usually referred to as the Galactic bulge [42]. We remark that Einasto et al. suggested a much smaller size ~ 0.2 kpc for the bulge [64]. Sometimes the bulge is considered as just the inner part of the halo mentioned above [61, 83], and at other times, instead, as a new unrelated central component [78]. We note that the origin of the bulge is a complicated problem and we are far from its final solution.

5. Optical depth and microlensing rate

Now let us consider the microlensing probability [144]. The parameter is expressed in standard terms used in astronomy and is called the optical depth for microlensing. Let us suppose that there are a lot of gravitational microlenses on the celestial sphere. The part of the celestial sphere which is

covered by Einstein–Chwolson circles, defines the probability of microlensing. We assume that all lenses have the same mass M. Let us consider a thin shell at a distance D_d from an observer and with depth ΔD_d. Thus, there is one lens on average in a shell surface having an area $\pi R_M^2 = M/(\rho \Delta D_d)$, where ρ is the average density of lenses in the volume $\pi R_M^2 \Delta D_d$. Each lens has a cross-section $\pi \xi_0^2$, where ξ_0 in the Einstein – Chwolson radius for a gravitational lens mass M. The shell contribution to the optical depth is determined by the following expression

$$\Delta\tau = \frac{\pi\xi_0^2}{\pi R_M^2} = \left[\frac{4\pi G\rho}{c^2}\,\frac{D_d(D_s - D_d)}{D_s}\right]\Delta D_d\,.$$

Therefore, the total optical depth due to the influence of all gravitational lenses between a source and an observer may be calculated as

$$\tau = \int_0^{D_s} \frac{4\pi G\rho}{c^2}\,\frac{D_d(D_s - D_d)}{D_s}\,\mathrm{d}D_d = \frac{4\pi G}{c^2}\,D_s^2 \int_0^1 \rho(x)x(1-x)\,\mathrm{d}x\,,$$

where $x = D_d/D_s$. We note that the optical depth τ depends on the total mass of all lenses, but does not depend on the masses of separate lenses M. If the mass density distribution is constant then we obtain

$$\tau = \frac{2\pi}{3}\,\frac{G\rho}{c^2}\,D_s^2\,. \tag{24}$$

If we consider a self-gravitational system of gravitational lenses then it will be possible to obtain a rough but very clear estimate of the gravitational depth [57]. Let us assume that the distance from an observer to a source D_s is approximately equal to the size of a galaxy formed of gravitational lenses. Therefore, we obtain from the virial theorem the expression for the velocity dispersion V^2, the density ρ and the size D_s:

$$\frac{GM_{\mathrm{tot}}}{D_s} \approx \frac{G\rho D_s^3}{D_s} \approx V^2\,. \tag{25}$$

We obtain the following estimate $\tau \approx V^2/c^2$ from Eqns (24) and (25). The precise estimate for the optical depth may be obtained by substitution of the mass density distribution along the line of sight into integral (24).

When the observations are performed in a given direction, one has to take into account, especially for bulge observations, that sources may be distributed along the line of sight. In this case, one has to perform an average over the source distribution to obtain the actual optical depth [84]

$$\tau = \frac{1}{N_s}\int \mathrm{d}D_s\,\frac{\mathrm{d}n_s}{\mathrm{d}D_s}\,\tau(D_s)\,, \tag{26}$$

where the normalization factor is $N_s = \int \mathrm{d}D_s\,\mathrm{d}n_s/\mathrm{d}D_s$, and $\mathrm{d}n_s/\mathrm{d}D_s$ describes the number density profile of detectable sources along the line of sight. For observations in the Galactic bulge it can be parameterized as $\mathrm{d}n_s/\mathrm{d}D_s \propto \rho_s D_s^{2-2\beta}$ [42]. The factor D_s^2 describes the change of the volume element with distance. The parameter β arises because the observations are magnitude limited and the fraction of sources with luminosities larger than L is assumed to scale as $L^{-\beta}$, implying that the fraction of stars which remain detectable behave as $D_s^{-2\beta}$. Thus, we obtain

$$\tau = \frac{\int \mathrm{d}D_s\,D_s^{2(1-\beta)}\rho_s\tau(D_s)}{\int \mathrm{d}D_s\,D_s^{2(1-\beta)}\rho_s}\,. \tag{27}$$

Zhao et al. (1995a) estimate the parameter β in Baade's Window as $\beta = 1 \pm 0.5$ so Roulet and Mollerach suppose that $\beta = 1$ for analysis of microlensing in the Galactic bulge [166, 42].

Similarly to the approach of Mao and Paczynski, we will try to estimate the number of expected microlensing events N, assuming the number of events n_s is observed during the time interval Δt [53]. We will consider only the microlensing events which have a maximum amplification factor greater than $3/\sqrt{5}$, i.e. their dimensionless impact parameter is greater than unity.

Let us consider the simplest case when all the lenses have the same mass M and the same velocity V. We also assume that the velocity vector is described by a random isotropic distribution, the source at a distance D_s is stationary and the lens concentration is statistically homogeneous. The model is analysed in detail in paper [53]. The main results of their analysis are also discussed in the book [9].

The typical time scale for microlensing is defined by the following expression

$$t_0 = \frac{\theta_0}{\dot{r}} = \frac{\xi_0}{V_{\mathrm{t}}} = \frac{\xi_0}{V\sin i}\,, \tag{28}$$

where i is the angle between the lens velocity vector and the line of sight, $V_{\mathrm{t}} = V\sin i$ is the transverse velocity of the lens. If all microlensing events have the same time scales, then the total number of microlensing events during the time interval Δt, will be determined as

$$N = \frac{2}{\pi}\,n_s\tau\,\frac{\Delta t}{t_0} \tag{29}$$

where $t_0 = \mathrm{const}$, the factor $2/\pi$ is the Einstein–Chwolson diameter divided by its area (in dimensionless units), τ is the optical depth, n_s is the number of observed sources [53].

6. Non-symmetrical light curves

One of the basic criteria for microlensing event identification is the symmetry of the light curve. If we consider a spherically symmetric gravitational field for a lens, a point source and a short duration microlensing event then the statement about the symmetry of a light curve will be a strong mathematical conclusion, but if we consider a more complicated distribution of gravitational field lens or an extensive light source then some deviations of symmetric light curves may be observed and (or) the microlensing effect may be chromatic. In this section we will consider these effects which increase the level of information extraction from microlensing observations. We will start from a discussion of the weak distortion of a light curve, connected with the parallax effect.

6.1 Parallax effect

A long time ago Refsdal expressed the idea of performing simultaneous observations of a microlensing event from ground and space-based telescopes as a way to obtain the constraints of the distances and masses of the lensing objects [106]. Grieger et al. proposed measuring the parallax effect on

lensed quasars in order to gain information about the relative transverse velocities involved [107]. Gould proposed using the same ideas for searches towards the LMC and the bulge [108, 73]. Parallax observations allow us to determine the projection of the Einstein–Chwolson radius $R_{\rm E}$ onto the observer's plane, i.e. the so-called reduced Einstein–Chwolson radius [42]

$$\tilde{R}_{\rm E} = R_{\rm E}\,\frac{D_s}{D_{ds}}\,. \tag{30}$$

Using the parameter together with event duration, one can obtain the reduced velocity modulus

$$\tilde{v} := \frac{\tilde{R}_{\rm E}}{T} = v^{\perp}\,\frac{D_s}{D_{ds}}\,, \tag{31}$$

which is a kinematic variable independent of the lens mass.

The main point for measuring the parallax is the following [42]: if the lensing event is monitored from two telescopes with no relative motion between them, the position of the lens with respect to the line of sight to the star from the Earth telescope in units of the Einstein–Chwolson radius can be expressed as

$$\mathbf{u}(t) = \frac{\mathbf{b}}{R_{\rm E}} + \frac{\mathbf{v}^{\perp}}{R_{\rm E}}\,(t - t_0)\,, \tag{32}$$

and that from the satellite telescope as

$$\mathbf{u}'(t) = \frac{\mathbf{b}'}{R_{\rm E}} + \frac{\mathbf{v}^{\perp}}{R_{\rm E}}\,(t - t_0')\,, \tag{33}$$

with $\mathbf{b}\cdot\mathbf{v}^{\perp} = 0 = \mathbf{b}'\cdot\mathbf{v}^{\perp}$. From the observed light curves $A(u(t))$ and $A(u(t'))$, the values t_0, t_0', $u_{\rm min} = l/R_{\rm E}$, $u'_{\rm min} = l'/R_{\rm E}$ and T can be obtained. Denoting by $\mathbf{r}$ the projection orthogonal to the line of sight of the satellite position with respect to the Earth, $\mathbf{u}(t)$ and $\mathbf{u}'(t)$ can be related through [42]:

$$\mathbf{u}'(t) = \mathbf{u}(t) + \frac{\mathbf{r}}{\tilde{R}_{\rm E}}\,. \tag{34}$$

Combining Eqns (32)–(34), we obtain $\Delta\mathbf{u} = \mathbf{u}' - \mathbf{u}$, so that

$$\Delta\mathbf{u} = \frac{\mathbf{r}}{\tilde{R}_{\rm E}} = \mathbf{u}'_{\rm min} - \mathbf{u}_{\rm min} - \frac{\mathbf{v}^{\perp}}{R_{\rm E}}\,(t_0' - t_0)\,. \tag{35}$$

From an analysis of light curves one can determine the moduli of $u_{\rm min}$, $u'_{\rm min}$ and $v^{\perp}/R_{\rm E} = T^{-1}$, but not the directions. Therefore, the variable $\Delta u := |\Delta\mathbf{u}|$ can be determined up to a two-fold degeneracy (the variable depends on choosing the sign in the right hand side of the following expression):

$$\Delta u_{\pm} = \sqrt{(u'_{\rm min} \pm u_{\rm min})^2 + \frac{(t_0' - t_0)^2}{T^2}}\,. \tag{36}$$

Hence, one can determine two possible values of the reduced Einstein–Chwolson radius

$$\tilde{R}_{\rm E\pm} = \frac{r}{\Delta u_{\pm}} \tag{37}$$

and the modulus of the reduced velocity

$$\tilde{v}_{\pm} = \frac{r}{T\Delta u_{\pm}}\,. \tag{38}$$

Thus, we obtain the resulting components of $\tilde{\mathbf{v}}_{\pm}$ in the directions parallel and perpendicular to $\mathbf{r}$, which are

$$\tilde{v}_{\pm}^{\parallel} = \frac{r(t_0' - t_0)}{T^2(\Delta u_{\pm})^2}\,, \qquad |\tilde{v}_{\pm}^{\perp}| = \frac{r(u'_{\rm min} \pm u_{\rm min})}{T(\Delta u_{\pm})^2} \tag{39}$$

respectively. There are various ideas for lifting the degeneracy. In particular, Gould suggested performing observations from a second satellite. If the positions of the two satellites with respect to the Earth $\mathbf{r}$ and $\mathbf{r}'$ are not parallel the sign of $\tilde{v}$ can also be determined [73].

The parallax effect can be measured from the Earth (without satellite observations), but now it is possible to detect the effect only for events of very long duration for which the Earth's motion leads to a significant correction to the light curve.

Alcock et al. detected an event of this kind in their first season of bulge observations by the MACHO collaboration. Their longest event, lasting 110 days, presents a significantly asymmetric, but still achromatic, light curve, as is expected to be the case when the approximation of constant velocities of the lens, the source and the observer does not hold [109].

The correction of the orbital motion of the Earth significantly improves the fit to the observed light curve, which is shown in Fig. 7 and presented originally in the article by Bennett et al. [110]. Bennett et al. [110] presented a theoretical model where they use the reduced velocity $\tilde{v} = 75 \pm 5$ km s^{-1}, and the velocity should be pointing at an angle of 28° with respect to the direction of increasing longitudes, supporting the interpretation that the lens is in the disk. The best fitting values obtained for the lens parameters are $D_d = 1.7^{+1.1}_{-0.7}$ kpc and $m = 1.3^{+1.3}_{-0.6} M_{\odot}$, so one can conclude that the lens is probably an old white dwarf or a neutron star†. Thus, the observation of parallax in one event allows one to achieve a better knowledge of the lens characteristics than in other events. However, parallax measurements can be performed from the ground only for a

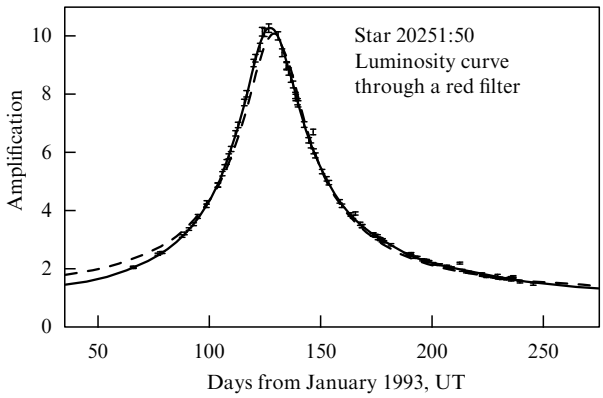

Figure 7. Parallax effect detection by the MACHO collaboration in microlensing searches. The dashed line is the fit without taking into account the Earth's motion while the solid line does include it. The horizontal axis corresponds to time (in days), the vertical axis corresponds to the amplification factor [42].

† However, Roulet and Mollerach remark [42] that Bennett et al. [110] neglect the possible rotational motion of the source. If the source were moving in the direction of the Sun's rotation, e.g. if it were a disk star (or a rotating bulge star), then the value D_d would be larger and hence the lens mass smaller.

small fraction of the events, those with very long durations. Since the majority of events have T between 10 and 50 days, the value $\tilde{v}$ cannot be obtained from the ground and it is necessary to use a space based telescope [42].

6.2 Proper motions of lenses

For some particular microlensing events it may become possible to obtain information on the Einstein – Chwolson angle $\theta_{\rm E}$ defined as mentioned above,

$$\theta_{\rm E} = \frac{R_{\rm E}}{D_d} \,. \tag{40}$$

Hence we know the 'proper motion' [42], which is defined as

$$\mu := \frac{\theta_{\rm E}}{T} = \frac{v^{\perp}}{D_d} \,, \tag{41}$$

which is the angular velocity of the lens relative to the source. We also note that the proper motion is a kinematic variable, independent of the lens mass while $\theta_{\rm E}$ is independent of the lens velocity [42].

The simplest situation in which the proper motion can be measured is when the radial extension of the source R_s, projected onto the lens plane is comparable to the impact parameter of the lens trajectory b, or equivalently that the angle subtended by R_s ($\theta_s = R_s/D_s$) is larger than the angle subtended by b ($\beta = b/D_l$). In this case the point-like source approximation breaks down and it is necessary to use the circle-like source approximation [111] and the light curve of the microlensing event is modified allowing the proper motion of the lens to be extracted from it [73, 111, 112, 42].

The amplification factor of a circular source with uniform brightness lensed by a point-like mass was given in paper [111]. If $\beta \gg \theta_s$, then the light curve is almost identical to that of a point-like source, but if β is comparable with or smaller than θ_s, the light curve is significantly different. When $\beta > \theta_s/2$, the peak amplification factor is larger than that for a point-like source while when $\beta \ll \theta_s/2$, the maximal amplification factor is smaller than in the point-like case. Particularly, when the alignment is perfect ($\beta = 0$), the amplification factor does not diverge as the point-like source expression indicates, but instead reaches a maximum value (assuming a uniform surface brightness)

$$A_{\max} = \sqrt{1 + \frac{16GmD_{ds}D_s}{R_s^2 c^2 D_d}} \,. \tag{42}$$

Comparing the peak amplification factor with that expected from the point-like source light curve determined by a fit to the measured amplifications far from the peak, one can obtain the ratio of the impact parameter to the projected source radius [42]

$$Z = \frac{bD_s}{R_s D_d} = \frac{\beta}{\theta_s} \,. \tag{43}$$

One can determine the parameter $u_{\min} = b/R_{\rm E}$ from the expression for the amplification factor of a point source. Now it is possible to determine the angle

$$\theta_{\rm E} = \frac{b}{u_{\min} D_d} = \frac{ZR_s}{u_{\min} D_s} \tag{44}$$

from the source radius R_s and the distance D_s. Thus, the 'proper motion' is

$$\mu = \frac{\theta_{\rm E}}{T} = \frac{ZR_s}{Tu_{\min} D_s} \,. \tag{45}$$

Since this effect appears when the lens transits the surface of the source, it is only expected to be present in some high amplification events for which large values of amplification factor correspond. If all events with $u_{\min} < 1$ (i.e. those with $\beta < \theta_{\rm E}$) can be detected, since μ can be measured only for those with $\beta < \theta_s$, one has that the fraction of events with measurable proper motions is $\simeq \theta_s/\theta_{\rm E} \propto 1/\sqrt{m}$ [42]. For LMC observations, if one assumes $m = 0.1 M_{\odot}$, this fraction is $\simeq 10^{-3}$ for Galactic lenses and 10^{-2} for lenses in the LMC.

The measurement of the proper motion for LMC events would allow one to distinguish between LMC and Galactic lenses. LMC lenses would give rise to proper motions $\mu \leqslant 2$ km (s kpc)$^{-1}$. Larger values would indicate a Galactic lensing population and could also help to distinguish among the different scenarios proposed. For bulge observations, somewhat shorter proper motions are expected for bulge lenses than for disk ones but a clear distinction between the two populations is not possible using observations of proper motions [42].

6.3 Binary sources

We have a very simple model in the case in which both the source and the lens are single objects. However, it is well-known that most stars are components of binary (or multiple) systems. Abt estimated that the fraction of binary stars is between 60% and 100% [113]. We will consider the microlensing model for the case of binary lenses below. Let us discuss the changes of the microlensing model for the case of binary sources.

Griest and Hu [114]; Sazhin and Cherepashchuk [115 – 118] analysed in detail the case of possible microlensing events of binary sources. In the case of binary sources the light curve differs from the light curve for a single source. For example, if both sources are lensed the light curve may have two peaks or be strongly asymmetric. In the case when one star is lensed the light curve may be symmetric, but it has a deviation from the light curve of a single (lensed) source connected with the influence of the luminosity of the companion if these two stars cannot be resolved. We remark that if the dimmer star is lensed, the shape of the light curve may be significantly affected. If these two stars have different colors, then the important signature of achromaticity may be lost.

By analysis of the motions of different types and considering different distributions of the orbital period and the ratio of masses Griest and Hu concluded that a small fraction $\sim 10-20\%$ of microlensing events of binary sources may be distinguished from microlensing of single sources (for LMC observations), and only about $2-5\%$ of microlensing events have unusual light curve or light curve changes greater than 0.1^m [114]. If we take into account binary sources then the total microlensing rate will increase by $\sim 5-15\%$.

If we consider two point-like sources with luminosities L_1 and L_2, then the amplification factor will have the standard expression through the parameter which is the normalized distance from the lens to the line of sight, $A_1(t) = A(u_1(t))$ and $A_2(t) = A(u_2(t))$. Then the total amplification factor is

$$A = \frac{A_1 L_1 + A_2 L_2}{L_1 + L_2} = A_1(1 - r) + A_2 r \,, \tag{46}$$

where the parameter

$$r = \frac{L_2}{L_1 + L_2} \tag{47}$$

is the deviation according to Griest and Hu [114]†. One can suppose without loss of generality that $L_2 \leqslant L_1$ and $0 \leqslant r \leqslant 0.5$. In the case when both stars have different colors, there are two different deviations of luminosities for each color. For example, if we consider star 1 with visible luminosity L_{1V} in the V-band and luminosity L_{1B} in the B-band, the visible star magnitude is connected with the luminosity as $V = -2.5 \log L_{1V} + \text{const}$. One can write the same expression for the B-band. Thus, it is possible to determine

$$r_V = \frac{L_{2V}}{L_{1V} + L_{2V}} = \left[1 + 10^{(V_2 - V_1)/2,5}\right]^{-1} \tag{48}$$

and

$$r_B = \frac{L_{2B}}{L_{1B} + L_{2B}} = \left[1 + 10^{(B_2 - B_1)/2,5}\right]^{-1} . \tag{49}$$

If the color index of star 1 is $B_1 - V_1$, the color index of star 2 is $B_2 - V_2$, then the color index of a binary system is

$$(B - V)_{tot} = -2.5 \log\left[(L_{1V} + L_{2V})(L_{1B} + L_{2B})\right] . \tag{50}$$

The luminosity of the binary system components changes during microlensing as follows:

$$\begin{aligned} &L_{1V} \to L_{1V} A_1 , \quad L_{1B} \to L_{1B} A_1 , \\ &L_{2V} \to L_{2V} A_2 , \quad L_{2B} \to L_{2B} A_2 , \end{aligned} \tag{51}$$

so the total color change is $\Delta(B - V) = 2.5 \log A_{B-V}$, where

$$A_{B-V} = \frac{(1 - r_V) A_1 + r_V A_2}{(1 - r_B) A_1 + r_B A_2} . \tag{52}$$

We note that if both stars have the same color then $r_V = r_B$ and $\Delta(B - V) = 0$. Similarly if both stars have the same amplification factor $A_1 = A_2$ then $\Delta(B - V) = 0$. Griest and Hu presented a microlensing event classification depending on the deviation r and the normalized distances between components d and described typical light curves for events of different types; a set of examples and corresponding figures are presented in paper [114] (also see the papers of Sazhin and Cherepashchuk [115, 116]).

6.4 Binary lenses and planets

Let us consider a set of point lenses [57], located between an observer and a source at the same distance D_d from the observer. The distance between the observer and the source is equal to D_s. We assume that lens number i has mass M_i and its location is determined by the vector (X_i, Y_i) in the lens plane. A light ray crossing the lens plane at the point (X, Y) is at a distance R_i from lens i

$$R_i = \left[(X - X_i)^2 + (Y - Y_i)^2\right]^{1/2} . \tag{53}$$

† Griest and Hu noted about the MACHO experiment that astronomers are searching for light curves which correspond to a single source. So, the deviation parameter r characterizes the influence of the second companion on the light curve. Such microlensing events are called events with a deviation in the MACHO experiment [114].

Therefore, the contribution of lens i to the deflection angle is determined by the angle

$$\alpha_i = \frac{4GM_i}{R_i c^2} , \tag{54}$$

and its components are equal to

$$\alpha_{x,i} = \alpha_i \frac{X - X_i}{R_i} , \quad \alpha_{y,i} = \alpha_i \frac{Y - Y_i}{R_i} , \tag{55}$$

respectively. In this case as a result of the deflection due to influence of all masses the light ray crosses the source plane at the point (X_S, Y_S) and

$$\begin{aligned} X_S &= X \frac{D_s}{D_d} - \sum_i \alpha_{x,i} (D_s - D_d) , \\ Y_S &= Y \frac{D_s}{D_d} - \sum_i \alpha_{y,i} (D_s - D_d) . \end{aligned} \tag{56}$$

We note that the variables X, Y, X_i, Y_i, and R_i are measured in the lens plane but X_s and Y_s are measured in the source plane. So, we obtain from Eqns (54)–(56)

$$x_s = x - \frac{D_s - D_d}{D_s D_d} \sum_i \frac{4GM_i}{c^2} \frac{x - x_i}{r_i^2} , \tag{57}$$

$$y_s = y - \frac{D_s - D_d}{D_s D_d} \sum_i \frac{4GM_i}{c^2} \frac{y - y_i}{r_i^2} , \tag{58}$$

where the angles are determined as $x_s = X_S/D_s$, $y_s = Y_S/D_s$ and $x = X/D_d$, $y = Y/D_d$, $x_i = X_i/D_d$, $y_i = Y_i/D_d$, $r_i = R_i/D_d$. The dimensionless mass m_i is determined as

$$m_i = \frac{D_s - D_d}{D_s D_d} \frac{4GM_i}{c^2} . \tag{59}$$

So, one can write Eqns (57) and (58) in the following form:

$$x_s = x - \sum_i \frac{m_i (x - x_i)}{r_i^2} , \quad y_s = y - \sum_i \frac{m_i (y - y_i)}{r_i^2} . \tag{60}$$

From Eqns (60) one can find all possible images formed by a set of point masses lying in the same plane which is perpendicular to the line of sight. The gravitational lens system formed by point masses is analysed in detail in paper [94]. The system of two point lenses is analysed in paper [95] and there is a wide family of different caustic and critical curves for this case in the paper. Erdl and Schneider consider the most general statement of the problem for the analysis of the system of two point lenses. They analysed in particular the case when the lenses are in different planes which are orthogonal to the line of sight [96]. Witt and Petters obtained critical and caustic curves for the system with one point mass (or two point masses) in an external gravitational field with non-vanishing shear [97].

We restrict our consideration to the general case of a binary gravitational lens [98, 57]. In this case Eqns (60) have the following form:

$$x_s = x - \frac{m_1 (x - x_1)}{r_1^2} - \frac{m_2 (x - x_2)}{r_2^2} , \tag{61}$$

$$y_s = y - \frac{m_1 (y - y_1)}{r_1^2} - \frac{m_2 (y - y_2)}{r_2^2} . \tag{62}$$

It is customary to adopt $m_1 + m_2 = 1$. Thus, all the angles are expressed in Einstein – Chwolson angle units for a lens with unit mass. If we consider the case of a static binary lens, or, in other words, we neglect the orbital motion of the binary system, then there are three additional parameters: the mass ratio m_1/m_2, the distance between components of a binary system in Einstein – Chwolson radius units and the angle characterizing the source motion with respect to the line connecting the two masses in the celestial sphere. As Paczynski noted, the variety of possible light curves is surprising [57]. Mao and di Stefano developed the numerical code and using it one can obtain not only theoretical light curves for a binary lens system but the best theoretical model for the interpretation of observational data [99]. The code was used for the theoretical interpretation of two events which are connected with two binary lenses: OGLE #7 [89, 85, 57] and DUO #2 [100].

Some samples of light curves corresponding to source motions relative to the caustic curve of a binary lens are shown in Fig. 8a. The geometry of critical and caustic curves is presented in Fig. 8b. The binary system is formed by two identical point masses (drawn in Fig. 8b as two points): $M_1 = M_2 = 0.5M$. We assume that the distance between the lenses is equal to the Einstein – Chwolson radius corresponding to mass M (or the total mass of the binary system). The caustic curve is shown by a solid line. The closed curve shown by a dashed line in the lens plane is the critical curve. The source located on the caustic curve has its image on the critical curve. We recall that in the case when the source crosses the caustic curve two images appear or disappear on the critical curve represented by the dashed line. In the case when the source is outside the region bound by the caustic curve, there are three images, one outside the critical curve and two images inside the critical curve. Usually they are close to one of the two point masses. If the source is the region bound by the caustic curve then two additional images appear, one of which is inside and the other image outside the critical curve. Five sources shown by small circles with a radius equal to 0.05 Einstein–Chwolson radii are shown in Fig. 8b. The trajectories of the sources are shown by straight lines.

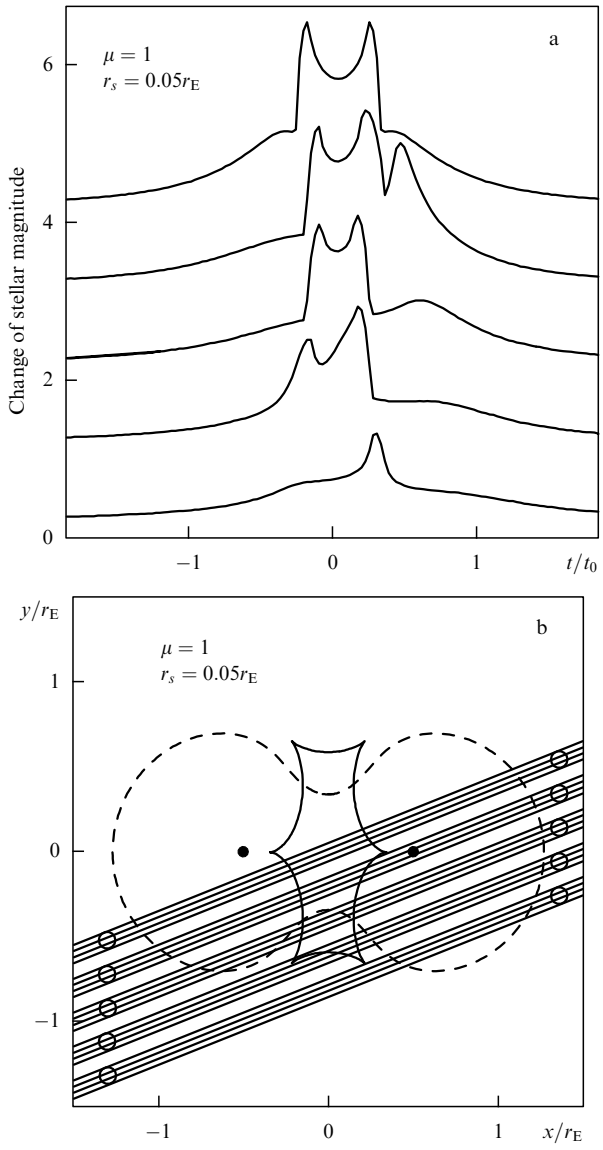

Figure 8. Five light curves as examples of microlensing by binary lenses (a) and the corresponding source trajectories (b). The top light curve here corresponds to the top trajectory. The peaks of the light curves correspond to caustic crossing by the source. (The light curves are shifted by one magnitude for clarity of illustration). Five identical sources are moving along the straight trajectories as marked. All sources have radii of $r_s = 0.05r_E$. (Figure from Ref. [57].)

It is clear that it is necessary to analyse a huge quantity of microlensing observations for planet discovery. Mao and Paczynski [98]; Gould and Loeb [101] showed that if all stars have Jupiter mass planets at a distance of several astronomical units then only a small fraction of all microlensing events will demonstrate a measurable deviation of the light curve. Therefore, if only a small fraction of all stars have Jupiter-like planets at distances of several astronomical units, then the fraction of all microlensing events which may be disturbed by giant planets is correspondingly reduced. Paczynski supposed that $\sim 5\%$ of all stars have planets with masses not smaller than Jupiter's mass at distances not greater than 5 astronomical units [57]. The duration of the most probable perturbation of the light curve is of the order of 1 day in this case, thus, it is necessary to carry out observations very often to have confidence that an event will not be missed.

Let us analyse the possibility of discovering a planet of Earth mass using the data of microlensing observations. The Earth's mass is about $3 \times 10^{-6} M_\odot$ and a typical star has a mass which is slightly less than that of the Sun [57]. So, we suppose that there is a ratio of masses for a fixed binary system of gravitational lenses: $M_2/M_1 = 10^{-5}$.

If we consider a single point object with a planet mass then the Einstein – Chwolson radius $r_{Ep} = r_E \times (M_2/M_1)^{1/2}$ will correspond to the planet. If the planet is not far from the star then the planet mass will perturb the light curve only over short length scale (or on a short time scale) and one can take into account the perturbation together with a long length (or long time) perturbation which is caused by the gravitational field of the star. An example of the (possible) influence of planets on the distortion of the light curve is shown in Fig. 9, where a microlensing event which is caused by the star and has a great amplification factor, is perturbed by eight planets with Earth mass [the planets are located along the trajectory of the source (the background star)]. One may note that the perturbation caused by each planet is practically independent of the perturbations caused by other planets. It is clear that such a model is fairly artificial but the analysis allows us to demonstrate the possible influence on microlensing of planets with Earth mass in a single figure. The dimensionless

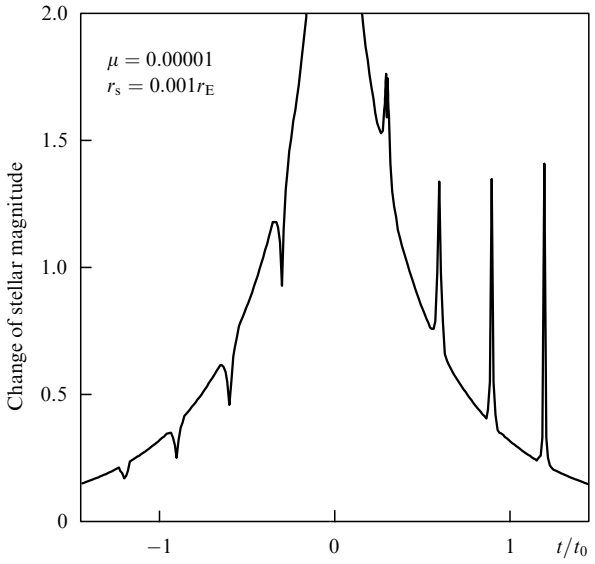

Figure 9. Variations of the amplification factor by a planetary system as a function of time. The system is formed by a star and eight planets, each with the mass fraction $\mu = 10^{-5}$, all located along a straight line. The source with a radius $r_S = 10^{-3} r_E$, moves along the line defined by the planets with an impact parameter equal to zero. The planets are located at these distances from the star: $r_p/r_E = 0.57$, 0.65, 0.74, 0.86, 1.16, 1.34, 1.55, 1.76 in the lens plane which corresponds to the disturbances in light variations at the times $t/t_0 = -1.2$, -0.9, -0.6, -0.3, 0.3, 0.6, 0.9, 1.2, as shown in the figure. Note, that planetary disturbances create local light minima for $r_p/r_E < 1$ $(t/t_0 < 0)$ and local maxima for $r_p/r_E > 1$ $(t/t_0 > 0)$. (Figure from Ref. [57].)

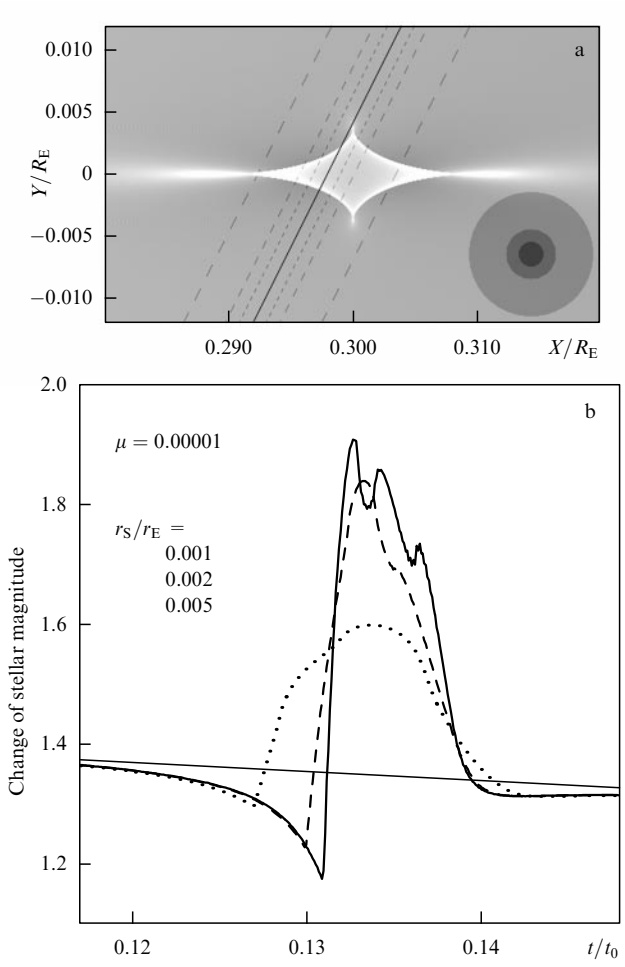

Figure 10. (a) Sample of the illumination pattern in the source plane formed by a planet with mass fraction $\mu = 10^{-5}$. The planet is located at the distance $r_p/r_E = 1.16$ from the star in the lens plane, which corresponds to $r_p/r_E = 0.03$ in the source plane. The centers of three circular sources are moving upwards along the solid straight line, with the dashed lines indicating the trajectories of the source edges. The source radii are $r_S/r_E = 0.001$, 0.002, 0.005, and their sizes are shown in the lower right corner. (b) Variations of the amplification factor as dependencies on time. The three light curves shown with thick solid, dashed and dotted lines are caused by an Earth-like planet with mass ratio $\mu = 10^{-5}$, and they correspond to the three sources with radii $r_S/r_E = 0.001$, 0.002, 0.005, respectively. The thin, slowly descending solid line corresponds to the fragment of the microlensing light curve in the absence of planetary disturbance. (Figure from Ref. [57].)

time t/t_0 is equal to the dimensionless coordinate characterizing the source position r_S/r_E, and both variables are connected with the planet's position through the following expression [57]: $t/t_0 = r_S/r_E = r_p/r_E - r_E/r_p$. If the planets are located not far from the star for $r_p/r_E < 1$, then a local minimum of the light curve (which is shown in Fig. 9) is formed. The effect is associated with reducing the brightness of the image which is closest to the gravitational lens on the celestial sphere. If the planets are located too far from the star for $r_p/r_E > 1$, then a local maximum (or double maximum) of the light curve is formed. The effect is associated with the splitting of image which is farthest from the lens and with enhancing the combined brightness [57]. If the planet is near the Einstein–Chwolson circumference or if $r_p \approx r_E$, the light curve is changed near the light curve peak because the celestial sphere area of one image is changed. We note that the light curve distortion is fairly significant for planets with Jupiter mass but is small for planets with Earth mass [98]. A detailed analysis of the possibility of planet discovery is presented in papers [102–105]. In particular, Bennett and Rhie showed that if a planet with Earth mass is from 1 to 4 astronomical units from a lens and if it is possible to detect a deviation of 4% from the light curve, then one can discover more than 2% of planets with Earth mass or more than 10% planets of 10 Earth masses [102].

The changes of the light curve for the idealized microlensing model are shown in Fig. 10b. We recall that the light curve shown in Fig. 9 corresponds to motion of the source along the X axis and the source radius is equal to $r_S/r_E = 0.001$. The event corresponds to a change of the amplification factor at the moment $t/t_0 = 0.3$ in Fig. 9, but different trajectories of the source are considered in the two cases. The source moves along the X axis for the light curve in Fig. 9, but the trajectory is inclined at an angle $\sim 64°$ relative to the axis X for the light curves in Fig. 10. The total time shown in Fig. 10b corresponds to ~ 10 hours, but the time $t_0 = 0$ corresponds to the light curve peak for microlensing by the star in the absence of a planet. The event corresponding to a planet's distortion of the microlensing lasts longer for the model shown in Fig. 9 than for the model shown in Fig. 10b, since the region of great values of the amplification factor is stretched strongly along the axis X. So, we note (following to Paczynski [57]), that the variety of possible light curves distorted by a planet is great.

6.5 Non-compact microlenses

The character of gravitational microlenses is unknown up to now although the most widespread hypothesis assumes that

they are compact dark bodies such as brown (or cold white) dwarfs. Nevertheless, they could be other objects, in particular, dark objects consisting of sypersymmetrical weakly interacting particles (neutralinos) as discussed in the papers of Gurevich et al. [122, 123, 48]. The authors show that neutralino stars may have been formed in the early stages of the evolution of the Universe and be stable over cosmological timescales.

The microlensing of a distant star by a neutralino star is considered in this section.

We consider microlensing in the framework of a rough model which is rather clear and we obtain analytical expressions for the results. Of course, a more exact model may be considered (see, for example, Ref. [123]); nevertheless, we think that the qualitative estimation of the effect has been considered correctly.

We approximate the density of mass distribution of a neutralino star in the form

$$\rho_{\mathrm{NeS}}(r) = \rho_0 \frac{a_0^2}{r^2}\,, \tag{63}$$

where r is the current value of the distance from the star's center, ρ_0 is the mass density of a neutralino star at a distance a_0 from the center, and a_0 is the radius of the neutralino star. The dependence is an approximation of the density distribution considered in the paper by Gurevich and Zybin [122]:

$$\rho_{\mathrm{NeS}}(r) = Kr^{-1,8}\,.$$

We introduce the following notation

$$R_0 = \frac{\pi\rho_0 a_0}{\Sigma_{cr}} = \frac{M}{a_0^2}\frac{2\pi GD}{c^2}\,, \qquad D = \frac{D_d D_{ds}}{D_s}\,, \tag{64}$$

where M is the microlens mass. Thus, we obtain the lens equation in a dimensionless form:

$$y = x - R_0\frac{x}{|x|}\,. \tag{65}$$

If we normalize the distances in the lens plane and in the source plane using R_0, namely if we introduce the variables $\hat{y} = y/R_0, \hat{x} = x/R_0$ then the lens equation has a quite clear form

$$\hat{y} = \hat{x} - \frac{\hat{x}}{|\hat{x}|}\,. \tag{66}$$

The symbol $\hat{}$ will not be written below. It is easy to see that the lens equation in a dimensionless form is the same as the lens equation for the model of galactic mass distribution corresponding to an isothermal sphere. We recall some results concerning the lens equation (66). First we will consider the solutions of the lens equation. Without loss of generality we may consider that $y > 0$. In the case when $y < 1$, the lens equation has two solutions $x_+ = y + 1$, $x_- = y - 1$. In the case when $y > 1$, there is only one root $x = y + 1$.

The circular source and its images are shown in Fig. 11 for different images between the source center and the gravitational lens center. We note that in the case of a non-compact lens the radial width of the images is larger than the width of images for the Schwarzschild microlens case (for small y by approximately 2 times).

Since for a spherically symmetric mass distribution of the gravitational lens we have the following expression for the

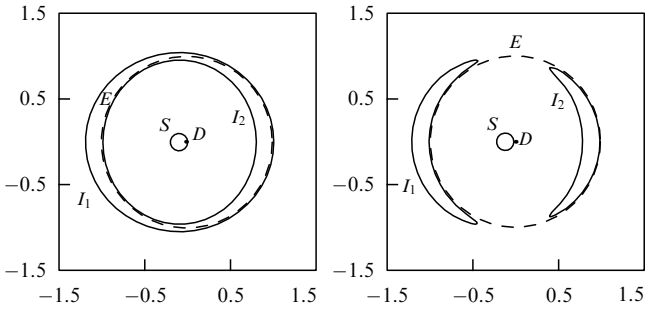

Figure 11. Boundary of a circular source S, which has two images I_1 and I_2. The dashed line shows the critical curve, namely the Einstein – Chwolson circumference. The source radius is $r = 0.1$, and the angular distances between the source center and the gravitational lens center are $d = 0.099$ (left panel) and $d = 0.11$ (right panel).

Jacobian:

$$\det A(\mathbf{x}) = 1 - \frac{1}{|x|}\,, \tag{67}$$

the amplification factor is equal to $A = |x|/(|x| - 1)$. So, if the critical curve is determined by the equation $|x| = 1$ (or the critical curve is a unit circle), the caustic curve degenerates into the point $y = 1$. It is not difficult to see how the sources are distorted by a gravitational lens. It is clear that the images are not distorted in the radial direction, but in the tangential direction they are expanded according to relation (67). We recall that there is a contraction of the images by two times for a Schwarzschild lens for $y \ll 1$ in the radial direction and there is the same expansion (as for a neutralino star) in the tangential direction, which is approximately equal to $1/y$. If we consider the case $y > 1$, then

$$A_P(y) = A(x_+) = \frac{y+1}{y} = 1 + \frac{1}{y}\,. \tag{68}$$

In the case $0 < y < 1$, we have

$$A(x_+) = \frac{|x_+|}{|x_+| - 1} = \frac{y+1}{y} = 1 + \frac{1}{y}\,, \tag{69}$$

$$A(x_-) = \frac{|x_-|}{|x_-| - 1} = \frac{y-1}{y}\,. \tag{70}$$

Since $A(x_-) < 0$, the total amplification factor is defined by the expression

$$A_P(y) = A(x_+) + |A(x_-)| = \frac{2}{y}\,. \tag{71}$$

Recall that in the case when the gravitational microlens is a point gravitating body (a Schwarzschild lens) then the amplification factor is determined by the following expression:

$$A_P(y) = \frac{y^2+2}{y\sqrt{y^2+4}}\,. \tag{72}$$

Thus, the difference between the amplification factor of a Schwarzschild lens and a neutralino star is an essential factor which distinguishes these objects.

We consider two asymptotes to show the difference between the amplification factors for these cases. First, we write $A_{\rm tot}$ for a neutralino star:

$$A(y)=\frac{2}{y} \quad \text{for} \quad y<1 \quad \text{and} \quad A(y)=1+\frac{1}{y} \quad \text{for} \quad y>1\,, \tag{73}$$

which are simultaneously precise equations. The similar expressions for the amplification produced by a compact body (Schwarzschild lens) are:

$$A(y)=\frac{1}{y} \quad \text{for} \quad y\ll 1 \quad \text{and} \quad A(y)=1+\frac{2}{y^4} \quad \text{for} \quad y\gg 1\,. \tag{74}$$

Thus, if we consider the case when the variable y (which is proportional to the minimal angular impact distance of a microlensing event) is the same for the neutralino star case and the compact body case then for the first case the light curve has higher maximum and wider wings and this fact may yield a test to distinguish the events.

We will discuss some possibilities for distinguishing these objects using observational data and the different dependencies of amplification factors on impact parameters for this case.

Light curve of a non-compact lens. We consider the amplification factor for different parameters R_0. We recall that the gravitational lens equation is correct for small values of the parameters y, x only. We consider the case when the light ray passes not only inside the non-compact body but also passes outside it. In that case the gravitational lens equation is

$$y=x-\frac{x}{|x|} \quad \text{for} \quad |x|\leqslant\frac{1}{R_0}\,,$$

$$y=x-\frac{1}{R_0}\frac{x}{|x|^2} \quad \text{for} \quad |x|>\frac{1}{R_0}\,. \tag{75}$$

We consider three different sets for the parameter R_0.

Case I. Let $1/R_0\geqslant 2$.

Case Ia. If $0<y<1$, then the gravitational lens equation has two solutions, both of which correspond to the values of the impact parameter that are smaller by absolute value than the size of the neutralino star, i.e. the corresponding light rays pass through the neutralino star. The solutions of the gravitational lens equation are (we assume that the axes are chosen so that $y>0$, as in all other cases which will be considered below) $x_+^{\rm NeS}=1+y$, $x_-^{\rm NeS}=y-1$. We recall that we have the following expressions for the amplification factor $A_+^{\rm NeS}=1+1/y$, $|A_-^{\rm NeS}|=1/y-1$. In this case the total magnification is determined by expression (71).

Case Ib. If $1\leqslant y\leqslant 1/R_0-1$, then the gravitational lens equation has one solution corresponding to the value of the impact parameter, which has a smaller absolute value than the radius of the neutralino star, i.e. the corresponding light ray passes through the neutralino star. Namely the solution of the gravitational lens equation is $x_+^{\rm NeS}=1+y$. The magnification corresponding to this solution is $A_+^{\rm NeS}$.

Case Ic. If $1/R_0-1\leqslant y$, then the gravitational lens equation has one solution corresponding to the value of the impact parameter, which has a greater absolute value than the size of the neutralino star i.e. the corresponding light ray passes outside the neutralino star. The solution is $x_+^{\rm S}=(y+\sqrt{y^2+4/R_0})/2$. The corresponding magnification is

$$A_+^{\rm S}=\frac{1}{4}\left(\frac{y}{\sqrt{y^2+4/R_0}}+\frac{\sqrt{y^2+4/R_0}}{y}+2\right).$$

Case II. Let $1<1/R_0<2$.

Case II a. If $0<y<1/R_0-1$, then the total magnification is determined by relation (71).

Case IIb. If $1/R_0-1\leqslant y\leqslant 1$, then the gravitational lens equation has two solutions. One of them corresponds to the impact parameter which has a greater absolute value than the size of the neutralino star, i.e. the corresponding light ray pass outside the neutralino star. This solution is

$$x_+^{\rm S}=\frac{y+\sqrt{y^2+4/R_0}}{2}\,.$$

The magnification factor corresponding to it is $A_+^{\rm S}$. The other solution corresponds to an impact parameter which has a smaller absolute value than the size of the neutralino star, i.e. the corresponding light ray passes inside the neutralino star. This solution of the gravitational lens equation is $x_-^{\rm NeS}=1-y$. The magnification factor corresponding to this solution is $A_-^{\rm NeS}$.

Case IIc. If $1<y$, then the gravitational lens equation has one solution corresponding to the impact parameter, which has a greater absolute value than the radius of the neutralino star, i.e. the corresponding light ray passes outside the neutralino star. The solution in this case is $x_+^{\rm S}$. The magnification corresponding to this solution is $A_+^{\rm S}$.

Case III. Let $0<1/R_0<1$.

Case III a. If $0<y<1-1/R_0$, the gravitational lens equation has two solutions, both of them corresponding to impact parameters, which have greater absolute values than the size of the neutralino star, i.e. the corresponding light rays pass outside the neutralino star. Namely there is a solution

$$x_+^{\rm S}=\frac{y+\sqrt{y^2+4/R_0}}{2}\,.$$

The corresponding magnification is $A_+^{\rm S}$. The other solution is also similar to the solution of the Schwarzschild lens equation

$$x_-^{\rm S}=\frac{y-\sqrt{y^2+4/R_0}}{2}\,.$$

The magnification corresponding to this solution is

$$|A_-^{\rm S}|=\frac{1}{4}\left(\frac{y}{\sqrt{y^2+4/R_0}}+\frac{\sqrt{y^2+4/R_0}}{y}-2\right).$$

Case IIIb. If $1/R_0-1\leqslant y\leqslant 1$, then the gravitational lens equation has two solutions, one of which corresponds to the impact parameter which has smaller absolute value than the radius of the neutralino star, i.e. the corresponding light ray passes outside the neutralino star. This solution of the gravitational lens equation is

$$x_+^{\rm S}=\frac{y+\sqrt{y^2+4/R_0}}{2}\,.$$

The magnification is $A_+^{\rm S}$. The other solution corresponds to the impact parameter which has smaller absolute value than the radius of the neutralino star, i.e. the corresponding light

ray passes through the neutralino star. This solution of the gravitational lens equation is

$$x_{-}^{\mathrm{NeS}} = 1 - y\,.$$

The magnification corresponding to this solution is A_{-}^{NeS}.

Case IIIc. If $y > 1$, then the gravitational lens equation has one solution which corresponds to the value of the impact parameter, which has a greater absolute value than the size of the neutralino star, i.e. the corresponding light ray passes outside the neutralino star. This solution is x_{+}^{S}. The magnification which corresponds to this solution is A_{+}^{S}.

So, the magnification of a non-compact body (neutralino star) has no difference from the amplification coefficient of the Schwarzschild lens only in case IIIa. In all other cases in principle one can distinguish these astronomical objects.

In Figure 12 the light curves for a non-compact body and a Schwarzschild lens for cases I – III are shown. One can note that the light curve for a non-compact body has a discontinuity in the case when the image is x_{+}, corresponding to an impact parameter which has an absolute value equal to the radius of the neutralino star. This is very easy to understand since the lens equation has a discontinuous derivative at this point, therefore the light curve also has a discontinuity for the general case. This is the result of two of our assumptions; the first one is that $a_0 \gg \xi$ and therefore $\Sigma(\xi) \approx 1/\xi$ (the factor $\arctan[(a_0^2 - \xi^2)^{1/2}/\xi]$ is considered to be equal to $\pi/2$). This assumption becomes rather rough for $\xi \approx a_0$. The second assumption is the approximation of a point source. It is clear that in this case if we suppose that one of the assumptions is incorrect then the light curve will be continuous for a non-compact object. Nevertheless, the model is rather clear, so we can investigate it in detail and thereby define the limits of its usage.

Thus, the magnification (the amplification factor) of a non-compact body (a neutralino star) coincides with the magnification of a Schwarzschild lens only in case IIIa (when case III holds and $y < 1 - 1/R_0$). In principle it is possible to distinguish these two objects in the other cases.

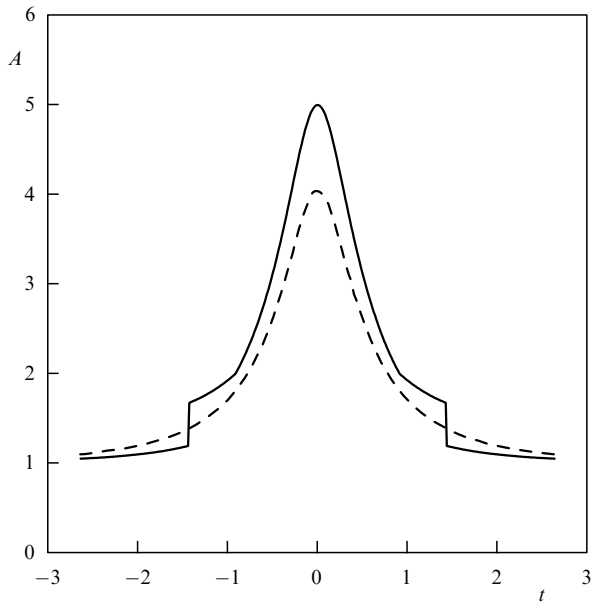

Figure 12. Light curve for a non-compact object (solid line) and for a Schwarzschild lens (dashed line) corresponding to $R_0 = 0.4$.

Let us consider case Ia. If the amplification factor is greater than 2, then $A = 2/y$. We suppose that the microlensing event is caused by a non-compact lens. If the amplification factor is greater than $2 (A_t > 2)$, then we have the following dependence of the amplification factor on the impact parameter $y_t = 2/A_t$. The maximal amplification factor corresponds to the minimal impact parameter y, or $y_{\min} = 2/A_{\max}$. Therefore, we have the following criterion to distinguish non-compact and compact lenses using the data of microlensing, namely it is necessary to check if $f = (y_t^2 - y_{\min}^2)^{1/2}$ is a linear function of time. We have $f(t) = (2/A_t^2 - 2/A_{\max}^2)^{1/2}$ in this case.

If the amplification factor is smaller than 2, we have case Ib and the following expression for the amplification factor on impact parameter $y_t = 1/(A_t - 1)$. It is clear that one can obtain an expression for the variable y_t which depends on A_t in case Ic, namely $y = 4/[R_0(z^2 - 1)]$, where $z = 2A_t - 1 + 2\sqrt{A_t(A_t - 1)}$.

One can check if the function $f(t)$ is a linear dependence on time. It is clear that if the microlensing event is caused by a Schwarzschild lens the dependence on time $f(t)$ is another.

In paper [124] the light curves of the OGLE project were analysed and it was shown that the two light curves are approximated much better in the framework of the non-compact lens model than in the framework of the Schwarzschild lens model. The first MACHO event was analysed in the paper of Gurevich et al. [48] and the authors showed that the event may be interpreted much better in the framework of the non-compact lens model in comparison with the standard model. Another interpretation of the light curve which corresponds to the first MACHO event was analysed in the paper [126]. The authors suppose that deviations of the observational data from the standard microlensing model are explained by the influence of the luminosity of an additional light source.

7. Source polarization during microlensing

In this section we consider the effect of partial polarization of a star's light during microlensing. In the previous sections we analysed only changes of the total luminosity, the light curve and its features. However, the light of any celestial object is characterized not only by the total luminosity since the star radiation is characterized more precisely by four Stokes parameters which describe the polarization. Changes of the source polarization have been observed, but nobody has observed the effect during microlensing. However, the polarization degree may give us important information about the motion of a lens and the background source. Therefore, the polarization effect is a very important point of the theoretical analysis of the microlensing effect.

It is known that scattering radiation in atmospheres of stars leads to polarization of the star's light. As was shown by Chandrasekhar [127] and Sobolev [128], radiation outgoing from a plane-parallel Rayleigh atmosphere is partially polarized and the direction of primary polarization of the electrical vector is perpendicular to the plane which is formed by the line of sight and the normal to the surface. Soon an increase of the polarization on approaching the edge of the disk was found on the Sun. The observation of this phenomenon for other stars excluding the case of mutual eclipse of components of binary systems requires an ability to resolve separate space elements on their disks and, hence, an application of methods of increasing the telescope angular

resolution. Ways to solve this problem using interferometers are suggested in papers [129, 130]. The method of observations during Lunar occultation of stars was considered by Bogdanov [131]. Speckle-interferometry methods are suggested in paper [132]. During normal observations of stars the total flux of radiation from the whole disk is registered which is non-polarized by virtue of the symmetry of the problem. The possibility of partial polarization of the total flux is connected with loss of symmetry, caused by fast rotation, tidal deformation of a star, the presence of hot spots, an asymmetric environment or a combination of these factors. It is obvious that the presence of a gravitational lens also destroys the symmetry of the problem. The amplification factor of a gravitational lens decreases non-linearly with the distance from its optical axis and consequently the contribution from the visible stellar-disk edge closest to the lens is enhanced in the total flux. The registered total flux should become partially polarized and the plane of polarization is always perpendicular to the line connecting the centers of the star's disk and the gravitational lens.

Let us consider the polarization of radiation scattered by the star's atmosphere. We introduce the intensities I_l, I_r as follows: I_l is the intensity lying in the plane of the line of sight and the normal to the surface, and I_r is the intensity in the plane perpendicular to it. We shall assume for simplicity that the lensing star has a plane parallel Rayleigh atmosphere. Therefore, one can express the intensity distribution with the approximate formula

$$I_r + I_l = I_0 + I_1\mu\,, \qquad I_r - I_l = u_0(1-\mu)\,, \tag{76}$$

where μ is the cosine of the angle between the line of sight and the normal to the star's surface. One can find more precise expressions for the intensities in papers [127, 133].

We choose a Cartesian coordinate system Oxy and direct the axis Ox along the major axis of the polaroid. Thus, the intensities I_R and I_L corresponding to a fixed point on the stellar disk are functions of the coordinates $r = \sqrt{x^2+y^2}$, $\varphi = \arcsin(x/\sqrt{x^2+y^2})$:

$$I_L(r,\varphi) = I_r(r)\sin^2\varphi + I_l(r)\cos^2\varphi\,, \tag{77}$$

$$I_R(r,\varphi) = I_l(r)\sin^2\varphi + I_r(r)\cos^2\varphi\,. \tag{78}$$

If distorting factors are absent then the radiation flux H_L which is observed through the polaroid L is the sum of intensities from all dish elements, namely

$$H_L = \int_0^{2\pi} \mathrm{d}\varphi \int_0^R I_L(r,\varphi) r\,\mathrm{d}r\,, \tag{79}$$

where R is the star's angular radius. The flux H_R for the polaroid R is determined by the following expression

$$H_R = \int_0^{2\pi} \mathrm{d}\varphi \int_0^R I_R(r,\varphi) r\,\mathrm{d}r\,. \tag{80}$$

The degree of polarization which is defined as

$$P = \frac{H_R - H_L}{H_R + H_L}\,,$$

is equal to zero from symmetry arguments.

Therefore, it is impossible to observe the effect of partial polarization on the stellar disks since the stellar disks are usually unresolvable, and the average polarization over the disk is exactly equal to zero. If the symmetry is broken then we have another situation. For example, we suppose that the stellar disk is partially eclipsed by a body which is located between the star and the observer. In this case the integral in Eqns (79), (80) is calculated only on part of the stellar disk, thus the symmetry is broken, the fluxes H_R, H_L may be unequal and the polarization may be non-vanishing.

There are several causes for the appearance of partial polarization during observations of an unresolvable stellar disk: an eclipse (for example, in the binary star system), hot spots on the stellar surface, tidal distortions of the stellar disks, etc. We consider another cause, namely a nonuniform dependence of the amplification factor of the source on the angular distance during the passage of light rays from the source near a gravitational microlens.

If there is a source amplification factor which is caused by the microlens then monochromatic radiation flux H_L, being observed through the polaroid L, is the sum of intensities from the disk elements multiplied by the amplification factor at the point in contrast to the previous case

$$H_L = \int_0^{2\pi} \mathrm{d}\varphi \int_0^R A(x,y) I_L(r,\varphi) r\,\mathrm{d}r\,. \tag{81}$$

Similarly, we obtain for the flux H_R observed through the polaroid R

$$H_R = \int_0^{2\pi} \mathrm{d}\varphi \int_0^R A(x,y) I_R(r,\varphi) r\,\mathrm{d}r\,. \tag{82}$$

Let us consider a simple case which is analysed analytically. If the spatial scale of changes of the amplification factor $A(x,y)$ is much greater than the star disk sizes then we expand the amplification factor into a Fourier series

$$A(x,y) = A(0,0) + \frac{\partial A}{\partial x}\,x + \frac{\partial A}{\partial y}\,y + \frac{\partial^2 A}{\partial x^2}\,x^2 + 2\,\frac{\partial^2 A}{\partial x\,\partial x}\,xy + \frac{\partial^2 A}{\partial y\,\partial y}\,y^2 + \ldots \tag{83}$$

Here $\partial^2 A/\partial x\,\partial x$, $\partial^2 A/\partial y\,\partial y$ are the partial derivatives of the amplification factors in the star's disk center. In this case the fluxes H_L and H_R are not equal and the total flux is

$$H_R + H_L = A_0 H_0 + \frac{1}{4}\,\pi R^2\left(\frac{\partial^2 A}{\partial x^2} + \frac{\partial^2 A}{\partial y^2}\right)\left(I_0 + \frac{2}{3}\,I_1\right), \tag{84}$$

but the degree of polarization is calculated according to

$$H_R - H_L = \frac{7}{120}\,u_0\pi R^2\left(\frac{\partial^2 A}{\partial x^2} - \frac{\partial^2 A}{\partial y^2}\right)R^2\,. \tag{85}$$

Here $A_0 = A(0,0)$, H_0 is the total flux. One can introduce an approximate expression for the degree of polarization

$$P = \frac{7}{60}\,\frac{u_0}{I_0 + 2I_1/3}\,A_0\left(\frac{R_*}{R_s}\right)^2,$$

where R_s is a typical scale of changes of the amplification factor.

It should be noted that the degree of polarization is inversely proportional to the square of the typical scale of changes of the amplification factor. This strong dependence points to a great degree of polarization which may exist

during the intersection of the caustic curve with a star trajectory when the amplification factor is discontinuous.

7.1 Polarization by a spherically symmetric microlens

First, we consider the polarization due to a spherically symmetric microlens. Following papers [134 – 136], we place the origin of coordinates at the center of the visible disk of the lensed star, the x axis is directed to the gravitational lens which is located at the angular distance p from the origin of the coordinates (Fig. 13a). We determine the location of a point on the star by the angular distance r from the origin and the angular distance φ from the x axis. It is obvious that by virtue of the circular symmetry of the initial distribution of intensities I_r and I_l on the disk, the flux and the degree of polarization of the registered radiation of a fixed star during microlensing depend only on the angle φ. Let $I_L(r,\varphi)$ and $I_R(r,\varphi)$ be the intensities of radiation at a point of the visible stellar disk with coordinates (r,φ) for observation through polaroids which are oriented parallel and perpendicular to the x axis, respectively.

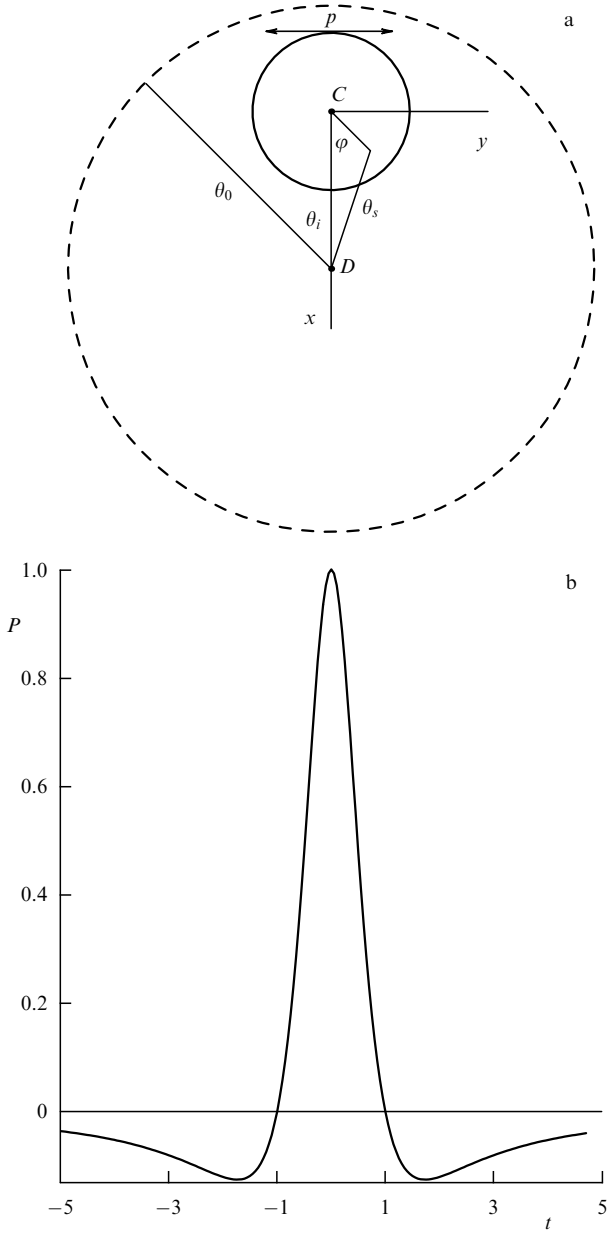

Figure 13. Schematic picture of the true position of a star inside the Einstein–Chwolson cone. The straight line CD connects the star center and the gravitational lens center. The twin arrow shows the polarization orientation, θ_0 is the angular size of the Einstein–Chwolson cone, θ_i is the impact parameter for the source center relative to the lens, and θ_s is the angular distance of the arbitrary point of the source from the gravitational lens. (b) Polarization curve. The first derivative of the curve is equal to zero for $t = 0$. The ratio of the degree of polarization and the maximal degree of polarization is measured along the vertical axis. Time is measured along the horizontal axis in dimensionless units.

In the presence of a gravitational lens with a spherically symmetric field the flux from an infinitely small surface element dS on the star's disk dH^0 is amplified in dependence on the angle p_s between the true direction to the center of the surface element and the direction to the gravitational lens so that dH can be written as $dH = A(p_s)dH^0$. For the amplification factor $A(p_s)$ we have the following expression

$$A(p_s) = \frac{1}{2}\left[\left(1 + 4\,\frac{p_0^2}{p_s^2}\right)^{1/2} + \left(1 + 4\,\frac{p_0^2}{p_s^2}\right)^{-1/2}\right], \qquad (86)$$

where p_0 is the angular radius of the Einstein – Chwolson cone for the gravitational lens. We recall the expression for the Einstein – Chwolson radius:

$$p_0^2 = \frac{4GM}{c^2}\,\frac{D_{sd}}{(D_{sd} + D_d)D_d}\,, \qquad (87)$$

where G is the gravitational constant, M is the lens mass, c is the speed of light, D_{sd} is the distance between the star and the lens, and D_d is the distance between the lens and the observer [115]. Therefore, one can write expressions for the fluxes H_L and H_R of polarized radiation

$$H_L(p) = \int_0^{2\pi} \mathrm{d}\varphi \int_0^R A\left(\sqrt{p^2 + r^2 - 2pr\cos\varphi}\,\right) I_L(r,\varphi) r\,\mathrm{d}r\,, \qquad (88)$$

$$H_R(p) = \int_0^{2\pi} \mathrm{d}\varphi \int_0^R A\left(\sqrt{p^2 + r^2 - 2pr\cos\varphi}\,\right) I_R(r,\varphi) r\,\mathrm{d}r\,. \qquad (89)$$

In this case $H_L(p)$ and $H_R(p)$ are not equal and the registered total flux has the following degree of polarization

$$P(p) = \frac{H_R(p) - H_L(p)}{H_R(p) + H_L(p)}\,. \qquad (90)$$

Note, that the plane of primary polarization should always be perpendicular to the direction from the center of the star disk to the gravitational lens. Thus, for sufficiently accurate observations one can detect a rotation of the plane of polarization during the visible motion of a star with respect to the lens. The time corresponding to the maximum degree of polarization coincides with the maximum amplification of the lensed star and is determined by the angle between the velocity vector of the star and the line connecting the centers of the star and the lens. By virtue of the symmetry of the problem, the direction of motion remains uncertain. This effect is of large interest, since it permits us to obtain information about the proper motion of dark bodies, causing the phenomenon of gravitational microlensing.

One can approximate the amplification factor by the first term in a Taylor expansion, thus, we obtain the expression for the degree of polarization

$$\frac{H_R - H_L}{H_R + H_L} = \frac{7}{160}\left(\frac{R}{p_c}\right)^2.$$

The polarization is always perpendicular to the line connecting the centers of the star and the gravitational lens. An arbitrary location of the star inside the Einstein–Chwolson cone is shown in Fig. 13a. In this case when we consider the polarization along the line CD, the observable degree of polarization has an additional dependence on the time connected with the projection of a Stokes vector ($\cos 2\psi$) varying with the star's motion. This additional time dependence is described by the following expression

$$\cos 2\psi = \frac{p_i^2 - v^2 t^2}{p_i^2 + v^2 t^2} .$$

We would like to mention that after time $T = p_i/v$, the degree of polarization becomes negative. This is caused by the fact that the line connecting the star's and lens's centers is rotated through 45° respective to the line CD.

More precise calculations for the parameters R and p_i show, as was expected, that the effect is not large and the degree of polarization really does not exceed 0.5% for the most favorable assumptions concerning the microlensing conditions.

7.2 Polarization by a binary microlens

Much higher values for the degree of polarization appear during microlensing by binary lenses. The degree of polarization is not too large during the motion of the background star inside the Einstein–Chwolson cone, but great changes of the amplification factors may appear at the time of intersection of the caustic curve and the degree of partial polarization increases significantly.

We consider changes of the degree of polarization when the stellar disk passes through the caustic curve. We use the approximate expression for the amplification factor [95]:

$$A = \sqrt{\frac{x_s}{x - x_c}} + 1 ,$$

where x_s is the typical spatial scale of changes of the amplification factor, and x_c is the location of the critical curve on the axis Ox. We suppose that the amplification factor is equal to unity in the region outside the closed boundary of the critical curve. We suppose that the critical curve is a line parallel to the axis Oy.

The changes of H_R and H_L are determined by the following expressions:

$$H_R = \int_{x_c}^{R_*} \mathrm{d}x \int_{y_-}^{y_+} \mathrm{d}y \sqrt{\frac{x_s}{x - x_c}} \times \left(I_r(x,y) \frac{x^2}{x^2 + y^2} + I_l(x,y) \frac{y^2}{x^2 + y^2} \right) ,$$

$$H_L = \int_{x_c}^{R_*} \mathrm{d}x \int_{y_-}^{y_+} \mathrm{d}y \sqrt{\frac{x_s}{x - x_c}} \times \left(I_r(x,y) \frac{y^2}{x^2 + y^2} + I_l(x,y) \frac{x^2}{x^2 + y^2} \right) ,$$

where $y_+ = \sqrt{R_*^2 - x^2}$, $y_- = -\sqrt{R_*^2 - x^2}$. The maximal degree of polarization (for $I_1/I_0 = 0.2$) is 2%. We also note that the polarization plane is parallel to the caustic curve.

Precise calculations were presented in paper [137]. The degree of polarization depends on the ratio R_*/R_E and may be about 1.5%.

A similar situation may appear during microlensing by non-compact objects. In this case the amplification factor may have discontinuities, therefore great gradients of the variable may be at the caustic boundary. So, the degree of polarization could reach noticeable values for the case of a non-compact object [138]. A possibility to observe the degree of polarization and the requirements on the equipment are analysed in paper [137].

8. Gravitational microlens observations

8.1 Introduction

For the first time the possibility of discovering microlensing using observations of star light curves was discussed in the paper by Byalko [142]. Systematic searches for dark matter using typical variations of light curves of separate stars from millions of observable stars started after Paczynski's discussion of the discovery of halo dark matter by monitoring stars from the Large Magellanic Cloud (LMC) [143]. We remark that at the beginning of the nineties new computer and technical possibilities enabling the storage and processing of huge arrays of observational data appeared and promoted the rapid realization of Paczynski's proposal. Griest offered to call the microlenses MACHOs (Massive Astrophysical Compact Halo Objects) [144]. Besides, MACHO is the name of the project of observations of the US-English-Australian collaboration which observes the LMC and Galactic bulge using the 1.3 m telescope of the Mount Stromlo observatory in Australia. Some information about the experiment is on the sites http://wwwmacho.mcmaster.ca/ and http://wwwmacho.anu.edu.au/. Information about possible microlensing events from current observational data of MACHO collaboration in real time is on the site http://darkstar.astro.washington.edu/.

The first papers about the discovery of microlensing were published by the MACHO collaboration [145] and the French collaboration EROS (Expérience de Recherche d'Objets Sombres) [146]. Some information about the EROS experiment is on the site http://www.lal.in2p3.fr/EROS/eros.html.

The first papers about the discovery of microlensing towards the Galactic bulge were published by a US-Polish collaboration (the Optical Gravitational Lens Experiment), which used the 1 m telescope at Las Campanas Observatory. Some information about the OGLE experiment is on the sites http://www.astrouw.edu.pl and http://www.astro.princeton.edu/ogle/. The results of the OGLE collaboration which include the photometry of OGLE microlensing event candidates, papers of the OGLE collaboration, as well as a regularly updated status report can be found over the Internet from the host sirius.astrouw.edu.pl (148.81.8.1) using the 'anonymous ftp' service.

We note that the addresses of these sites have been changed (or the access modes for the data) in the past, and probably the addresses will be changed in future. However, we have indicated the sites for the collaborations which were used by the groups in 1997 (perhaps the addresses will be used in future).

8.2 Microlensing features

A microlensing event may be characterized by the following main features, which allow a microlensing event and stellar variability to be distinguished (see, for example, Refs [42, 9]).

• Since microlensing events have a very small probability, they should never be repeated for the same star. Stellar variability is usually connected with periodic (or quasi-periodic) events of the fixed star.

• In the framework of a simple model of microlensing when a point source is considered, the microlensing effect must be achromatic (deviations from achromaticity for a non-point source have been considered, for example in paper [149]), but a proper change of luminosity of the star is usually connected with temperature changes and thus the light curve depends on color.

• The light curves of microlensing events are symmetric, but the light curves of variable stars are usually asymmetric (often they demonstrate the rapid growth before the peak and a slow decrease after the peak of luminosity).

• Observations of microlensing events are interpreted quite well by a simple theoretical model, but some microlensing events are interpreted by a more complicated model in which one can take into account that the source (or microlens) is a binary system, the source has non-vanishing size, or the parallax effect may arise.

The features of the light curve of the first microlensing event observed by the MACHO collaboration in the LMC are shown in Fig. 14, where the light curves are shown for two spectral bands†. The light curve (in two bands) is fitted by the simple model well enough, but the ratio of luminosities for the bands is shown in the lower panel of figure (the ratio shape is adjusted with the event achromaticity). However, one can note that near the maximal observable luminosity the theoretical curve does not fit the data of the observations very well.

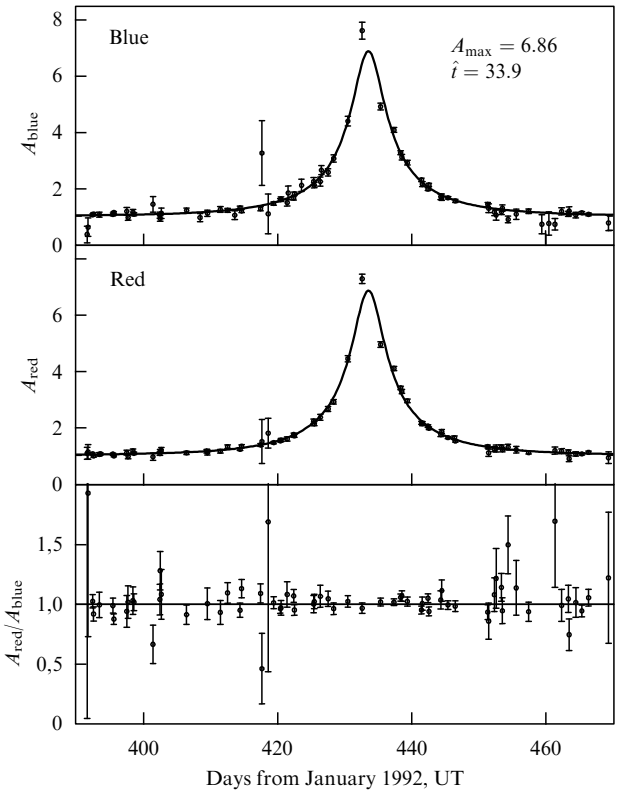

Figure 14. First microlensing event detected by the MACHO collaboration during microlensing searches towards the LMC (Alcock et al. [145]).

† A more recent MACHO fit to the observed amplification of this event gives $A_{\max} = 7.2$.

Now one can carry out accurate testing of the achromaticity and moreover the stability of the source spectrum during a microlensing event with the Early Warning systems implemented both by the MACHO [150] and OGLE [85] collaborations. This allows one to study the source properties using large telescopes and to organize intense follow-up studies of light curves using a telescope network around the globe [150].

In addition to the typical properties of individual microlensing events, Roulet and Mollerach note that the population of observed events should have the following statistical properties [42]:

(a) unlike star variability, microlensing events should happen with the same probability for any kind of star therefore the distribution of microlensing events should correspond to the distribution of observed stars in the color-magnitude diagrams‡.

(b) the distribution of the maximal amplification factor $A_{\max}$ should correspond to a uniform distribution of the variable $u_{\min}$.

(c) the distributions of the amplification $A_{\max}$ and the microlensing event time T should be uncorrelated.

The basic point of microlens discovery is the very small probability of the microlensing event. It is not difficult to obtain a simple estimate of the optical depth for the searches towards the LMC. Based on the estimate $\tau \simeq V^2/c^2$ obtained in the previous section and thus, we find $\tau_{\text{halo}} \simeq 5 \times 10^{-7}$ for the halo case [42]. The average duration of microlensing events is connected with the average velocities in the halo as $T \simeq R_{\text{E}}/\sigma \simeq 100$ days $\sqrt{m/M_{\odot}}$ (using the assumption $x = D_d/D_s = 1/4$). Hence, one can obtain that, for lenses with masses in the range $10^{-2} - 10 M_{\odot}$, the typical event durations are between a week and a year. Using these estimates one can conclude that several million stars should be monitored for more than a year and it is necessary to measure the observable luminosity of stars with a typical time interval of several days. In the case when the lenses have masses in the range $10^{-7} - 10^{-4} M_{\odot}$, the events last less than a day, but the event rates $\Gamma \propto \tau/\langle T \rangle$ are much higher than the event rates for lenses of stellar mass. To discover the lenses in this mass range it is necessary to observe with a much better time coverage, i.e. performing several measurements per night. Thus, for the exploration of the possible range of the lens masses $10^{-7} < m/M_{\odot} < 10$ it is necessary to perform measurements of the same star fields several times per night and with a time interval of about a day.

Roulet and Mollerach present a simple estimate of the optical depth $\tau \simeq 10^{-6}$ for bulge stars which are lensed by stars in the bulge and the disk with typical event durations of a few weeks, so that in this case several million stars also need to be monitored for more than a year to get reliable statistics [42].

Since for microlens searches one can monitor several million stars for several years, the ongoing searches have focused on two targets: (a) stars in the Large and Small Magellanic Clouds (LMC and SMC) which are the nearest galaxies having lines of sight which go out of the Galactic

‡ However, Roulet and Mollerach noted that for observations in the bulge, since observed stars have a non-negligible spread along the line of sight, the optical depth is significantly larger for a star lying behind the bulge, thus the lensing probabilities should increase for fainter stars [42].

plane and well across the halo; (b) stars in the Galactic bulge which allow us to test the distribution of lenses near the Galactic plane.

8.3 Searches towards the LMC and SMC

There are some collaborations which are devoted to searches for microlensing events toward the Magellanic Clouds. Below we will discuss results of the MACHO and EROS collaborations.

8.3.1 The EROS experiment. The first experiment was realized by the French collaboration which actually had two different programs at La Silla Observatory in Chile: (i) they used a CCD camera in a 40 cm dedicated telescope to make short exposures (10 min each) so as to be able to test short duration events; (ii) they analysed plates from a 1 m Schmidt telescope which made two exposures per night in different colors from which they have followed the light curves of several million stars since 1991 [42]. Using the information in the plates which had been collected since 1990 one can obtain several million light curves. The plates were obtained using a Schmidt telescope with a 1 m aperture and a 3 m focal length. Each plate was of size 30×30 cm^2 and corresponded to a celestial sphere element of $5^\circ \times 5^\circ$, so it covers the larger part of the LMC area.

During one night of observations the EROS collaboration usually got two plates (red and blue filters were used); the time exposure for each plate was about 1 hour. During the first winter of observations in 1990 – 1991 the EROS collaboration got 28 plate pairs (total 56 plates). The collaboration had about 200 plate pairs by the end of 1994. The data from the plates were digitized using MAMA† of the Paris Observatory; the digital data density was about 10^4 pixels mm^{-2}. Digitizing one plate took 6 hours (the data size was about 1.6 Gb); each image had 784 cadres, each cadre had 1024×1024 pixels, each pixel corresponding to 0.67 angular square seconds on the celestial sphere. Analyzing 1 cm^2 of the plate one can estimate the luminosities of 10000 stars. However, only about 50% of the observed stars (about 4×10^6 stars) were suitable for microlensing searches [87].

A CCD camera (for searching for events with short durations) was fixed in the focus of the 40-cm dedicated telescope at the end of 1991. The camera consists of 16 separate matrices, has about 4×10^6 pixels and may be used for observations of a celestial sphere element with size $0.4^\circ \times 1^\circ$. One pixel corresponds to a square angle equal to 1.1 angular square seconds. The typical time exposure is about 10 min. The collaboration got 46 images in blue and red colors [151]. The goal of the observations using the camera is the search for microlensing events with small duration ($\gtrsim 1$ hour). Using the CCD camera about 10^5 stars were monitored in the bar of the LMC.

From July 1996 the EROS collaboration started to use the 1 m dedicated telescope MARLY for microlensing searches which is located in the Observatory of ESO [152] (the observations on this telescope are called EROS 2). This telescope may carry out observations simultaneously in the blue ($\lambda \in [420\text{ nm}, 720\text{ nm}]$ with maximal sensitivity $\lambda \sim 560$ nm) and in the red band ($\lambda \in [620\text{ nm}, 920\text{ nm}]$ with maximal sensitivity $\lambda \sim 760$ nm) using a dichroic cube for splitting the beam of light. CCD-camera is fixed in each channel, each camera having 8 CCD-matrices with 2048×2048 pixels. The field sizes are 0.7 angular degrees (right ascension) $\times$ 1.4 angular degrees (inclination). The pixel size is about 0.6 angular seconds. As the main targets for observations the collaboration chose stars near the Galactic center in Galactic plane, and stars in the LMC and SMC.

† MAMA is the abbreviation of the French words Machine Automatique a Mesurer pour l'Astronomie.

8.3.2 The MACHO collaboration. The Australian – US – English MACHO collaboration carries out observations using the 1.27 m telescope of the Mount Stromlo Observatory near Canberra. The collaboration uses an optical corrector with a field of about $0.7^\circ \times 0.7^\circ$, the dichroic beamsplitter taking simultaneous images in the red and blue bands. Two large CCD-cameras are fixed in the focuses of the system, each camera having 4 chips containing 2048×2048 pixels. The typical time exposure is about 300 seconds, so during a clear night one can get up to 60 images. The collaboration had 50000 images by October 1996 [153]. The Galactic bulge was observed when the LMC and SMC were too low on the celestial sphere.

8.3.3 The PLANET project. As Albrow et al. noted, in 1995 the program PLANET (Probing Lensing Anomalies NETwork) started. The aim of the project is to follow the announcements of real time detection of microlensing events (currently implemented by the OGLE and MACHO collaborations) with frequent multi-color observations on four telescopes: the 0.6 m telescope of the Perth Observatory at Bickley in Australia, the 1 m telescope near Hobart in Tasmania, the 1 m telescope of the South African Astronomical Observatory at Sutherland in South Africa and the Dutch-ESO 0.92 m telescope at La Silla in Chile.

8.3.4 Observational results of the EROS collaboration. Let us present the theoretical estimates for the basic parameters of the microlensing model based on the analysis of the light curves of stars in the LMC. In Table 1 the values for τ, Γ_{th}, $\langle T \rangle_{th}$ and $\langle D_l \rangle$ are given for observations towards the LMC, for different dark lensing components. The estimates were calculated in the paper by Roulet and Mollerach [42]. The theoretical estimates for event rates and average durations in Table 1 were calculated assuming a common lens mass and unit efficiency ($\epsilon = 100\%$). Really, the actual efficiencies are typically $\leqslant 30\%$ and T dependent. Anyway, taking into account the efficiencies of the MACHO and EROS collaboration, more than 10 microlensing events might have been detected in each experiment [42]. However, one can note that it is very difficult to estimate precisely the fraction of

Table 1. Predicted optical depth τ, theoretical ($\epsilon = 1$) rates Γ_{th}, average event duration $\langle T \rangle_{th}$ and average distance between the lens and observer $\langle D_l \rangle$ for microlensing events of LMC stars by different Galactic lensing populations: a standard halo, a heavy spheroid [where $\rho_*^{\mathrm{S}} := \rho_0^{\mathrm{S}}/(0{,}0015 M_\odot\ \mathrm{pc}^{-3})$], a dark thick disk [with $\Sigma_{45} := \Sigma_0/(45 M_\odot\ \mathrm{pc}^{-2})$] and a thin disk [with $\Sigma_{30} := \Sigma_0/(30 M_\odot\ \mathrm{pc}^{-2})$], $m_{0.05} := M/0.05 M_\odot$. (Table from Ref. [42].)

Lensing component	τ, 10^{-7}	Γ_{th} $(10^7$ stars $\cdot$ years$)^{-1}$	$\langle T \rangle_{th}$, days	$\langle D_d \rangle$, kpc
Halo	5.4	$89 m_{0.05}^{-1/2}$	$14 m_{0.05}^{1/2}$	14
Spheroid	$0.44 \rho_*^{\mathrm{S}}$	$6.7 \rho_*^{\mathrm{S}} m_{0.05}^{-1/2}$	$15 m_{0.05}^{1/2}$	9.0
Thick disk	$0.47 \Sigma_{45}$	$5.5 \Sigma_{45} m_{0.05}^{-1/2}$	$20 m_{0.05}^{1/2}$	3.6
Thin disk	$0.11 \Sigma_{30}$	$1.1 \Sigma_{30} m_{0.05}^{-1/2}$	$23 m_{0.05}^{1/2}$	1.1

microlensed binary sources which have a chromatic or non-symmetrical light curve.

Observing more than 80000 stars during 10 months (from 21 August 1992 to 31 March 1993) using a CCD-camera, the EROS collaboration found no events. If we consider the standard halo model ($4 \times 10^{11} M_\odot$), then one can estimate the expected number of microlensing events using Monte Carlo simulations. The theoretical estimate of the expected event number is calculated using the assumption that all microlenses have the same mass. Since the estimated number of microlensing events is greater than 2.3 for a lens mass in the range $5 \times 10^{-8} < M_d/M_\odot < 7 \times 10^{-4}$, so, based on results of the observations Magneville concluded that with probability 90% the lenses could not form a component which would contribute essentially to the halo mass [151]. In the case when the lens mass is in the range $3 \times 10^{-7} < M_d/M_\odot < 1.5 \times 10^{-5}$, the expected number of microlensing events is greater than 6.9, and Magneville gave the statistical conclusion that the total mass of microlenses of such mass could not form more than one third of the halo mass [151].

Using the observations of the first three years on the Schmidt telescope with a total exposure $E = 3$ years $\times$ 3.33×10^6 stars, the EROS collaboration found two candidates for microlensing events with durations $T_1 = 23$ days and $T_2 = 29$ days [146]†.

Table 2. Theoretical estimates of microlensing events for the standard halo model depending on the microlens masses which could be observed in the EROS experiment using the CCD camera. (Table from the review by Ansari [87].)

Lens mass, $M_\odot$	Event number
10^{-7}	5.6
10^{-6}	9.7
10^{-5}	4.3
10^{-3}	1.9

We recall that the efficiency depends on the event duration $[\epsilon = \epsilon(T)]$, so if we suppose that the EROS collaboration found one microlensing event then we would be able to obtain the following estimate of the optical depth towards the LMC‡

$$\tau_{\rm est}^{\rm EROS} \equiv \frac{\pi}{2E} \sum_{\rm events} \frac{T_i}{\epsilon(T_i)} < 4 \times 10^{-8} \,. \qquad (91)$$

From July 1996 to February 1997 and since July 1997 using modified equipment the EROS collaboration has been carrying out the observations of the SMC region, which is covered by 10 fields with a total area of about 10 square degrees and with the maximal number of observable stars [152]. From 1996 to 1997 they got from 60 to 120 images for each field. A repeat observation for each star field was made after 2–4 days. The total exposure was from 5 to 15 min. Thus, the EROS collaboration got the light curves of 5.3 million stars. After processing these observations the EROS collaboration reported one candidate for a microlensing event, or more exactly speaking the authors wrote that "one star had a light curve which could be interpreted best of all as a microlensing event by an invisible body" [152]. The crossing time of the Einstein–Chwolson radius was about 123 days. The EROS collaboration estimates the lens mass as $2.6^{+8.2}_{-2.3} M_\odot$, the maximal amplification factor is equal to 2.6. Analyzing the parallax effect they showed that if the lens is located in the halo then its mass should be not less than $1.2 M_\odot$, but if the lens is located in the SMC then its mass will be about $0.1 M_\odot$. They estimated the optical depth towards the SMC as $\sim 3.3 \times 10^{-7}$.

8.3.5 Observational results of the MACHO collaboration. As Sutherland et al. reported, by October 1996 the MACHO collaboration had completed the analysis of more than two years observations for 22 well investigated regions of the LMC, which have about 8 million stars. For each star from 300 to 800 luminosity observations had been collected [153, 154]. Thus, the total exposure was about 1.8×10^7 star · years. First, the MACHO collaboration selected only the microlensing event candidates which satisfied strong selection rules, namely the light curves had to be characterized by the essential changes of luminosity (the maximal amplification factor was $A_{\rm max} > 1.75$), but outside the amplification region the stellar luminosity had to be approximately constant. Then the selection rules were slightly changed since the MACHO collaboration gained experience in analysis of the observational data from the observations towards the Galactic bulge. In particular, the selection rules on the standard shape and the achromaticity were reduced, but the requirements on the statistical level and the amplification factor were strengthened. Thus, events #2 and #3, which were observed during the first year of observations and selected first, do not correspond to the new selection rules, but the researchers found new candidates which were observed during the first year and correspond to the new selection criteria. During the processing of observational results, 12 objects were found satisfying the final criteria, four of them corresponding to only two stars (the stars were in the intersection region of two neighboring fields), two objects were excluded from the consideration since, probably, their light curves cannot be explained by microlensing and, as Sutherland et al. noted, one of the stars is most probably a supernova [153]. As a result 8 candidates for microlensing events were found with typical durations of 34 to 145 days; the respective light curves are shown in Fig. 15. The events are numbered 1, 4–10 (numbers 2 and 3 are omitted since the events which were selected earlier do not satisfy the new criteria). Six from the eight candidates correspond well enough to the standard light curve for a simple microlens model; three of them (numbers 5, 7 and 9) demonstrate a weak dependence on color. The event #9 has a light curve with two typical maxima which most probably corresponds to a binary lens [157]. Event #10 has a slightly asymmetric light curve. The event probably corresponds to a variable star but Sutherland et al. proposed that there was microlensing of a binary background star [153]. The final statistical results do not depend on the inclusion (or exclusion) of this event. Sutherland et al. think that the selected events are actually connected with microlensing and cannot be connected with errors of observations, such as the influence of cosmic rays and other causes. Besides event MACHO #1 was also confirmed by the EROS collaboration, and event #4 was detected in real time and observed

† However, Ansari et al. reported that the event EROS #2 is an eclipsing binary system possibly with an accretion disk. The system has a characteristic period of about 2.8 days [156]. Paczynski noted that the event EROS #1 is probably an emission line Be type star (or a variable star of a new kind [57]). The new class of variable stars was found as a serendipitous result of the MACHO collaboration.

‡ Assuming that the EROS collaboration found two microlensing events, Ansari et al. estimated the optical depth towards the LMC as $\tau_{\rm est}^{\rm EROS} = 8.2 \times 10^{-8}$ [87].

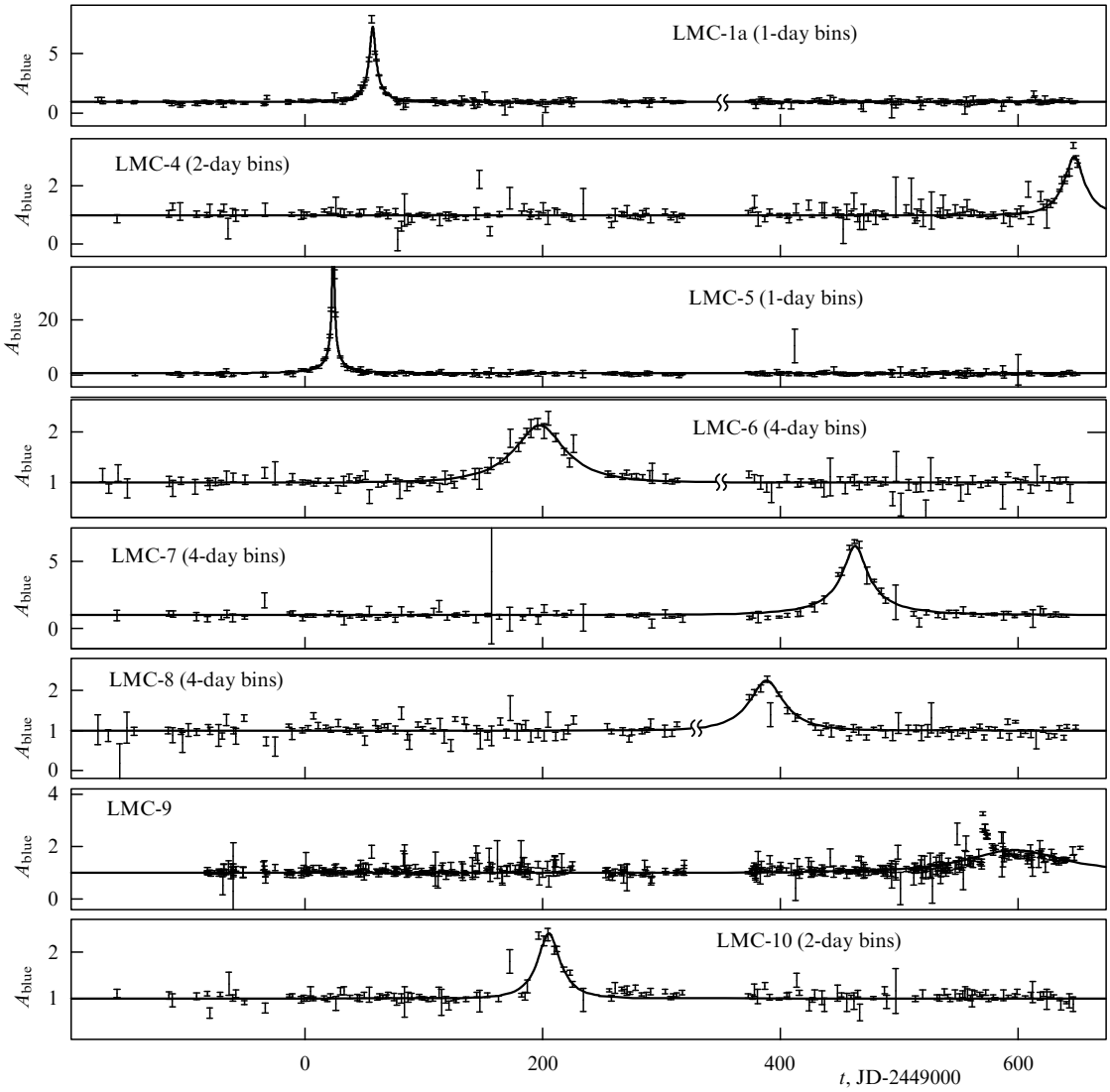

Figure 15. Light curves of 8 microlensing event candidates based on the processing of observational data collected over two years by the MACHO collaboration. Light curve variations (only in the blue) are shown on a linear scale corresponding to the average standard deviation 1σ; the observations were averaged in each time bin (of one to four days), light curves are normalized to basic light curves which correspond approximately to constant luminosity. The solid line for the observational data of each microlensing event candidate corresponds to the single lens model. The time is measured in days. (Figure from Ref. [153].)

using other telescopes [153]. Sutherland et al. note that it is very difficult to exclude proper stellar variability however some microlensing candidates demonstrate an essential growth of luminosity and it is not easy to explain the light curves in another way (not using the microlensing model) [153]. The spectral data were also obtained for event #4 which confirm the hypothesis of microlensing. As Alcock thinks, the distribution of the maximal amplification factor and color–magnitude diagram agree with the estimated parameters [158]. In October 1996 the MACHO collaboration thought that at least five of the suggested event candidates are connected with microlensing, however Alcock et al. noted that if only the 'high quality' events are considered (for example, the events 1, 4, 5 and 9), then the probability of the observable distribution for the variable $A_{\max}$ would be very small [158].

To obtain quantitative estimates of the results, the MACHO collaboration numerically simulated their experiment using the Monte Carlo method. In the simulation star light curves were imitated (they included the data of real observations) with different amplification factors. The group also modeled different conditions of observations because of bad weather, variable conditions of observations and other factors. The artificial light curves (together with the observable light curves) were processed using standard software. From the analysis of the light curves the group obtained the event detection efficiency dependencies on time, which are shown in Fig. 16 (the different lines correspond to different simulation procedures). It is clear that the detection efficiency depends, although not essentially, on a lot of other parameters (for example, on the maximal amplification factor) and on stochastic parameters such as the conditions of observations.

Following Sutherland et al. [153] we suppose that the halo is formed by objects with identical mass, so that the expected number of microlensing events is shown in Fig. 17a. As was noted earlier the typical duration of microlensing events depends essentially on the lens mass, therefore, if the lens mass is about $m \gtrsim 0.01 M_\odot$ then most of the microlensing events have a typical duration of $\hat{t} \gtrsim 10$ days, where the

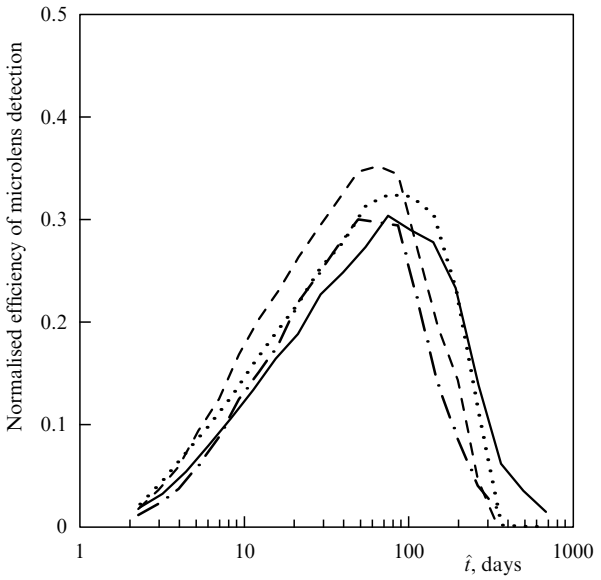

Figure 16. Solid line shows the efficiency of detection of the microlensing event candidates (relative to the rate of the event detection which is described by the inequality $u_{\min} < 1$) for the MACHO observations towards the LMC over two years. (Figure from Ref. [153].)

detection efficiency is high enough, but the rate of such events decreases with increasing lens mass as $\propto m^{-0.5}$. For small lens masses $m < 0.001 M_\odot$ the estimated rate of such events is fairly high, but most of the events have durations shorter than $\hat{t} \sim 3$ days, where the detection efficiency of the MACHO experiment is small. As a result Sutherland et al. conclude that if the halo is formed by objects with mass $m \sim 2 \times 10^{-3} M_\odot$ then the maximal expected number of microlensing events in the MACHO experiment is about ~ 45 [153].

From the absence of microlensing events with a short typical duration one can estimate the contribution of low mass lens to the halo mass. So, since events with typical duration shorter than $\hat{t} < 20$ days were not found in the MACHO experiment, Sutherland et al. concluded that the objects with masses in the range from 6×10^{-5} to $0.02 M_\odot$ contribute less than 20% of the halo mass with confidence 95% [153]. To increase the possibility of finding a low mass microlens (with a corresponding short duration), some regions of the LMC were observed twice per night which allowed 4 points to be obtained (two luminosities per night in each of two spectral bands) for the luminosity of any object in the regions. Microlensing events with typical durations $\sim 0.3-3$ days were not found after processing the observational data.

Analyzing the data of the MACHO experiment, Sutherland et al. conclude that lenses with masses in the range 10^{-6} to $0.02 M_\odot$ contribute less than 20% to the halo mass. In other words, such objects contribute less than $10^{11} M_\odot$ of the halo mass inside 50 kpc, as shown in Fig. 17b [153].

In this case the estimated optical depth towards the LMC (taking into account the detection efficiency of the MACHO experiment) is [153]

$$\tau^{\mathrm{MACHO}} = 2.9^{+1.4}_{-0.9} \times 10^{-7} . \qquad (92)$$

We note that earlier, based on the data of the first year of observations (using 3 events), the value for the optical depth τ^{MACHO} was estimated to be approximately three times smaller [42].

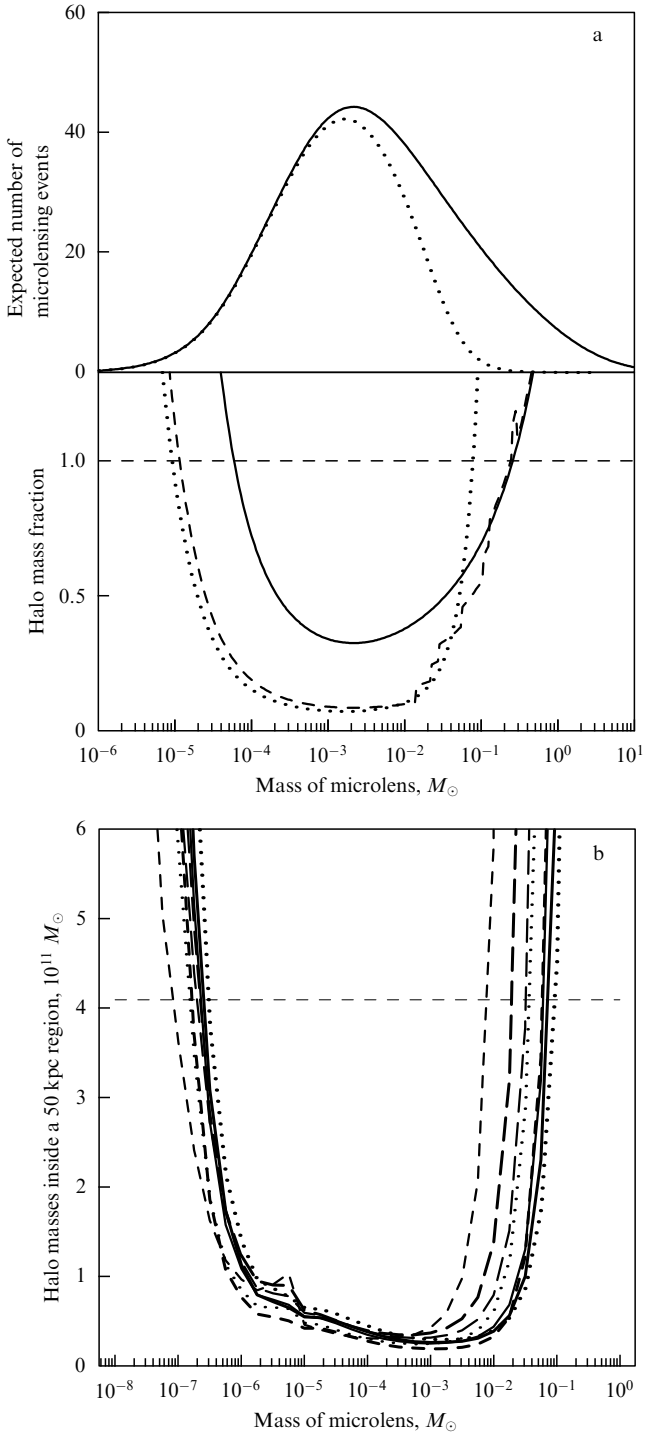

Figure 17. (a) Top figure shows the expected number of microlensing events for the case when all lenses have the same mass m. The bottom figure shows the restrictions to the halo mass fraction corresponding to lenses with such a mass. The regions which are higher than the drawn curves are excluded with 95% confidence. The solid line is drawn using 8 observed events, the dashed line is shown based on the observational result that there were no events with typical duration $\hat{t} < 20$ days. (b) The high limits (with 95% confidence) of the total halo mass which is formed by gravitational microlenses inside the region 50 kpc using the results of the processing of the observational data of the MACHO experiment for 8 different halo models. (Figure from Ref. [153].)

Roulet and Mollerach note that it is necessary to accept the estimates for the optical depth τ from expressions (91) and (92) critically because the statistical data size of microlensing

event candidates is not very large and the detection efficiency for lens masses greater than $\sim M_\odot$ is also small [42]. On the other hand, some microlensing event candidates are probably not associated with real microlensing events. In this case the optical depth estimate must be smaller.

If the standard light curve is observed then generally it is impossible to determine the distance between the lens and the observer. Since microlensing could be caused by stars in our Galaxy as well as the stars in the LMC (as Sahu suggested [92]) or by halo objects. However, as Alcock et al. noted [159], microlensing by known stars could lead to the detection of about 1.1 events in the MACHO experiment and the optical depth $\tau_s \sim 0.5 \times 10^{-7}$ could be associated with these stars. So, the optical depth estimate exceeds the optical depth corresponding to observable stars. Bennett et al. give a more conservative estimate of the optical depth of the halo $\tau_{\rm halo} = 2.1^{+1.1}_{-0.7} \times 10^{-7}$, obtained from the data analysis by the exclusion of event #9 (since the lens corresponding to this case could be in the LMC) and event #10 (since the corresponding background star could be variable) [157]. Sutherland et al. give the lens mass estimate, starting from the observable event durations. The variable $\hat{t}$ depends on three unknown parameters: the lens mass, the distance between lens and observer, and the transverse velocity. Therefore, the mass estimate has only a statistical significance and generally speaking depends only on the halo model [153]. Using the maximal likelihood method one can determine the most probable interval of the lens mass to be $0.5^{+0.3}_{-0.2} M_\odot$ for the standard halo model (Fig. 18). If the lenses are located in the halo in this mass range, they cannot be hydrogen-burning stars which would be easily detectable [160]. Thus, Sutherland et al think that cold white dwarfs could be the most natural microlenses [153].

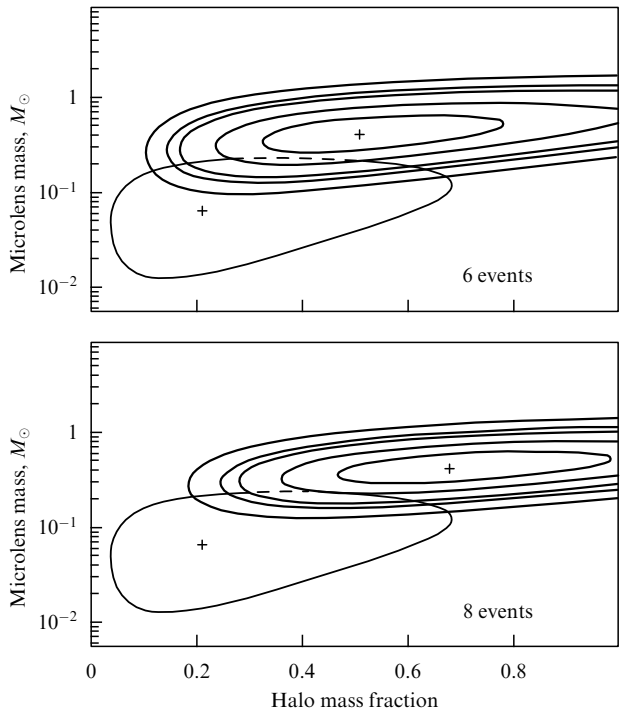

Figure 18. Thick lines show the contours (with the confidence probabilities 34, 68, 90, 95, 99% for the region inside the curves) for the lens mass and contributions of the lens masses to the halo mass for the standard halo model for the cases of 6 and 8 detected events. The thin line shows the contour corresponding to the confidence probability of 90% using the MACHO data of the first year of observations. (Figure from Ref. [153].)

Although the formal significance of the experiment is great enough, Sutherland et al. do not assert that they have found dark matter since several microlensing events suggested earlier are actually variable stars [153]. Zhao suggested [161] that the cause (which is artificial enough according to the opinion of Sutherland et al. [153]) of the observable optical depth could be associated with the hypothesis that there is a dwarf galaxy between the LMC and the Earth, although the theoretical probability of this is very small $\sim 1\%$.

8.4 Observations towards the Galactic bulge

The extensive observations of the Galactic bulge realized by the MACHO and OGLE collaborations have already been mentioned. The French DUO (Disk Unseen Objects) collaboration has also carried out observations towards the bulge since 1993 at the La Silla Observatory of ESO in Chile using the Schmidt telescope. As Ferlet reported, based on communications of the group's participants, the DUO collaboration has obtained the light curves of about 15 million stars and found several microlensing event candidates [20]. We shall discuss some results of the observations of the OGLE and MACHO collaborations.

8.4.1 Observational results of the OGLE collaboration. Now at least three collaborations carrying out observations towards the Galactic bulge for the detection of the microlensing events are known. These collaborations have found a lot of microlensing events (more than was estimated before observations). The first group which started such observations was the OGLE collaboration which has been monitoring more than 10^6 stars since 1992. The most part of the observations of the collaboration are carried out in the I-band but some observations were performed in the V-band. If we take the time at which a microlensing event reached its maximum, then the first microlensing event was event OGLE #10, which peaked on June 29, 1992 [89, 57]. The event was found by the OGLE collaboration after six other events were observed that summer. However, the event was extracted by a computer from observational data only in the spring of 1994. The OGLE collaboration discovered the first event (OGLE #1) on September 22, 1993, but this event peaked on June 15, 1993, almost a full year later than OGLE #10†. An example of a microlensing event (OGLE #2) is shown in Fig. 19. This microlensing event took place in 1992. The event was in the overlap area of two separate fields, so it had a large number of measurements in the I-band: 93, 187, and 94 in the observing seasons 1993, 1994, and 1995 respectively. Paczynski pointed out, based on a private communication with M Szymanski, that the stellar luminosity was constant during these three years with average I-band magnitudes of 19.07, 19.10 and 19.13 respectively, and the standard deviation of individual measurements was 0.13, 0.10 and 0.09, respectively [57].

The distribution of OGLE events in the $(V-I)-V$ color–magnitude diagram of stars seen through Baade's Window, i.e. at $(l, b) \approx (1, -4)$ is shown in Fig. 20. Following Paczynski, we note that the events are scattered over a broad area of the diagram populated by galactic bulge stars,

† As Paczynski noted [57], based on a private communication of Alcock, the first event ever to be noticed by a human was MACHO # 1 — Will Sutherland saw it come out of a computer on Sunday September 12, 1993.

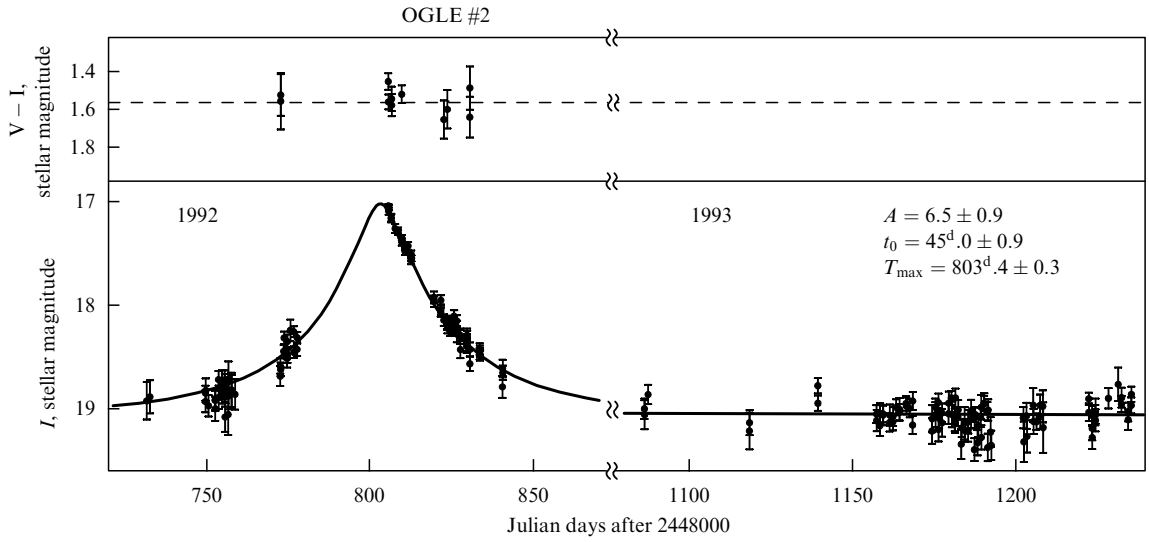

Figure 19. Example of the observed light curve corresponding to the point lens model: the event candidate OGLE #2 [89]. (Figure from Ref. [57].)

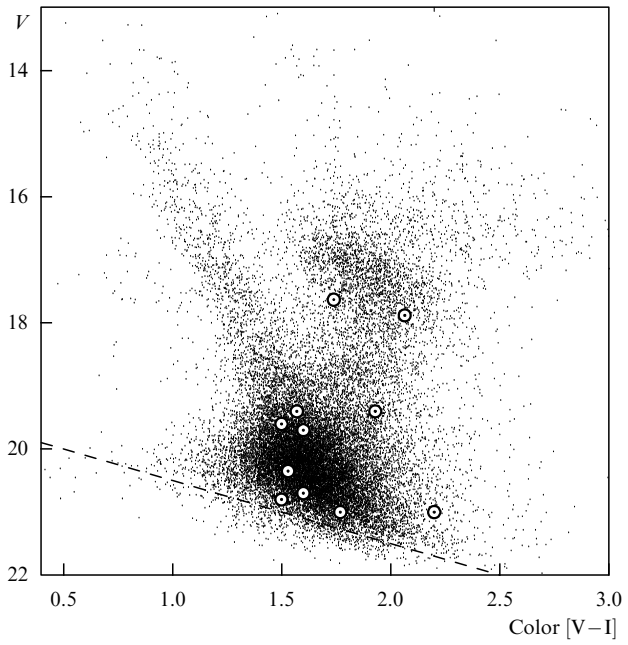

Figure 20. Color – magnitude diagram for stars in the Baade's Window. The location of 11 OGLE microlensing event candidates is shown by small circles. The region which is accessible to the OGLE observations is shown above the straight dashed line [85]. Most stars in the bulge are at the main sequence turn-off point of the galactic bulge, near $V-I \approx 1.6$, $V \approx 20$. The bulge red clump stars are near $V-I \approx 1.9$, $V \approx 17$. The disk main sequence stars form a distinct band between $(V-I, V) \approx (1.5, 19)$ and $(V-I, V) \approx (1.0, 16)$. (Figure from Ref. [57].)

in proportion to the local number density of stars multiplied by the local efficiency of event detection [57, 85].

The most surprising result was the OGLE discovery that the optical depth is as high as $3.3 \pm 1.2 \times 10^{-6}$ (based on 9 events) towards the Galactic bulge [85]. In the first theoretical papers by Griest et al. [162] and Paczynski [163], where the optical depth towards the Galactic bulge was estimated, the effect of microlensing by Galactic bulge stars was ignored. Kiraga and Paczynski supposed that the effect may be dominant for observations towards the Galactic bulge [84], however they still ignored the fact that there is a bar in the inner region of our Galaxy (the possibility of the bar's existence was discussed by de Vaucouleurs [164] and Blitz and Spergel [77]). However, the preliminary results of the OGLE collaboration forced upon us the 'rediscovery' of the Galactic bulge [89, 67, 165 – 167]. So, Dwek et al. think that the microlensing searches are becoming a useful new tool for studies of the Galactic structure [168].

Besides the rediscovery of the Galactic bar the OGLE collaboration found an event corresponding to the light curve formed by a binary gravitational lens, when the source projection crosses the caustic curve being formed by the binary gravitational lens. Udalski et al. presented the example of the light curve corresponding to the first binary lens (OGLE #7); the light curve is shown in Fig. 21 [170]. The star was found to be constant in 1992, 1994 and 1995. The average magnitude based on 32, 45 and 41 I-band measurements in these three observing seasons was 17.53, 17.52 and 17.54 respectively with the variance of single measurements being 0.07, 0.04 and 0.03 magnitudes, respectively [57]. The object was also found in the MACHO database [110] and the MACHO group confirmed the presence of the second caustic crossing event near JD 2449200 and demonstrated that the light curve variation was achromatic.

The standard interpretation of the light curves of OGLE #7 is the intersection of the caustic curve which is formed by a binary gravitational lens. However, the caustic curve formation is also possible in the framework of the model of a transparent gravitational microlens formed by a non-compact object [171].

8.4.2 Observational results of the MACHO collaboration. Alcock et al. reported the MACHO results of processing the observational data for the first year of observations towards the Galactic bulge [172]. The MACHO collaboration analysed 24 fields having about 12.6 million stars observed over 190 nights in 1993, and reported the detection of 45 microlensing event candidates with durations of 4.5 to 110 days (Fig. 22)†. The MACHO collaboration observed the

† Sutherland et al. reported that the MACHO collaboration has detected more than 100 microlensing events towards the bulge [153].

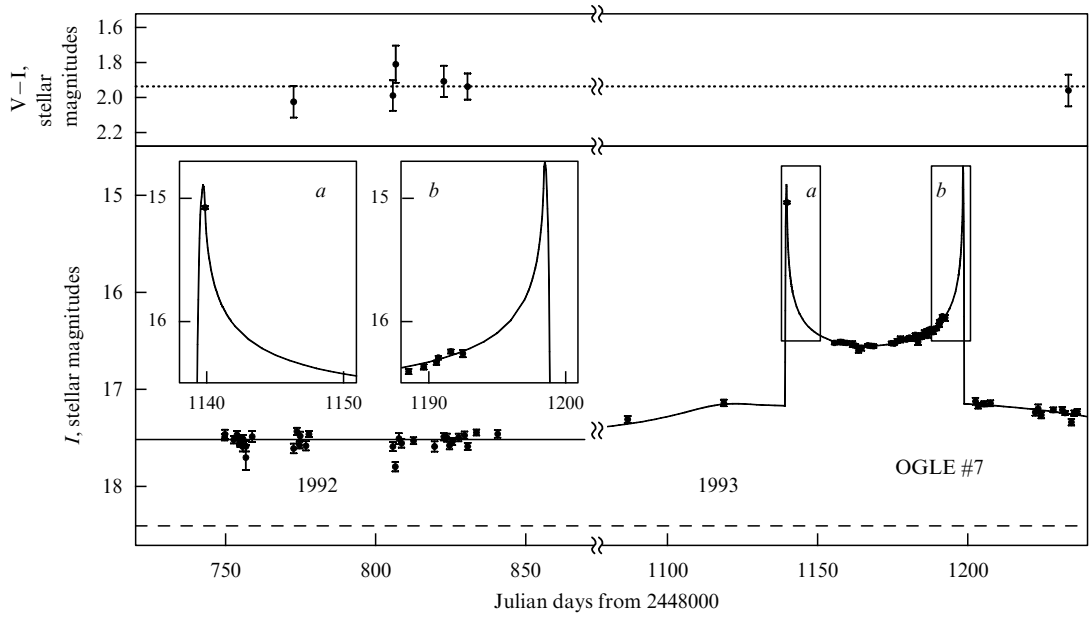

Figure 21. Possible example of a binary lens: the microlensing event candidate (OGLE #7) [170]. The regions of the two caustic crossing $s(a)$ and (b) are shown in the enlarged insert. The MACHO collaboration has a few dozen additional points in two bands showing that the light curve variations are achromatic; three MACHO points correspond to the second caustic crossing (b) [110]. (Figure from Ref. [57].)

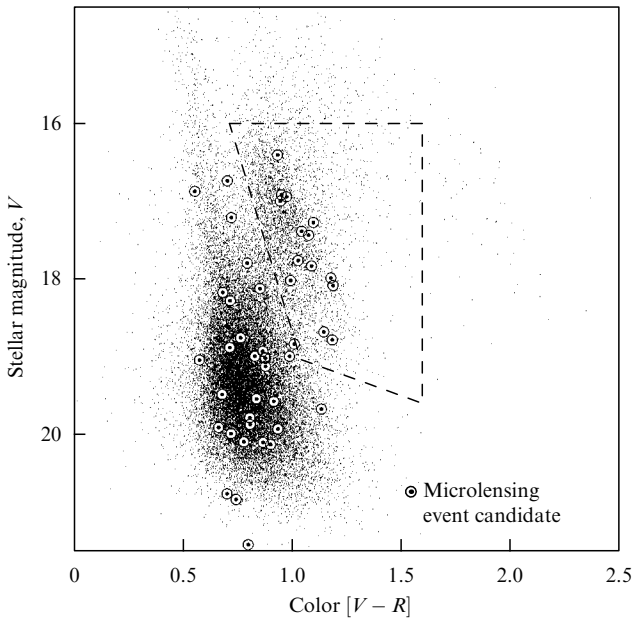

Figure 22. Color–magnitude diagram for bulge observations of the MACHO collaboration. The light circles show the stars which correspond to microlensing event candidates (there are 45 microlensing event candidates). (Figure from Ref. [172].)

bulge region having the galactic coordinates in the ranges $0^\circ < \ell < 7^\circ$ and $-2^\circ > b > -6^\circ$. Many of the event candidates had large signal/noise ratios and demonstrated remarkable examples of light curves. Using observations of 1.3 million stars from 'the group of giants', whose typical distances and detection efficiencies are well known, the MACHO collaboration found 13 microlensing event candidates in the region which had an area of about 13 square degrees on the celestial sphere and a center with the galactic coordinates $\ell = 2.55^\circ$ and $b = -3.64^\circ$. Using the observational data the MACHO group calculated the optical depth as $\tau^{\mathrm{MACHO}} = 3.9^{+1.8}_{-1.2} \times 10^{-6}$. Preliminary results of the MACHO collaboration demonstrate that the optical depth grows with decreasing coordinate $|b|$. The preliminary estimates of the optical depth (as dependencies on the galactic latitudes) towards the Galactic bulge are presented in Table 3. The estimates are based on processing the observational data of the first year of the MACHO experiment.

Table 3. Estimated optical depth towards the Galactic bulge and respective confidence intervals. The stars which are monitored for microlensing searches are given in the first column, the average galactic latitude and longitude and the number of detected events are given in the columns 2–4 respectively, the lower limits of the confidence interval are in columns 5 and 6, the higher limits are in columns 8 and 9. (Table from the paper by Alcock et al. [172].)

	$\langle\ell\rangle$	$\langle b\rangle$	N	0.05	0.16	Estimate	0.84	0.95
1	2	3	4	5	6	7	8	9
All stars	2.7	−4.08	41	1.69	1.98	2.43	2.97	3.33
"Group of Giants"	2.55	−3.64	13	1.90	2.66	3.92	5.79	7.09
"Group of Giants" $\lvert b\rvert < 3.5$	2.18	−2.95	10	2.75	4.07	6.32	9.89	12.32
"Group of Giants" $\lvert b\rvert > 3.5$	2.88	−4.33	3	0.44	0.80	1.57	3.21	4.59

8.4.3 Interpretation of the observations. As noted earlier, originally it was supposed for the planning of observations towards the Galactic bulge that microlensing is caused by faint stars in the disk, thus, the microlensing events must be found independently of the existence of compact objects in the halo. The optical depth for bulge stars lensed by faint stars was estimated by Griest et al. [162] and Paczynski [163] to be $\leqslant 10^{-6}$ and is given in the row labeled 'faint stars' in Table 4.

Griest et al. assumed a fixed local density of disk stars and a constant density of gravitational microlenses [162]. Originally, it was suggested that the contribution of the dark matter

Table 4. Predictions of the optical depth τ, 'theoretical' rates Γ_{th}, average event duration $\langle T\rangle_{th}$ and lens distances $\langle D_d\rangle$ for microlensing stars in Baade's Window by different lens populations [$M_2 = M/(10^2 M_\odot)$, $m_{0.2} = M/(0.2M_\odot)$] [42].

Lensing component	τ, 10^{-6}	Γ_{th} $(10^6$ stars · years$)^{-1}$	$\langle T\rangle_{th}$, days	$\langle D_s\rangle$, kpc
Faint stars	0.29 – 0.96	2.2 – 7.5	~ 30	5.7
Bar ($\alpha = 10°$)	$1.74M_2$	$19M_2 m_{0.2}^{-1/2}$	$20m_{0.2}^{1/2}$	7.0
Bar ($\alpha = 30°$)	$0.97M_2$	$12M_2 m_{0.2}^{-1/2}$	$18m_{0.2}^{1/2}$	7.4
Disk ($D_d < 12$)	$0.42\Sigma_{30}$	$4.3\Sigma_{30} m_{0.2}^{-1/2}$	$22m_{0.2}^{1/2}$	5.5
Disk ($D_d < 6$)	$0.31\Sigma_{30}$	$2.5\Sigma_{30} m_{0.2}^{-1/2}$	$28m_{0.2}^{1/2}$	4.1
Thick disk	$0.37\Sigma_{45}$	$3.3\Sigma_{45} m_{0.2}^{-1/2}$	$25m_{0.2}^{1/2}$	6.2
Spheroid	$0.72\rho_*^{\rm S}$	$14\rho_*^{\rm S} m_{0.2}^{-1/2}$	$12m_{0.2}^{1/2}$	7.7
Halo	0.24	$4.7m_{0.2}^{-1/2}$	$12m_{0.2}^{1/2}$	5.4

halo should not be dominant. However, Gates et al. [59] found that the conclusion depends on the assumed halo core radius a and the contribution grows with decreasing a and with halo flattening. As Guidice et al. showed in the heavy spheroid models, the contribution of spheroid lenses was comparable to that of disk lenses and arose mainly from the inner 2 kpc of the Galaxy, where this component describes the bulge [81]. However, the associated event durations were typically smaller than the disk ones. Using Kent's axially symmetric model Kiraga and Paczynski studied the bulge – bulge microlensing and concluded that averaging over the source distribution increases both the bulge — bulge rates and the average event durations by $\sim 25\%$ (increasing τ by $\sim 50\%$) [84]. However, this averaging does not significantly change the rates due to disk lenses because these are on average more distant from sources and less centrally concentrated than the bulge lenses [42]. Kiraga and Paczynski also analysed how the rates due to disk lenses are reduced in models where a 'hole' in the central distribution is present [84].

Since the observed optical depth towards the Galactic bulge is above the expectations from all these models, as already noted, Kiraga and Paczynski [84] and Paczynski et al. [67] suggested that the cause of these large rates could be the fact that the bulge is actually triaxial with the larger axis making a small angle with respect to the line of sight. In this case, the average distance between sources and lenses is larger, with a corresponding increase of the associated Einstein–Chwolson radii and also the line of sight to the source goes through a larger number of lenses. Therefore, the microlensing observations could help to construct a more precise model of our Galaxy. In addition, the velocities of stars in the bar would be smaller in the directions orthogonal to the major axis, helping to explain the event durations observed, i.e. $T \sim 10 - 50$ days, which would be too long for faint stars in a spherically symmetric model [811] or axially symmetric bulge model [84]. Predictions of the bar mass are consistent with the dynamical estimates $M_{\rm bar} \simeq 2 \times 10^{10} M_\odot$, and the angle between the major axis and the line of sight is consistent with the inferred range $\alpha = 20° \pm 10°$ of Dwek et al. [168] (see, for example, the review [42] and references in the paper).

Thus, the observed optical depth could be caused both by bar stars and faint stars of the disk or lenses which form dark matter. Moreover, as Roulet and Mollerach noted due to the small velocity dispersions of disk constituents, the observed durations of microlensing events could even correspond to stars near the hydrogen burning limit ($0.08M_\odot$) [42]. If lenses (and sources) belong to the bar one can expect that there should be a rate asymmetry for positive and negative latitudes and the effect could be detected based on the (observed) estimate of the rate in different fields. One may observe a magnitude offset between stars observed at opposite longitudes, with those at negative ℓ, which are further away, being fainter. Stanek et al. reported the detection of the effect [165] by the OGLE collaboration. On the other hand, sources in the bar are more likely to be lensed if they are on the far side and hence there may also be an observed magnitude offset of the lensed stars with respect to the whole sample in a given field [42]. This prediction was also confirmed in the OGLE experiment [165].

As Mollerach and Roulet noted, a complication in the interpretation of the bulge results is that a non-negligible fraction of the source stars actually belong to the disk [173]. For example, Terndrup estimated that $\sim 15\%$ of the giant stars in Baade's Window are in the disk and this fraction may be even larger for main sequence stars [174, 42]. Moreover, in fields at larger longitudes and similar latitudes the number of disk stars is practically unaffected while that of bulge stars decreases significantly, making the effects of disk stars relatively more important in those fields [42]. The different distribution and the motion of source stars belonging to the disk affect the predictions about the parameters of microlensing.

The main result of the observations towards the Galactic bulge is the fact that the observed optical depth is greater than the estimated optical depth. If the disk is not void then the rate of events caused by disk stars is non-negligible and since in this case both a lens and a source are in the disk, the events have particularly long durations. The conclusion could explain the origin of events with long durations (such as the long duration event which was found in the MACHO experiment according to the communication of Alcock et al. [172]). If disk stars are microlensed by bar objects the optical depth could be greater for positive longitudes (in contrast to events when both the source and lens are in the bar), and features of the asymmetry would be decreased in the fields of observations.

Using the results of observations towards the Galactic bulge, one can estimate the lens mass. As already noted, Mao and Paczynski concluded that it is necessary to analyse about 1000 events to get a reliable estimate of the lens mass in the case when the kind of lens mass distribution is known but a few parameters of the distribution are unknown [53]. According to Alcock et al., a preliminary analysis of the observations yields the lens mass estimate as $0.1 - 1M_\odot$ [172]. However, as Roulet and Mollerach noted, the lens mass function could be formed by two lens populations, i.e. the disk and bulge stars, the populations may have different lens mass distributions, and the interpretation of observational data would be more complicated in this case [42].

8.4.4 Simulation results and comparison with observations. Using Monte Carlo simulations, Mao and Paczynski showed that even in the case when the spatial and kinematic distributions are completely known or in the other words, the duration distribution by the lens mass is known, it could be difficult to determine the lens mass distribution parameters [53]. The problem is most difficult in the case when the lens mass function is small ($\beta \lesssim 1$). Moreover if the lens mass function exponent differs significantly from –1.5, then it is

difficult to determine the high mass limit for $\alpha \ll -1.5$ and the low mass limit $\alpha \gg -1.5$.

Mao and Paczynski compared their results with the results of Han and Gould [169], who obtained stronger constraints on the lens mass function of disk stars using the observational data about 50 microlensing events towards the Galactic bulge. However, one can note that the high mass limit which is equal to $10M_{\odot}$ was considered by Han and Gould as the initial suggestion [169]. The results of Han and Gould agree with the results of Mao and Paczynski in the case when the high mass limit is known; the other parameters of the distribution are determined more precisely [53]. Thus, the approach of Mao and Paczynski is more realistic and it is necessary to estimate the high mass limit using the maximal likelihood method to avoid *a priori* assumptions about the ranges of physical parameters [53].

In the general case, if we would like to estimate three independent parameters, for example, M_0, α and β, then any statistical method should use the information about first three moments. However, if the moment is higher then it is determined with greater uncertainty for a relatively small number of microlensing events. Therefore, the precision of the determination of any distribution is lower for three parameter determination than for two parameter determination. However, small errors for the two parameter estimate could give the correct result only in the case when there is correct independent information about the third parameter.

In the second sample, which was analysed by Mao and Paczynski [53] the detection range simulated the MACHO detection range and one could obtain the information about a fairly wide range of lens masses. Mao and Paczynski concluded that the amplification factor A and the lens mass function exponent α could be estimated precisely using observations of ~ 100 events. However, the lens mass estimate range ($\beta_{\min}$ or $\beta_{\max}$) in the detection region have more uncertainty for the event number $n = 100$.

In the case when the lens mass range is wider than the detection range, the total rate of events or the total optical depth (or the total mass) could not be measured since the larger part of the events are outside the detection range and the events are characterized by too long or too short durations t_0.

Therefore, there is a problem in expanding the detection range. Some attempts to expand the range were realized by the EROS collaboration [87] and the MACHO collaboration [88]. Mao and Paczynski presented the criterion to determine when the high (low) mass limit is reached [53]. For this determination it is necessary to expand the detection region and to find essential number of microlensing events to verify that there is an asymptotic power law [53]. It is necessary to find much more than 100 microlensing events for this determination. Such a great number of microlensing events could be detected towards the Galactic bulge since the event rate is great enough [85, 89–91]. If we have only 10 detected events then an estimation of these parameters could lead to large uncertainties.

In the discussion of numerical simulation results Mao and Paczynski noted that the spatial distribution of lenses and the lens kinematics are unknown in general [53]. For observations towards the LMC most lenses could be in our Galaxy (as Alcock et al. [86] supposed), or in the LMC (as Sahu [92] and Wu [93] assumed). For observations towards the Galactic bulge lenses could be as in the bulge (as Kiraga and Paczynski [84]; Udalski et al. [89, 85]; Paczynski et al. [67]; Zhao et al. [166, 167] assumed) or in the Galactic disk (as Alcock et al. [90, 91] supposed). Depending on the positions and lens kinematics the relation between the lens masses and typical durations could be very varied and the effect could yield additional uncertainties on the background of pure statistical uncertainties which were discussed in the paper by Mao and Paczynski [53]. Therefore, it is a very difficult problem to determine all the parameters which are necessary for a full description of the spatial distribution and the lens kinematics based on the analysis of the observed distribution of the typical duration of microlensing events.

Fortunately, future investigations of the optical depth variations depending on the directions could help to determine the positions of most lenses. So, if we analyse the microlensing searches towards the Galactic bulge and microlensing is caused mainly by stars in the Galactic bulge then the optical depth could change strongly depending on the Galactic longitude [84]. If the variation is not observed then the lenses are located mainly in the Galactic disk. If we analyse the microlensing searches towards the LMC and microlensing is caused mainly by stars in the LMC, then the optical depth could increase essentially for the direction towards the LMC center. If the optical depth is approximately constant for variations of the direction towards the LMC, then probably the lenses are mainly located in our Galaxy.

Although the ideas discussed by Mao and Paczynski are very simple in principle, it is necessary to detect several hundreds of microlensing events to obtain a reliable conclusion about the lens positions [53]. Such a great number of microlensing events could be detected towards the Galactic bulge, but the observations towards the LMC need much more time, since the observed event rate is much smaller in this case [86]. According to the remark of Mao and Paczynski, only when the location of gravitational lenses is known, can one develop more realistic models of their kinematics and consider more reliable expressions between the lens masses and the typical duration distribution [53].

So, there is a serious problem which is connected with the relation used between the observed durations and the lens masses, since now a model for the spatial distribution and the velocity distribution of lenses is unknown in general. Mao and Paczynski assumed that there is a uniform spatial distribution and uniform distribution for lens velocities [53]. However, there is no generally accepted model of the spatial distribution and velocity distribution of gravitational microlenses towards the Galactic bulge and the LMC. To create the model one can determine the optical depth variations as dependencies on galactic coordinates and use the information to determine the spatial distribution of lenses which contribute essentially to the microlensing effect. Future observations will allow us (possibly) to specify the distribution of the Galactic gravitational potential and to obtain a more precise estimate of the distribution of lens velocities. Only after future observations and their analysis according to the opinion of Paczynski, could one discuss the connections between the typical duration distribution and the lens mass distribution using much more reliable arguments [57].

However, one could remark that the problem would be solved only in the case when the spatial distribution of lenses is described correctly enough by a function having a small number of parameters and it could be incorrect in principle, if the microlenses form numerous clumps which are distributed in a complicated way in space.

8.5 Results and unsolved problems

Let us cite the well established results of microlensing searches and discuss the questions for which we have now different answers which do not contradict the observational data [57]. Now it is generally recognized that the microlensing searches towards the Galactic bulge or nearby galaxies are very important for solutions of a lot of problems in astronomy and cosmology. As Paczynski noted, the most important is the consensus that the microlensing phenomenon has been discovered [57]. Now it is impossible to tell which of the microlensing event candidates are actually connected with the effect since there are probably some variable stars among the event candidates, and it could be stellar variability of an unknown kind†.

(1) The observed light curves are achromatic and their shapes are interpreted by simple theoretical expressions very well, however, there is not complete consent about 'very good interpretation' since even for the event candidate MACHO # 1 the authors of the discovery proposed two fits. Dominik and Hirshfeld suggested that the event could be interpreted very well in the framework of the binary lens model [147, 148], but Gurevich et al. assumed that the microlensing event candidate could be caused by a non-compact microlens [123].

(2) As expected, binary lenses have been detected and the observed rate of these events correspond to the expected value.

(3) As expected, the parallax effect has been detected.

(4) Bennetti et al. reported that the spectrum of the only event monitored spectroscopically has been found to be constant throughout the intensity variations [175].

(5) Since the observed optical depth is essentially greater than the estimated value, an independent confirmation of the Galactic bar existence was made.

Now the following results are generally accepted [57]:

(1) The optical depth towards the Galactic bulge is equal to $\sim 3 \times 10^{-6}$, so it is larger than the estimated value.

(2) The optical depth towards the LMC is equal to $\sim 10^{-7}$, so it is smaller than the estimated value. We recall that now the MACHO collaboration presented the estimate 3×10^{-7}, but the first MACHO estimate based on three events and the first EROS estimate based on two events coincided remarkably and were equal to 8×10^{-8}.

(3) A lot of new interesting scientific results could be extracted from the giant data base which has been collected during microlensing searches, thereby, as Schneider wrote, microlensing searches are 'eldorado' for experts in stellar variability. New kinds of stellar variability have already been found using microlensing observations, but probably the data base contains other interesting information and has a great scientific significance.

However there are different suggestions (which do not contradict the observational data) about the following issues [57]:

What is the location of objects which dominate the microlensing observed towards the Galactic bulge?

Kiraga and Paczynski [84], Paczynski et al. [67], Zhao et al. [166, 167] suggested that most lenses are in the bulge, but Alcock et al. assumed that the most microlenses are in the Galactic disk [90].

Where are the most microlenses for searches towards the LMC? The microlenses may be in the Galactic disk, Galactic halo, the LMC halo or in the LMC itself. *Are the microlenses stellar mass objects or are they substellar brown dwarfs?*

What fraction of microlensing events are caused by binary lenses?

What fraction of microlensing events are connected with binary sources?

Paczynski suggested that we shall have definite answers for some of the presented issues after some years and since the optical depth towards the Galactic bulge is essentially greater than the optical depth towards the LMC, we shall have more information about the lens distribution towards the Galactic bulge, however, probably, some problems in the theoretical interpretation will appear after the detection of new microlensing event candidates [57].

8.6 Microlensing searches towards M31

In this section we discuss the method of searching for microlensing unresolved stars towards the Andromeda galaxy (M31). Recently several groups (Ansari et al. [177]; Crotts [179]; Shulga et al. [180]) have proposed monitoring the Andromeda galaxy. Ansari et al. call their project as AGAPE — Andromeda Galaxy and Amplified Pixel Experiment [177].

8.6.1 Arguments for the choice of the galaxy M31. Let us present the basic arguments for the choice of the galaxy M31 as a target for microlensing searches:

The galaxy M31 is the nearest large galaxy after the LMC and SMC (the galaxy is located at a distance of ~ 690 kpc). Therefore, as Shulga et al. noted, one can observe all lenses (at least in principle) in the Galactic halo, but not only lenses which are located inside the sphere with the radius ~ 52 kpc as for microlensing searches towards the LMC [180].

The Galaxy M31 is a giant galaxy roughly twice as large as our Milky Way. The galaxy M31 probably has its own halo and objects in the halo could cause the microlensing effect. Besides, as Crotts noted [179] there are some arguments that the Andromeda galaxy is tilted with respect to the line of sight, therefore, microlensing detection is more probable for stars on the far side of the galactic disk than for stars on the near side. On the other hand, there are no arguments that the asymmetry could be faked by variable stars.

One may remark that microlensing searches towards the galaxy M31 could help us to estimate the optical depth in a direction which is different from the directions towards the LMC, SMC or the bulge.

Gould estimated the optical depth towards the galaxy M31 due to known stars in the disk of the galaxy M31 itself as $\tau \sim 2 \times 10^{-7} e^{-r/d}$, where d is the disk scale, and r is the size along the major axis [181]. Thus, one can expect a significant effect for observations of the disk of galaxy M31 even if the galaxy M31 contains no dark compact objects. The optical depth has a strong dependence on the azimuthal angle: at fixed radius

$$\tau \propto \left(1 + \frac{h}{d} \tan i \cos\phi\right)^{-2},$$

where h is the scale height of the disk, $i = 75^\circ$ is the inclination angle of the galaxy M31, and ϕ is the azimuthal angle relative to the near minor axis. By measuring the optical depth as a function of the radial and azimuthal positions one can

† The microlensing event candidates proposed early by the EROS collaboration (#1 and #2) and by the MACHO collaboration (#2 and #3) are now considered as evidence of stellar variability.

estimate the parameters h and d for the mass of the M31 disk and so determine whether the disk light traces the disk mass distribution. Gould presented the following estimate: if one could realize ground observations (once per week) with an angular resolution of about $0.5''$ and an observation field of about 0.8 square degrees, then one could detect about 3 events per year. Gould considered the possibility of realizing a space based program of observations using the Wide Field Camera on the repaired Hubble Space Telescope. The WFC covers 4.4 square arcminutes. Hence observations would require about 250 hours per week, thus, the WFC camera is not suitable for the program and one must use a camera with a larger field of view [181].

If microlensing events are caused mainly by objects in the spheroid of the galaxy M31 (in comparison with objects in the disk), then event rate would be higher and the spheroid parameters could be determined. The optical depth distribution differs significantly for microlensing models in the disk and in the spheroid of the galaxy M31, respectively.

Using Monte Carlo simulations, Baillon et al. showed that in searches towards M31 the best sensitivity is achieved for lens masses in the range $10^{-3}-10^{-5}M_{\odot}$, and that most of the detectable events correspond to mild amplifications of bright stars rather than high amplifications of faint ones [182]. The authors proposed feasible observation programs which would lead to a few tens of events per year for brown dwarfs masses in the range $10^{-1}-10^{-5}M_{\odot}$ if the lenses form our Galaxy halo and the halo of the galaxy M31 [182].

Along with the AGAPE collaboration that has taken data using a 2 m telescope with a CCD camera at Pic du Midi in the French Pyrenees, observations of the galaxy M31 have been realized by the Columbia — VATT collaboration led by Crotts mainly using the Vatican Telescope in Arizona.

8.6.2 First observations of the galaxy M31. The first attempts of microlensing searches towards the galaxy M31 were carried out in 1990–1992 (the total duration of observations was about 1.5 years) at the Observatory of Sternberg State Astronomical Institute at Mount Maidanak and preliminary observational results were published in the paper by Shulga et al. [180]. The observational field of each plate was about $2.25^{\circ} \times 3^{\circ}$. The searchers have obtained 196 plates. The standard exposure time was 30 min. The average angular resolution was $\sim 1.4''$. The searchers have selected 75 events, which could be connected with the microlensing.

8.6.3 The AGAPE project. A problem of microlensing detection towards the galaxy M31 is caused by the difficulty of resolving single stars. A different approach (which differs from the discussed programs of monitoring light curves of a large number of stars) has been proposed by Baillon et al. [182], Crotts [179], Ansari [177]. It consists in monitoring the light flux which is measured by any single pixel of the CCD camera when one cannot measure the light flux corresponding to a single star. This approach allows one to detect the amplification due to the lensing of one of the many stars present in a crowded field, even if the star is not resolved. The light flux on a pixel comes from a group of stars in and around it plus the sky background radiation. The light flux of an individual star is spread among all the pixels of the seeing spot and only a fraction of the flux (the 'visible part' according to terminology of Ansari at al. [177]) is measured by the 'central' pixel. When the luminosity of the star is sufficiently amplified, the brightest pixel may emerge above the background radiation. So, the pixel measures the flux

$$F_{\text{pixel}} = \{\text{visible part}\}F_{\text{star}} + \langle F_{\text{other stars}}\rangle + F_{\text{background}}\,, \qquad (93)$$

where F_{star} is the flux of the microlensed star. If the star luminosity is amplified by a factor A, the pixel flux increases by

$$\Delta F_{\text{pixel}} = (A-1)\{\text{visible part}\}F_{\text{star}}\,. \qquad (94)$$

One can assume that the microlensing event is detected if the variable ΔF_{pixel} is Q times larger than the natural fluctuation of the pixel σ_{pixel} for at least few consecutive exposures, or

$$\Delta F_{\text{pixel}} > Q\sigma_{\text{pixel}}\,. \qquad (95)$$

For example, in the AGAPE experiment (Ansari et al. [177]) the searchers required that the variable Q should be larger than 3 for three consecutive exposures and larger than 5, for at least one of them.

Variable stars should be the main background. As Ansari et al. noted [178, 156] one can use ordinary typical features of microlensing (symmetrical light curves, single events, achromatic light curves) to distinguish microlensing events and stellar variabilities.

The AGAPE collaboration realized the first observations towards M31 during 57 half nights in the autumn of 1994. The observational field was about $4' \times 4'$, covered by 800×800 pixels of angular sizes $0.3'' \times 0.3''$ of a thin Tektronix CCD camera. However, the observational data were not enough to detect microlensing events. The observational data and some data of EROS were used to test the methods of processing observational data (Ansari et al. [177]).

9. Microlensing searches in future

Paczynski discussed possible experiments which can give additional information to answer some questions arising after experiments searching for the microlensing effect [57]. One future experiment could be connected with space observations using a satellite. There are natural reasons to carry out space observations, namely in this case there are no observational condition dependencies on weather conditions and atmospheric influence; there are possibilities to observe independently on a daily and yearly timescale (this could be realized only with a global network for microlensing searches); there is a possibility to access UV and IR observations. Besides these arguments, there are additional advantages for microlensing in putting a space telescope at a distance of about 1 AU from ground based telescopes as this allows the detection of the microlensing parallax effect. Any observations done at a single site provide only one quantity, namely the characteristic time scale t_0. The time scale t_0 depends on the lens mass, its distance, and its transverse velocity, none of which are known. The amplification factor depends on the impact parameter expressed in Einstein–Chwolson radius units, thus the illumination pattern created by the lens varies substantially on a scale of a fraction of the Einstein–Chwolson radius. Hence, even a small space telescope placed in a solar orbit could give us additional information and in the case as Gould noted, if the relative proper motion in the lens–source system is known, one can determine three additional parameters of the microlensing event [181, 42]. In particular, the determination of the lens mass might be possible. Paczynski discussed some problems

connected with the possible realization of the space experiment [57]. The main problem is the high cost, likely to be of the order of $\$10^8$, but the typical cost of a ground experiment is about $\sim \$10^6$ (although Paczynski supposed that "dollars in space weigh less" [57]). Moreover, even if the parallax effect alone can provide some constraints on the lens parameters, a unique determination of the lens mass may be made only for the cases when the amplification factors are very high. Such events are very rare. According to the opinion of Paczynski, probably the most important impact of the space experiment would be the direct proof that the observed event is really caused by gravitational microlensing and no other phenomenon can be responsible for the observed light curves [57]. Paczynski noted that only after future collection of the data of ground based observations one could describe more reliably the lens mass distribution, since as was noted above, one would need at least 10^3 events for a reliable determination of the lens mass distribution [57] (the conclusion is the consequence of the discussed Monte Carlo simulations of Mao and Paczynski [53]). Such a great number of microlensing events will be collected for observations towards the Galactic bulge in the coming years, but the collection of such a great number of events towards the LMC needs perhaps at least a decade.

Paczynski noted two cases when one can determine the lens masses [57]. One of the cases is when the lenses could belong to globular clusters seen against a rich stellar region of the galactic bulge or LMC (SMC), the second is when nearby high proper motion stars are seen against the distant stars of the Milky Way or LMC (SMC). In both cases the distances and proper motions can be measured directly or indirectly (for example, in the case when the lenses in the globular clusters are too dim to see). So, one can estimate the microlens mass in these cases.

10. Conclusions

The main result of the microlensing searches is that the effect predicted theoretically has been confirmed. This is one of the most important astronomical discoveries.

When new observational data are collected and the processing methods are perfected, probably some microlensing event candidates will lose their status, but perhaps new microlensing event candidates will be extracted from the analysed observational data.

Perhaps the optical depth estimates will be changed especially for observations towards the LMC since the recent MACHO estimate, given in 1996, is several times greater than the estimate given by the EROS and MACHO collaborations in 1995. Moreover, now one cannot affirm the coincidence of the estimates for the EROS and MACHO experiments. The lens mass estimates could be changed since the early MACHO estimates (for searches towards the LMC) differ significantly from the recent ones which we discussed above.

So, a general conclusion may be made. A very important astronomical phenomenon was discovered, but some quantitative parameters of microlensing will be specified in future.

Bibliographic remarks

First, we recommend the monograph [9] where there is a detailed description of microlensing theory. In our presentation of microlensing theory we also extensively used the recent comprehensive review [42] and the simple but very informative review [57]. The dark matter problem is also discussed in the comprehensive review [17], in the book [19] and in the brief review [45]. Microlensing by non-compact objects is analysed in the papers [122, 123, 48, 140, 141]. The discussion of the 'chromatic' features of microlensing is discussed in paper [149].

A detailed description of microlensing observations is in the book [9]. We used the papers [183, 177, 20, 151, 42] to describe the EROS experiment in detail. One could use these papers as useful bibliographic sources too. The results of the EROS experiment are described in the papers [183, 177, 20, 151, 42]. The MACHO results are presented in the comprehensive report of Alcock et al. [154] and in paper [153]. A brief description of the OGLE results is in the review by Paczynski [57].

Acknowledgements

We would like to thank V L Ginzburg for his interest which was the stimulus to write our review. We also acknowledge A V Gurevich for numerous useful discussions of different aspects of microlensing. The discussions significantly improved our review. We would like to thank K P Zybin and V A Sirota for useful discussions.

This work was partially supported by the "Cosmomicrophysics" project of the "Astronomy" program, by the Scientific and Educational Center "Cosmion" and by the Russian Foundation for Basic Research (grant No. 96-02-17434).

References

1. Soldner J G *Berliner Astron. Jahrbuch 1804* (1804) s. 161
2. Möller C *The Theory of Relativity* (Oxford: Clarendon Press, 1972) [Translated into Russian (Moscow: Atomizdat, 1975)]
3. Landau L D, Lifshitz E M *Teoriya Polya* (The Classical Theory of Fields) (Moscow: Nauka, 1988) [Translated into English (Oxford: Pergamon Press, 1975)]
4. Liebes S *Phys. Rev.* **133** B835 (1964)
5. Refsdal S *Month. Not. R. Astron. Soc.* **128** 295 (1964)
6. Refsdal S *Month. Not. R. Astron. Soc.* **128** 307 (1964)
7. Mukhanov V F *Usp. Fiz. Nauk* **133** 729 (1981) [*Sov. Phys. Usp.* **24** 331 (1981)]
8. Bliokh P V, Minakov A A *Gravitatsionnye Linzy* (Graviational Lenses) (Kiev: Naukova Dumka, 1989)
9. Zakharov A F *Gravitatsionnye Linzy i Mikrolinzy* (Gravitational Lenses and Microlenses) (Moscow: Janus-K, 1997)
10. Born M, Wolf E *Principles of Optics* (Oxford: Pergamon Press, 1968) [Translated into Russian (Moscow: Nauka, 1973)]
11. Burke W L *Astrophys. J.* **244** L1 (1981)
12. Schneider P, Ehlers J, Falco E E *Gravitational Lenses* (Berlin, New York: Springer-Verlag, 1992)
13. Erdl H, in *Proc. of the Workshop on Cosmology and Gravitational Lensing*, Preprint MPA/P3, Garching (1989) p. 79
14. Savelov A A *Ploskie Krivye* (Planar Curves) (Moscow: Nauka, 1960)
15. Doroshkevich A G, in *Fizika Cosmosa. Malen'kaya Entsiklopediya* (Cosmos Physics. Small Encyclopaedia) (Ed. R A Syunyaev) (Moscow: Sovetskaya Entsiklopediya, 1986) p. 622
16. Dolgov A D, Zel'dovich Ya B, Sazhin M V *Kosmologiya Ranneĭ Vselennoĭ* (Basics of Modern Cosmology) (Moscow: Izd. MGU, 1988) [Translated into English (Gif-sur-Yvette, France: Editions Frontieres, 1990)]
17. Carr B *Ann. Rev. Astron. Astrophys.* **32** 531 (1994)
18. Turner M S, in *Annals of the New York Academy of Sciences* Vol. 759 (Eds H Böhringer, G E Morfill, J E Trümper) (New York: The New York Academy of Sciences, 1995) p. 153
19. Peebles P J E *Principles of Physical Cosmology* (Princeton, N.J.: Princeton University Press, 1993)
20. Ferlet R, in *Annals of the New York Academy of Sciences* Vol. 759 (Eds H Böhringer, G E Morfill, J E Trümper) (New York: The New York Academy of Sciences, 1995) p. 56

21. Oort J *Bull. Astron. Inst. Heth.* **6** 249 (1932)
22. Rubin V C, Ford W K, Thonnard N *Astrophys. J.* **238** 471 (1980)
23. Faber S H, Gallagher J S *Ann. Rev. Astron. Astrophys.* **17** 135 (1979)
24. Bosma A *Astron. J.* **86** 1791 (1981)
25. Einasto J, Kaasik A, Saar E *Nature* (London) **250** 309 (1974)
26. Casertano S, Albada van T S, in *Baryonic Dark Matter* (Eds D Lynden-Bell, G Gilmore) (Dordrecht, Boston: Kluwer Acad., 1990) p. 159
27. Bahcall J M, Flynn C, Gould A *Astrophys. J.* **389** 234 (1992)
28. Valentijn E A *Nature* (London) **224** 891 (1990)
29. Burstein D, Haynes M P, Faber S M *Nature* (London) **353** 515 (1991)
30. Fich M, Tremaine S *Ann. Rev. Astron. Astrophys.* **29** 409 (1991)
31. Zaritsky D et al. *Astrophys. J.* **405** 464 (1993)
32. Zaritsky D, White S D M *Astrophys. J.* **435** 599 (1994)
33. Persic M, Salucci P *Astrophys. J. Suppl.* **99** 501 (1995)
34. Lin D N C, Faber S M *Astrophys. J.* **266** L21 (1983)
35. Aaronson M *Astrophys. J.* **266** L11 (1983)
36. Zwicky F *Helv. Phys. Acta* **6** 110 (1933)
37. White S D M et al. *Nature* (London) **366** 429 (1993)
38. Tyson J A, Fisher B *Astrophys. J.* **446** L55 (1995)
39. Linde A D *Fizika Elementarnykh Chastits i Inflyatsionnaya Kosmologiya* (Particle Physics and Inflationary Cosmology) (Moscow: Nauka, 1990) [Translated into English (Chur, New York: Harwood Acad. Publ., 1990)]
40. Copi C J, Schramm D N, Turner M S *Science* **26** 192 (1995)
41. Persic M, Salucci P *Month. Not. R. Astron. Soc.* **258** 14 (1992)
42. Roulet E, Mollerach S, astro-ph/9603119 (1996); *Phys. Rep.* **279** 2 (1997)
43. Evans N M *Month. Not. R. Astron. Soc.* **267** 333 (1994)
44. Bertschinger E, Dekel A *Astrophys. J.* **336** L5 (1989)
45. Spiro M *Nuclear Phys. B* (*Proc. Suppl.*) **43** 100 (1995)
46. Sadoulet B, in *Particle Astrophysics* (Eds G Fontaine, J Tran Thanh Van) (Gif-sur-Yvette: Editions Frontieres, 1993) p. 257
47. Gurevich A V, Zybin K P *Usp. Fiz. Nauk* **165** 723 (1995) [*Phys. Usp.* **38** 687 (1995)]
48. Gurevich A V, Zybin K P, Sirota V A *Usp. Fiz. Nauk* **167** 913 (1997) [*Phys. Usp.* **40** 869 (1997)]
49. Low C, Lynden-Bell D *Month. Not. R. Astron. Soc.* **176** 367 (1976)
50. Palla F, Salpeter E E, Stahler S W *Astrophys. J.* **271** 61 (1983)
51. De Rujula A, Jetzer Ph, Masso E *Month. Not. R. Astron. Soc.* **250** 348 (1991)
52. Bahcall J M et al., astro-ph/9406019 (1994)
53. Mao S, Paczynski B, astro-ph/9604002 (1996)
54. Pfennniger D, Combes F, Martinet L *Astron. Astrophys.* **285** 79 (1994)
55. De Paolis F et al. *Phys. Rev. Lett.* **74** 14 (1995)
56. Gerhard O, Silk J, astro-ph/9509149 (1995)
57. Paczynski B, astro-ph/9604011 (1996)
58. Komberg B V, Kompaneets D A, Lukash V N *Astron. Zh.* **72** 457 (1995) [*Astron. Rep.* **39** 402 (1995)]
59. Gates E I, Gyuk G, Turner M S, astro-ph/9508071 (1995), *Phys. Rev. D* **53** 4138 (1996)
60. Ostriker J P, Peebles P J E, Yahil A *Astrophys. J.* **193** L1 (1974)
61. Caldwell J A R, Ostriker J P *Astrophys. J.* **251** 61 (1981)
62. Bahcall J M *Ann. Rev. Astron. Astrophys.* **24** 577 (1986)
63. Sellwood J A, Sanders R H *Month. Not. R. Astron. Soc.* **233** 611 (1988)
64. Suchkov A A, in *Fizika Kosmosa. Malen'kaya Entsiklopediya* (Cosmos Physics. Small Encyclopaedia) (Ed. R A Syunyaev) (Moscow: Sovetskaya Entsiklopediya, 1986) p. 62
65. Marochnik L S, Suchkov A A *Galaktika* (Galaxy) (Moscow: Nauka, 1984)
66. Kent S M, Dame T M, Fazio G *Astrophys. J.* **378** 131 (1991)
67. Paczinsky B et al. *Astrophys. J.* **435** L113 (1994)
68. Lewis J R, Freeman K C *Astron. J.* **97** 139 (1989)
69. Bahcall J M *Astrophys. J.* **276** 169 (1984)
70. Gould A, Bahcall J M, Flynn C *Astrophys. J.* **465** 759 (1996)
71. Kuijken K, Gilmore G *Astrophys. J.* **367** L9 (1991)
72. Gould A *Month. Not. R. Astron. Soc.* **244** 25 (1990)
73. Gould A *Astrophys. J.* **465** L71 (1994)
74. Rich M *Astrophys. J.* **362** 604 (1990)
75. Bahcall J M, Casertano S *Astrophys. J.* **347** 347 (1990)
76. Binney J, May A *Month. Not. R. Astron. Soc.* **218** 743 (1986)
77. Blitz L, Spergel D N *Astrophys. J.* **370** 205 (1991)
78. Bahcall J M, Schmidt M, Soneira R M *Astrophys. J.* **265** 730 (1983)
79. Rohlfs K, Kreitschmann J *Astron. Astrophys.* **201** 51 (1988)
80. Richer H B, Fahlman G G *Nature* (London) **358** 383 (1992)
81. Giudice G F, Mollerach S, Roulet E *Phys. Rev. D* **50** 2406 (1994)
82. Ostriker J, Caldwell J A R, in *Dynamics and Structure of the Milky Way* (Ed. W L H Shuter) (Dordtrecht: Reidel, 1982)
83. Blanco V M, Terndrup D M *Astron. J.* **98** 843 (1989)
84. Kiraga M, Paczynski B *Astrophys. J.* **430** L101 (1994)
85. Udalski A et al. *Acta Astron.* **44** 227 (1994)
86. Alcock C et al. *Phys. Rev. Lett.* **74** 2867 (1995)
87. Ansari R *Nucl. Phys. B* (*Proc. Suppl.*) **43** 108 (1995)
88. Bennett D et al. *Talk at the 2nd Int. Workshop on Gravitational Microlensing Surveys* (1996)
89. Udalski A et al. *Acta Astron.* **44** 165 (1994)
90. Alcock C et al. *Astrophys. J.* **445** 133 (1995)
91. Alcock C et al., astro-ph/9511073 (1995)
92. Sahu K *Nature* (London) **370** 275 (1994)
93. Wu X-P *Astrophys. J.* **435** 66 (1994)
94. Witt H J *Astrophys. J.* **403** 505 (1993)
95. Schneider P, Weiss A *Astron. Astrophys.* **164** 237 (1986)
96. Erdl H, Schneider P, Preprint MPA 647, Garching (1992)
97. Witt H J, Petters A O, Preprint POP-509 (1993)
98. Mao S, Paczynski B *Astrophys. J.* **347** L37 (1991)
99. Mao S, Di Stefano R *Astrophys. J.* **440** 22 (1995)
100. Alard C, Mao S, Guibert J *Astron. Astrophys.* **300** L17 (1995)
101. Gould A, Loeb A *Astrophys. J.* **396** 362 (1992)
102. Bennett D, Rhie S H, astro-ph/9604031 (1996)
103. Rhie S H, Bennett D P, astro-ph/9607055 (1996); *Nucl. Phys. B* (*Proc. Suppl.*) **51B** 86 (1996)
104. Gaudi B S, Gould A, astro-ph/9610123 (1996)
105. Gould A, astro-ph/9608045 (1996); in *Proc. of the 12th IAP Astrophysics Meeting, France, 1996* (Eds R Ferlet, J P Maillard) (Gif-sur- Yvette: Editions Frontieres, 1997) p. 125
106. Refsdal S *Month. Not. R. Astron. Soc.* **132** 101 (1966)
107. Grieger B, Kayser R, Refsdal S *Nature* (London) **324** 126 (1986)
108. Gould A *Astrophys. J.* **386** L5 (1992)
109. Alcock C et al. *Astrophys. J.* **454** L125 (1995)
110. Bennett D et al., in *Dark Matter* (AIP Conf. Proc., Vol. 336, Eds S S Holt, C L Bennett) (New York: AIP Press, 1995)
111. Witt H J, Mao S, Preprint POP-531 (1993)
112. Nemiroff R N, Wichkramasinghe W A *Astrophys. J.* **424** L21 (1994)
113. Abt H A *Ann. Rev. Astron. Astrophys.* **21** 243 (1983)
114. Griest K, Hu W *Astrophys. J.* **397** 362 (1992)
115. Sazhin M V, Cherepashchuk A M *Pis'ma Astron. Zh.* **20** 613 (1994) [*Astron. Lett.* **20** 523 (1994)]
116. Sazhin M V, Cherepashchuk A M *Pis'ma Astron. Zh.* **21** 263 (1995) [*Astron. Lett.* **21** 230 (1995)]
117. Cherepashchuk A M, Sazhin M V, Trifalenkov I A *Astrophys. Space Sci.* **229** 265 (1995)
118. Khruzina T S, Cherepashchuk A M *Astron. Zh.* **74** 559 (1997) [*Astron. Rep.* **41** 492 (1997)]
119. Schneider S, Weiss A *Astron. Astrophys.* **260** 1 (1992)
120. Chang K, Refsdal S *Astron. Astrophys.* **132** 169 (1984)
121. Zakharov A F, Sazhin M V *Astron. Zh.* **74** 336 (1997) [*Astron. Rep.* **41** 291 (1997)]
122. Gurevich A V, Zybin K P *Phys. Lett. A* **208** 276 (1995)
123. Gurevich A V, Zybin K P, Sirota V A *Phys. Lett. A* **214** 232 (1996)
124. Sazhin M V, Yagola A G, Yakubov A V *Phys. Lett. A* **219** 199 (1996)
125. Gurevich A V, Zybin K P, Sirota V A, in *VIII Rencontres de Blois; Neutrino, Dark Matter and the Universe* (Gif-sur-Yvette: Editions Frontieres, 1996) p. 349
126. Bogdanov M B, Cherepashchuk A M *Astron. Zh.* **75** (1) 93 (1998) [*Astron. Rep.* **42** 81 (1998)]
127. Chandrasekhar S *Radiative Transfer* (New York: Dover Publ., 1960)
128. Sobolev V V *Perenos Luchistoĭ Energii v Atmosferakh Zvezd i Planet* (Radiation Transfer in Stellar and Planetary Atmospeheres) (Moscow: Gostekhizdat, 1956)
129. Sams D C, Johnston I D S *Month. Not. R. Astron. Soc.* **168** 463 (1974)

130. Cassinelli J P Hoffman N M *Month. Not. R. Astron. Soc.* **173** 789 (1975)
131. Bogdanov M B *Astron. Zh.* **64** 1300 (1987) [*Sov. Astron.* **31** 682 (1987)]
132. Bogdanov M B *Astron. Tsirk.* N1526 10 (1988)
133. Bochkarev N G, Karitskaya E A *Pis'ma Astron. Zh.* **9** 14 (1983) [*Sov. Astron. Lett.* **9** 6 (1983)]
134. Schneider P, Wagoner R V *Astrophys. J.* **314** 154 (1987)
135. Simmons J F L, Willis J P, Newsam A M *Astron. Astrophys.* **293** L46 (1995)
136. Bogdanov M B, Cherepashchuk A M, Sazhin M V *Astrophys. Space Sci.* **235** 219 (1996)
137. Agol E *Month. Not. R. Astron. Soc.* **279** 571 (1996)
138. Belokurov V A, Sazhin M V *Phys. Lett. A* **239** 215 (1997) (accepted)
139. Zakharov A F, Sazhin M V *Pis'ma Astron. Zh.* **23** 403 (1997) [*Astron. Lett.* **23** 349 (1997)]
140. Zakharov A F, Sazhin M V *Pis'ma Zh. Eksp. Teor. Fiz.* **63** 894 (1996) [*JETP Lett.* **63** 937 (1996)]
141. Zakharov A F, Sazhin M V *Zh. Eksp. Teor. Fiz.* **110** 1921 (1996) [*JETP* **83** 1057 (1996)]
142. Byalko A V *Astron. Zh.* **46** 998 (1969)
143. Paczynski B *Astrophys. J.* **304** 1 (1986)
144. Griest K *Astrophys. J.* **366** 412 (1991)
145. Alcock C et al. *Nature* (London) **365** 621 (1993)
146. Aubourg E et al. *Nature* (London) **365** 623 (1993)
147. Dominik M, Hirshfeld A C *Astron. Astrophys.* **289** L31 (1994)
148. Dominik M, Hirshfeld A C, Preprint DO-TH 95/19 (Dortmund, 1995)
149. Bogdanov M B, Cherepashchuk A M *Pis'ma Astron. Zh.* **21** 570 (1995) [*Astron. Lett.* **21** 505 (1995)]
150. Pratt M et al., in *IAU Symp. 173* (Eds C Kochanek, J Hewitt) (Dordrecht: Kluwer Academic, 1995)
151. Magneville C, in *Annals of the New York Academy of Sciences* Vol. 759 (Eds H Böhringer, G E Morfill, J E Trümper) (New York: The New York Academy of Sciences, 1995) p. 664
152. Palanque-Delabrouille N et al., astro-ph/9611059 (1996)
153. Sutherland W et al., astro-ph/9611059 (1996); in *Proc. of the 1st Intern. Workshop on the Identification of Dark Matter, Sheffield, UK, 1996* (Ed. N J C Spooner) (Singapore: World Sci., 1996) p. 200
154. Alcock C et al., astro-ph/9606165 (1996)
155. Albrow M, in *Proc. IAU Symp. 173* (Eds C S Kochanek, J N Hewitt) (Dordrecht, Boston, London: Kluwer Academic Publ., 1996) p. 227
156. Ansari R et al. *Astron. Astrophys.* **299** L21 (1995)
157. Bennett D P et al., astro-ph/9606012 (1996); *Nucl. Phys. B* (*Proc. Suppl.*) **51B** 152 (1996)
158. Alcock C et al., astro-ph/9606165 (1996)
159. Alcock C. et al., astro-ph/9603158 (1996)
160. Flynn C, Gould A, Bahcall J *Astrophys. J.* **466** L55 (1996)
161. Zhao H S, astro-ph/9606166 (1996)
162. Griest K et al. *Astrophys. J.* **372** L79 (1991)
163. Paczynski B *Astrophys. J.* **371** L63 (1991)
164. De Vaucouleurs G, in *The Galaxy and the Magellanic Clouds* (IAU Symp. 20, Eds F J Kerr, Rotgers) (IAU: Union Radio Scientifique Intern., 1963)
165. Stanek K et al. *Astrophys. J.* **429** L73 (1994)
166. Zhao H, Rich R M, Spergel D N *Astrophys. J.* **440** L13 (1995)
167. Zhao H, Spergel D N, Rich R M, astro-ph/9512065 (1995)
168. Dwek E. et al. *Astrophys. J.* **445** 716 (1995)
169. Han C, Gould A, astro-ph/9504078 (1995)
170. Udalski A et al. *Astrophys. J.* **436** L103 (1994)
171. Ossipov D L, Kuryan V E *Phys. Lett. A* **223** 157 (1996)
172. Alcock C et al., astro-ph/9512146 (1995)
173. Mollerach S, Roulet E *Astrophys. J.* **458** L9 (1996)
174. Terndrap D M *Astron. J.* **96** 884 (1988)
175. Benetti S et al. *Astron. Astrophys.* **294** L37 (1995)
176. Schneider P, Preprint MPA 901 (1995)
177. Ansari R, in *Annals of the New York Academy of Sciences* Vol. 759 (Eds H Böhringer, G E Morfill, J E Trümper) (New York: The New York Academy of Sciences, 1995) p. 608
178. Ansari R et al., astro-ph/9504078 (1995)
179. Crotts A P S *Astrophys. J.* **399** L43 (1992)
180. Shulga V V, Sazhin M V, Gorbatko N P *Astron. Astrophys. Trans.* **10** 187 (1996)
181. Gould A, Preprint OSU-TA-5/94 (1994)
182. Baillon P et al. *Astron. Astrophys. Trans.* **277** 1 (1993)
183. Ansari R, in *Particle Astrophysics* (Eds G Fontaine, J Tran Thanh Van) (Gif-sur-Yvette: Editions Frontieres, 1993) p. 243